Helsinki University of Technology Automation Technology Laboratory
Series A: Research Reports No. 24
Espoo, December 2002

ADAPTIVE AUTONOMOUS NAVIGATION OF MOBILE ROBOTS IN UNKNOWN ENVIRONMENTS

Jorma Selkäinaho

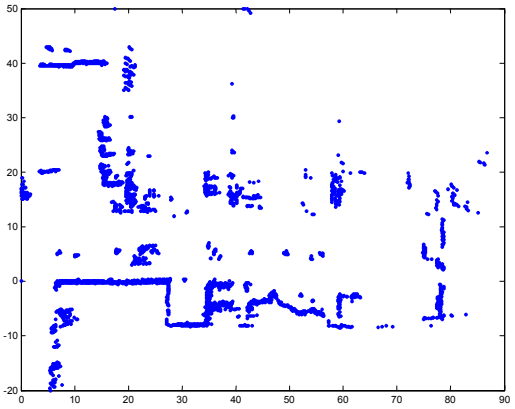

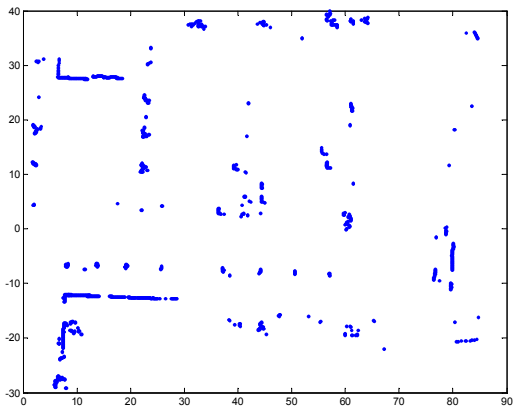

TEKNILLINEN KORKEAKOULU
TEKNISKA HÖGSKOLAN
HELSINKI UNIVERSITY OF TECHNOLOGY
TECHNISCHE UNIVERSITÄT HELSINKI
UNIVERSITE DE TECHNOLOGIE D'HELSINKI

Helsinki University of Technology - Automation Technology Laboratory
Series A: Research Reports No. 24, December 2002

ADAPTIVE AUTONOMOUS NAVIGATION OF MOBILE ROBOTS IN UNKNOWN ENVIRONMENTS

Jorma Selkäinaho

Dissertation for the degree of Doctor of Science in Technology to be presented with due permission of the Department of Automation and Systems engineering, for public examination and debate in Auditorium T2 at Helsinki University of Technology (Espoo, Finland) on the 12th of December 2002, at 12 o'clock noon.

Helsinki University of Technology
Department of Automation and Systems Technology
Automation Technology Laboratory

Teknillinen korkeakoulu
Automaatio- ja systeemitekniikan osasto
Automaatiotekniikan laboratorio

Distribution:

Helsinki University of Technology
Automation Technology Laboratory
P.O. Box 5400
FIN-02015 HUT
FINLAND

e-mail jorma.selkainaho@hut.fi
Tel +358-9-451 3302
Fax +358-9-451 3308

ISBN 951-22-6230-4
ISSN 0783-5477

Pica-set Oy
Helsinki 2002

ABSTRACT

Autonomous navigation of a mobile robot is a challenging task. Much work has been done in indoor navigation in the last decade. Fewer results have been obtained in outdoor robotics. Since the early 90's, the Global Positioning System (GPS) has been the main navigation system for ships and aircrafts. In open fields, satellite navigation gives absolute position accuracy. The absolute heading information is also obtained by satellite navigation when the mobile robot is in motion. However, the use of GPS satellite navigation is mainly restricted to open areas where at least three satellites can be seen. For example, mobile robots working in underground or deep open mines cannot use satellite navigation at all, and in forest or city areas, there are serious limitations to its use.

Laser range finder technology has evolved remarkably over the last decade, and offers a fast and accurate method for environment modeling. Furthermore, it can be used to define robot position and heading relative to the environment. It is obvious that the use of several alternative sensors according to the environment will make the navigation system more flexible. Laser range finder technology is particularly suitable for indoors or feature rich outdoor environments.

The goal of this thesis is to develop a multi sensor navigation system for unknown outdoor environments, and to verify the system with a service robot. Navigation should be possible in unstructured outdoors as well as indoor environments. The system should use all available sensor information and emphasize those that best suit the particular environment. The sensors considered in this thesis include a scanning laser range finder, a GPS receiver, and a heading gyro.

The main contribution of the thesis is a flexible navigation system developed and tested with a service robot performing versatile tasks in an outdoor environment. The used range matching method is novel and has not been verified earlier in outdoor environments.

No unique solution can be guaranteed in the developed map matching algorithm, although it seems to work well in the practical tests. Position and heading errors grow without bound in successive map matchings, which could be referred to as laser odometry. Therefore, the position and heading have been corrected by means of global matching when the robot returns to a place it has previously visited. Alternatively, structured landmarks have been used for position and heading correction. In field tests, tree trunks and walls have been used as structured landmarks. When structured landmarks are not present, navigation has been based on counting the translation and rotation between two successive maps based on a scanning laser range finder. In featureless environments, the robot is able to switch automatically from laser based to satellite navigation.

The biggest difference compared to other methods, such as iterative closest point, is that odometry is not needed since the matching is based on a global search. However, when included, mobile robot dynamics and odometry increase the reliability of the matching process.

The flexibility of the navigation system presented here means that a mobile robot can enter different environments, and the system automatically selects an appropriate set of sensors for each particular environment. It additionally means that the system can work without landmarks, but if they exist, they will be used to improve navigation accuracy. This kind of flexibility in the navigation system is of the utmost importance when in the near future increasingly mobile robots will move out from structured indoor environments into unknown outdoor environments.

Keywords: autonomous navigation, laser range finder, outdoor robotics

PREFACE

The work presented in this thesis was carried out at the Automation Technology Laboratory of Helsinki University of Technology during the period 2000-2002.

The conductor of this thesis was been professor Aarne Halme, the head of the laboratory. I thank him for an interesting research problem.

The main part of the work was done while working on the WorkPartner project, financed by the Technology Development Centre of Finland (TEKES). Almost half of the funding came from the Research Support Foundation of Helsinki University of Technology, which received a donation from Sandvik/Tamrock Ltd.

The expertise of Mr Janne Paanajärvi has been valuable in helping me become acquainted with correlation methods and the Hough transform. Moreover, he has always been ready for practical discussions throughout the work.

I also thank Dr Pekka Forsman for his practical advice throughout the work.

I owe a debt of gratitude to the members of WorkPartner project who built the robot used in my thesis. In addition, I thank Mr Tapio Leppänen and Mr Carl Gustaf Rosenblad for assembling the sensors in the navigation box.

Mr Maciej Gigon was kindly preparing figures 4.4 and 4.5.

I additionally thank my preliminary examiners, Dr. Hannu Mäkelä and Professor Alexander Zelinsky for their reviews and valuable suggestions on the thesis. Many thanks are also due to Ms Ruth Vilmi for the English language revision of the manuscript. In addition, I thank Dr. Mika Vainio for the English language revision in the early stage.

I am extremely grateful for the financial support I received earlier from the Walter Ahlström Foundation and the Heikki and Hilma Honkanen Foundation.

I thank to my wife Ritva for her supportive attitude to my work.

Espoo, November 2002 Jorma Selkäinaho

CONTENTS

LIST OF SYMBOLS

α	the angle variable in the Hough space
α_M	manipulator body pitching angle relative to robot body
α_P	pitch angle of the robot front body segment
α_R	roll angle of the robot front body segment
α_w	direction of the normal axis of the wall
β	laser beam bearing angle to an object
β_t	laser beam bearing to a tree
β_I	laser beam angle of incidence in line feature detection
γ	the angle between the front and rear body segment of the robot
ϕ	heading of the robot in local coordinates
ϕ_{GPS}	GPS heading measurement
ω_L	mean angular velocity of left wheel
ω_R	mean angular velocity of right wheel
$\Delta\alpha$	angle resolution in Hough line transform
$\Delta\beta$	laser beam resolution
Δb	heading search resolution
Δd	range resolution in Hough line transform
Δx	difference in position coordinate x between reference and current map
Δy	difference in position coordinate y between reference and current map
$\Delta\phi$	difference in heading between reference and current map
Δs	position search resolution
ΔT	measurement update period
a_x	measured acceleration in sway direction of the robot
a_y	measured acceleration in surge direction of the robot
d	line distance in the Hough transform
d_i	laser beam range to tree surface
d_k	radius of the respective point acceptance circle in pair wise matching
d_{max}	upper limit of laser beam range in the Hough line transform
d_p	distance between points on line
d_t	distance between robot and tree
d_{tw}	distance between tree and robot
d_w	distance between robot and wall
e_ϕ	heading error
e_{GPS}	GPS heading error
e_r	range error
$f()$	gyro filter output
g	gravity constant
g_g	gyro gain
G	gain of the Kalman filter
h_L	laser distance from ground
i	time index
ll	line length
L_B	distance between virtual back wheel axis and virtual articulation joint
L_F	distance between virtual front wheel axis and virtual articulation joint
m_i	number of detected movements of target o_i
n	number of points in tree feature

n_k	1 if respective point found else 0
N	number of common points in pair wise matching
o_i	target no i
o_w	width of a human person
p(|)	conditional probability
r	laser beam range to object
r_c	tree radius
r_{max}	upper limit of laser beam range
R_T	turning radius of the robot front body segment
R_W	wheel radius
s_ϕ	standard deviation of robot heading error
T	period of time
u_0	value of gyro measurement at zero angular velocity
u_g	gyro measurement
v	velocity of the robot
v_s	white noise
w_g	white noise
w_u	white noise with unit variance
x	local position coordinate
x_c	x-coordinate of tree trunk center
x_j	coordinate of object point in map
x_R	robot surge coordinate
x^R	object position in robot coordinates
y	local position coordinate
y0	difference between gps heading and local coordinate heading
y_c	y-coordinate of tree trunk center
y_j	coordinate of object point in map
y_R	robot sway coordinate
y^R	object position in robot coordinates

1 INTRODUCTION

1.1 Problem of robot navigation in outdoor environment

Navigation in engineering science is defined as estimating the attitude of a mobile vehicle in a local or global coordinate system. This thesis is limited to mobile ground vehicles, and the position is considered only in 2D. The main reason for the limitation is the fact that the distance from vehicle to ground is usually almost constant. The configuration space of position is a surface with constant distance to the ground. In addition, the available computing power in real time applications motivates this choice.

Since the early 90's, satellite navigation has been the primary navigation method outdoors. It is commonly used in sea and air navigation. However, its use is restricted to open areas above ground or sea. Thick forests and urban canyons cause losses in position fixes due to satellite invisibility problems. The accuracy of the conventional Global Positioning System (GPS) is not sufficient for a robot performing autonomous working tasks. Therefore, accurate navigation results obtained in structured indoor environments have raised the interest of using similar methods in unstructured outdoor environments. Such methods are landmark navigation and dense raw data registration. Used measurement technology includes laser range finder, wide angle sonar, camera, and wheel based odometry.

The history of robot indoor navigation began when Automated Guided Vehicles (AGV) were moving on factory floors. In the beginning, the AGV navigation was based on simple line following. The conventional technology was based on following AC-driven electrical cable embedded in the concrete floor. This technology restricts the AGV movements to predetermined paths and it is costly to change the route. A more flexible technology is based on following painted lines on the floor using cameras [Frohn and Seelen, 1989]. In the 90's, laser scanner based systems came onto the markets. Navigation was based on measuring the bearing of reflective tapes on walls. New routes could be given through a computer interface, which made the system more flexible.

At present, there is a trend away from teleoperated mobile robots to semi-autonomous robots that require more knowledge of the operating environment. Several autonomous or semi-autonomous mobile robots or robotic machines have been introduced so far. Cruise missiles (http://www.chinfo.navy.mil/navpalib/factfile/missiles/wep-toma.html) and unmanned surveying aircrafts are examples operating in the air and using GPS navigation. Remotely operated underwater vehicles are developing towards more autonomous operations. Most autonomous or semi-autonomous robots operate within specified indoor environments. The shop floor cleaning robot [Lawitzky, 2001], museum tour guide robot [Thrun et al., 1998a], hospital courier robot [Evans, 1994] and vacuum cleaner robot (http://trilobite.fi.electrolux.com) are some examples. In these examples, navigation is based on a structured environment and local coordinates. The lawn mower robot by Husqvarna works outdoors inside a surrounding cable. Robots operating in non-structured environments are extremely rare. The autonomous load-haul-dump (LHD) mining vehicle [Mäkelä, 2001] is able to haul and dump autonomously in an underground mine. Only the loading phase is remotely operated. Similar results with LHD vehicles in underground mines have been reported in [Roberts et al., 2000]. These methods are presented more accurately in [Madhavan et al., 1998a].

A car automated in Australia was able to navigate in sub-urban area autonomously [Bailey and Nebot, 2001]. Navigation was based on laser odometry and natural landmarks. They estimated the position and heading by comparing successive laser range readings.

It is possible to make the navigation task easier by adding artificial features to natural environments. Artificial landmarks have been used in laser based outdoor navigation in [Guivant et al., 2000a]. However, it is a time consuming and expensive method that leads to less flexible applications.

A robot that navigates autonomously must know its position and heading relative to the working environment. A robot can use several local coordinate systems depending on the work task. For example, the coordinate system may be fixed to an object in a grasping task. One or several local coordinates can be further fixed in global Earth fixed coordinates so that the robot can subsequently use the extracted landmarks. The problem is usually divided into two parts. Firstly, the robot must find its pose (position and heading) relative to the goal at startup or later on. Secondly, The robot must know its pose with sufficient accuracy when it attempts to reach the goal. This is referred to as 'pose tracking'. Accuracy is sufficient when the robot can detect and recognize the goal. Motion planning and obstacle avoidance is additionally required. This thesis concentrates on determining the position and heading of the robot. The mission route is given to the robot, and the robot moves on the route using reactive obstacle avoidance [Roberts et al., 2000].

1.2 Motivation for the study

Interest in developing mobile service robots has increased remarkably over the last decade. Most of the research has focused on developing robots for indoor use, but there is an increasing trend towards outdoor robotics. A good example of such a service robot is currently being developed at the Automation Technology Laboratory of Helsinki University of Technology. This centaur type service robot is known as WorkPartner and is intended to work together with a human operator mainly in outdoor environments. It has four wheeled legs and two hands [Halme et al., 2001a]. A typical task for the service robot could be to fetch a defined object from a defined place. The human operator gives the required definitions of the task. Carrying out service tasks in an unknown environment is a challenging task for the perception system. The robot must know its local position and heading relative to the working environment. The need for increased flexibility requires that there are no limitations for the work environment. The robot should be able to operate in a new environment without previous knowledge. On the other hand, if previous knowledge exists about the working environment, e.g., from the earlier visits, the information should be exploited.

The goal of this thesis is to develop a navigation system for a mobile robot such as WorkPartner. The obtained results are also largely valid for other mobile robots working in unstructured outdoor environments. The robot should be capable of moving autonomously in a previously unknown environment. In unknown environments, navigation cannot rely only on predefined landmark types such as trees or sharp corners. However, if landmarks can occasionally be detected, they should be used as additional information for navigation. Usually, the environment may consist of trees, cars, or buildings. An empty field can also form an environment for the robot.

The developed navigation system does not require a structured environment. However, if structured objects exist occasionally in an environment, they will be used. This thesis concentrates on navigation methods that use such natural landmarks as trees, lampposts, bushes, or even parked cars. The navigation system utilizes a 2D laser range finder as a main sensor and a low cost GPS receiver, a piezo gyro, inclinometers, and a 3D magnetometer can be used as alternative or additional sensors.

When Workpartner starts to work in an unknown place, it should be able to adapt quickly to the new working environment. Transitions from feature rich environments to open fields should not cause problems. In a new environment, there are no previously known landmarks but the robot should recognize potential landmarks and use them the next time.

A robot that operates in an unknown environment should be able to cope with dynamic objects such as people walking or moving cars. However, the navigation is based on static features in the environment.

Traditionally, scientific work proceeds in two stages. First, a theory is developed, and then it is verified with experimental work. In this thesis, the results derive merely from analyzed sensor data. A large amount of sensor data is at first collected from numerous test trials with the robot operating in an outdoor environment. The gathered data is then carefully analyzed and real time algorithms capable of utilizing the data are developed.

1.3 Scientific contribution

In this thesis, an adaptive navigation system has been developed and verified with a real robot performing versatile tasks in an outdoor environment. The adaptability has been obtained by using different combinations of navigation sensors according to the environmental requirements.

The main scientific contribution is a laser range data matching method that works in unstructured environments outdoors. The method is presented in Chapter 4.5. In Chapter 5.4, the method is tailored to the Workpartner robot, and the accuracy is presented in Chapter 5.5. An earlier version of the method has been published in [Selkäinaho et al., 2001]. Similar correlation methods based on evidence grids have previously been used in structured indoor environments [Schultz and Adams, 1998] and [Konolige and Chou, 1999]. The new matching method does not require odometry. Odometry-free laser based navigation has been used in an outdoor environment but only with structured landmarks [Bailey and Nebot, 2001].

The second contribution is the method that enables the presented navigation method to automatically change the navigation method according to the requirements of the environment. The adaptive navigation method is presented in Chapter 4.8. Results from robot pose initialization are shown in Chapters 5.2 and 5.3. Pose correction using landmarks is presented in Chapter 5.6. Robot heading estimate correction using GPS heading is presented in Chapter 5.8. The results of automatically changing the navigation method between satellite navigation and successive laser range scan matching are shown in Chapter 5.9. The commonly used wheel based odometry has not been used in navigation but it will be added to the system soon.

The third contribution is the error analysis that has been conducted for several navigation sensors. The GPS heading error model is presented in Chapter 5.8. The accumulation of heading errors in the real time matching algorithm is presented in Chapter 5.5.

The fourth contribution is a tree trunk position estimation algorithm based on only two or three laser range readings. That is presented in Chapter 5.1. The viewing angle based tree trunk recognition method has been used earlier by [Bailey et Nebot, 2001]. Individual landmark recognition is based on pair wise distances, as in [Nebot et al., 2000].

The fifth contribution is an automatic calibration method that minimizes the drift of a low cost piezo gyro to 1/100. The calibration method is presented in Chapter 4.1 and the results are shown in table 4.1. The idea of always calibrating gyro when the robot is not moving has been presented on a general level in [Balaram, 2000].

The sixth contribution is modeling the accuracy of Doppler based velocity and the heading measurement of a non-accurate GPS receiver in a dynamical situation. That is presented in Chapter 5.8. Static modeling has been carried out earlier [Selkäinaho and Paanajärvi, 2000]. GPS positioning was free from Selective Availability after May 1st, 2000. As far as the author is aware, no papers have since been published on the heading and velocity accuracy of conventional GPS receiver.

The scientific contributions mentioned above have been verified with a WorkPartner service robot in an outdoor environment.

1.4 Outline of the thesis

In Chapter 1, the problems of outdoor navigation are introduced. Then, the motivation of the study, scientific contributions, and the outline of the thesis are presented.

In Chapter 2, relevant research, mainly from indoor navigation but also from outdoors, is presented.

In Chapter 3, the problem of navigation is defined, and coordinate systems are explained. The test trial environment is also presented.

In Chapter 4, the WorkPartner robot is first presented and the used sensors are analyzed. The pose initialization and calibration methods are presented based on analyzed sensor data. Then, the navigation methods based on different sensors are explained. Additionally, it is explained how the navigation methods are changed automatically according to environmental requirements.

In Chapter 5, the methods presented in the preceding chapter are verified with the sensor data gathered from outdoor test trials.

In Chapter 6, additional results on simultaneous localization and mapping are presented. In addition, results on human target detection and tracking are shown.

In Chapter 7, the summary and considerations of the future are presented.

2 RELATED RESEARCH

Most related research into mobile robot navigation has been done indoors. These results cannot be applied directly to an unknown outdoor environment. Features that are common indoors are usually only temporarily available outdoors. Such basic algorithms as the Hough transform may still be useful.

Different kinds of objects can be used as navigation landmarks. In a city environment, walls, lampposts, and trees serve as useful landmarks. A wall is a line object that carries information about the direction and 1D distance. The robot position and heading can be computed when another wall corner can be detected. The most common cylindrical obstacle in a natural environment is a tree trunk. A lamppost or a tree trunk is a point type landmark that does not carry information about the heading. Two point type landmarks can be used to define two possible locations for the robot. The correct location can be computed when the bearing to point wise landmarks is known.

In indoor navigation, the walls, in particular their vertical or horizontal corners, are commonly used as landmarks. A horizontally scanning laser range finder measures distances to the wall in polar coordinates. The contact points of the laser beam and the wall are seen as points on a line in the Cartesian coordinates. By using the Hough transform, some of the points can be shown to belong to the same line.

Indoors, a robot can see up to four walls and corners that can be used as navigation landmarks. Two orthogonal walls are enough for pose determination. Outdoors sometimes only one wall of a building can be seen, which is not enough for pose determination. Therefore, it is useful to acknowledge that other objects can be used as navigation landmarks.

2.1 Indoor navigation

The Hough transform is useful when searching line features from 2D laser range pictures. The indoor environment is structured and includes walls and furniture. A sensor with a 180° viewing angle is able to see up to four walls in a room that are recognized as lines in 2D range maps. The Hough transform has been successfully applied indoors with both sonar sensors [Grossman and Poli, 2001] and scanning laser range finders [Jensfelt, 1999]. Outdoors, in an environment where only one building exists, not more than one wall can be seen most of the time. Depending on the viewing angle, no line features may exist. Two orthogonal walls are sufficient landmarks for robot pose estimation. Therefore, it is necessary to use additional landmarks outdoors. Possible landmarks include tree trunks, lampposts, cars, and bushes.

Larsson et al. [Larsson et al., 1996] used wall-lines as landmarks when integrating laser range measurements indoors. The wall lines have been extracted by using a 2D scanning laser range finder and the range weighted Hough transform. Range weighting makes it easier to find wall lines in cluttered rooms. Outdoors, the range weighted Hough transform occasionally finds faulty lines from maximal distances of the sensor.

Arras et al. [Arras and Tomatis, 1999] and [Arras and Vestli, 1998] built robots that are able to move autonomously in office corridors. Walls extracted by a laser range finder and vertical edges extracted by a camera were used as landmarks. The laser range finder and the camera

are complementary sensors. A closed door is easier to find with a camera than with laser range finder. On the other hand, the distance to the corridor end is more accurately measured with a laser range finder than extracted from camera picture. The constant level of artificial illumination indoors is advantageous for image processing compared to highly fluctuating illumination outdoors.

Lu and Milios[Lu and Milios, 1994] presented two algorithms for robot position and heading estimation; the first works in polygonal environments and the second in unstructured environments. These algorithms work in unknown environments and do not require landmark detection. Algorithms are based on 2D laser range scans. The approximate rotation and translation required to align two consecutive laser scans is at first solved by using odometry. In the tangent based method, rotation and translation are solved alternately. In the point based matching algorithm known as Iterative Dual Correspondence, the rotation and translation are similarly solved alternately. The error in rotation is solved by minimizing, in consecutive scans, the distance between points having equal distance to the origin. The linear translation is then solved using the Iterative Closest Point method. The tangent based method can handle large initial rotation and position errors. The point based method is more accurate. Practical tests have been successfully conducted in an office environment.

In [Lu, 1995], it was shown that convergence is faster if the rotation and translation are estimated alternately. ICP works better if the closest points belong to the same target like wall in an indoor environment. Without odometry, ICP may fail. In an outdoor environment, the closest point may belong to an incorrect target.

Groups in Carnegie Mellon University and the University of Bonn [Dellaert et al., 1999] have considerable experience of autonomous museum tour guide robots. They have developed Markov localization algorithms that work well even in museums full of people. When the robot starts, its position is a uniformly distributed random variable in the working environment. After a single range scan, the random probability that represents the robot position concentrates on few places in the environment. This method, unlike methods based on unimodal Gaussian distributions (Kalman filter), is capable of restoring after faulty localization. They also use an entropy filter for rejecting unreliable sensor readings originating from people. The entropy filter measures the uncertainty of position, and uncertainty increases after a faulty sensor reading. A distance filter is used to reject sensor readings originating from people standing in front of known objects in a map. The position and heading of the robot was presented using a 3DOF grid. The size of the position grid was less than 40cm and the angular resolution was less than 5°. The distances to landmarks were pre-computed for every grid cell and stored into a table.

Schultz and Adams [Schultz and Adams, 1998] used occupancy grid based correlation with odometry. The odometry errors were continually corrected by matching a current perception map with a consistent occupancy grid map in an office environment.

Occupancy grids are suitable for indoors where the area is limited. Outdoors, where the operating area has no limits, they are not so effective. Occupancy grids are useful in handling inaccurate sonar measurements.

Moreno et al. [Moreno et al., 1992] used ultra sonic sensors to detect multiple moving people indoors. An existence probability was connected to every potential target moving at least 0,1 m/s. A successful sensor reading increases the associated probability, and missing sensory

information decreases the probability. The trajectory of moving targets was tracked by using Kalman filtering.

Mobile robots move in populated environments, especially indoors. Schulz et al. [Schulz et al., 2001] used particle filters for tracking multiple moving targets around a mobile robot. The practical tests have been performed in a corridor environment with two moving targets (humans). A person was represented by a vector consisting of the x and y position components, as well as heading and velocity components. The detection of a person was based on detecting the legs. The robot position and heading was estimated by using the method by Lu and Milios [Lu and Milios, 1994]. The used joint probabilistic data association filter was found to be better than the Kalman filter in multiple target tracking.

Konolige and Chou [Konolige and Chou, 1999] presented a correlation based method that was two orders of magnitude faster than the original Maximum Likelihood (ML) method. Correlation was computed between occupancy grid maps.

Correlation based methods are interesting because they do not require identified features or odometry. Therefore, they are promising candidate for outdoor navigation in natural environments.

2.2 Outdoor navigation

Forsman [Forsman, 2001] and Guivant et al. [Guivant et al., 2000b], for example, used tree trunks as outdoor landmarks. Walls and vertical cylinder landmarks are complimentary because walls include information on direction and 1DOF distance whereas vertical cylinder objects carry information on 2DOF distance but not direction. In a thin forest or park, two or three tree trunks are enough for pose determination. However, in a thick forest of young conifer trees, for example, it is difficult to recognize tree trunks because of the branches hide them, in which case, the entire tree with branches or even a thick group of young trees can be used as a less accurate landmark.

Rotation and translation exist between two successive range images if the robot is moving. A second range image can be transformed to the coordinates of the first range image by using odometry. There is an error between corresponding points in the two images because of odometry errors. In iterative closest point (ICP) matching, it is assumed that the closest point in image two is also the corresponding point in image one. The distance between corresponding points in image one and two is minimized iteratively. Iteration is terminated when the sum of squared distances between closest points is below a threshold.

Madhavan [Madhavan et al., 1998b] demonstrated that ICP does not work reliably when an LHD vehicle is making fast turns in an underground environment. Immeasurable drift is large in such situations. ICP requires that the robot position can be predicted for example by using conventional wheel based odometry. Prediction errors may exceed the acceptable level when the vehicle is drifting in turns.

Bailey and Nebot [Bailey and Nebot 2001] installed a Sick PLS scanning laser range finder in front of a utility vehicle. They used two feature types, namely points and edges. The point features were further classified by using the circle radius of the point object. These features have then been used for laser dead reckoning. Laser dead reckoning has been found to be far

more accurate than the conventional dead reckoning based on wheel encoders. The data collection was done in a park and a suburban street environment. Because of the large-scale environment, a topological map was generated. In that map, a node defines the sub-map coordinates and a link defines the relation between sub-map coordinates. Sub-map spacing varied between 10 m and 150 m.

Mäkelä [Mäkelä, 2001] presented an industrial application in underground mining. The route from load place to dump place is first recorded while driving manually. After that, the LHD truck is able to haul autonomously the ore from the load place to the dump place and then return to loading. The loading of many trucks is accomplished by a single tele-operator. Route teaching and following is based on odometry and two 2D scanning laser range finders installed in front and back of the truck. Odometry errors are corrected by comparing instant range measurements with the wall profiles obtained in the teaching phase. The stability at high speed (20 m/s) during route following is accomplished by using predictive control.

Madhavan [Madhavan et al., 1998a] describes a similar scientific experiment in an underground mine. A poly-line map of the mine walls was built by using a 2D laser range finder. The position and heading of an LHD truck was predicted by using an adaptive extended Kalman filter. The laser range measurements taken in the predicted position were matched with the poly-line map of the mine walls, and the results were used as Kalman filter measurements. The iterative closest point (ICP) method was used to find the correspondence between the poly-line map and the laser range finder readings.

A good review of practical aspects in navigating off-road environments is presented in [Nebot et al., 2000]. They present a method for recognizing a set of point and line features. The method is based on using distances between point objects, normal distances from point objects to lines, and subtended angle between lines. These distances are used to build graphs to distinguish certain features. The graphs are independent of the robot position, and finding a maximum common sub-graph can be used to define the robot's position and heading.

In [Guivant et al, 2000a] and [Guivant et al., 2000b] a 2D laser range finder LMS200 and dead reckoning were used for a high accuracy navigation with a utility car. The absolute position in terms of Earth fixed coordinates was obtained with 2 cm accuracy from a kinematic GPS. A position accuracy of approximately 0,2 m was obtained by using extended Kalman filtering and artificial reflectors. The Kalman filter state included the vehicle position and heading as well the coordinates of the landmarks. The intensity information of the reflected laser beam was used to detect artificial reflectors. Tree trunk features were also extracted. Because the natural landmarks were too close together, the data association problem became extremely difficult. Tree trunk landmarks were associated correctly by using additional artificial beacons.

Hancock [Hancock, 1999] studied how to find small obstacles on a road from a medium speed car. He used the laser intensity signal to distinguish obstacles from road surface. The fast 3D laser range finder used amplitude modulated continuous wave technology.

The Carnegie Mellon UGV group [Brumitt et al., 2002] demonstrated outdoor navigation by using two highly mobile multi-wheeled vehicles (HMMWV). An amplitude modulated, continuous time of flight laser range finder was used at HMMWV2 to sense the environment from up to 50m. The laser produced two 60x1000 images per second at a vertical angular view of 30° and a horizontal angular view of 360°. HMMWV1 used a three camera stereo

system to sense obstacles at greater distances. The position and heading estimation was based on odometry and a kinematic GPS receiver. A problem in accurate GPS navigation was that it could take 20 s before the receiver could re-acquire the carrier lock after losing it because of satellite occlusions.

Satellite navigation cannot be used on planets other than Earth. The magnetic field is missing on some planets orbiting the sun. In [Balaram, 2000], a navigation system for a Mars rover was developed. It was based on accurate vehicle kinematics, inertial sensors, and extended Kalman filtering. The gyros were calibrated by averaging the gyro measurements when the robot was not moving.

Kalman filtering has been used to increase the accuracy of landmark positions. However, the computation load increases rapidly when the number of landmarks increases. The landmark position accuracy optimization is not so important as the landmark identification. When using modern laser range finders the measurement accuracy of a landmark is usually sufficient for robot navigation.

Most research relevant to this thesis is the correlation method presented by [Schultz et Adams, 1998], even though the results have been obtained by using evidence grids in structured indoor environment. The results obtained in a large scale outdoor environment by [Bailey et Nebot, 2001] are also relevant to this thesis although they used extracted landmarks instead of unstructured raw data as in this thesis. The term “laser odometry”, which they coined, is very descriptive, and is therefore used in this thesis. In conventional odometry, the robot position has been integrated from wheel revolutions and heading gyro values. In laser odometry, the robot position has been integrated from incremental position and heading changes estimated by using laser range finder.

Olson [Olson, 2000] presents a map-matching algorithm where the current map is compared to the global map. The best relative position between the maps according to the similarity measure was found by using divide-and-conquer search of the robot pose space. The localization was done infrequently to correct pose errors obtained by using deduced-reckoning. However, the algorithm does not require an initial estimate for the robot pose. The method is similarly applicable in unstructured outdoor terrain.

The papers presenting map matching by correlation methods [Konolige et Chou, 1999] have been the most influential in this thesis. In addition, the literature dealing with the Hough transform [Pears, 2000] has been crucial. Most of the results were obtained by using common sense when analyzing sensor data from test trials. A strong mathematical background has helped in this work. However, the Expectation Maximization (EM) [Shumway and Stoffer, 1982] algorithm has proved a novel discovery for the writer. The other related literature is studied in more detail after the results have been obtained.

3 PROBLEM OF NAVIGATION IN UNKNOWN OUTDOOR ENVIRONMENTS

3.1 Introduction

Outdoor navigation sets new challenges for a mobile robot when compared to indoor navigation. The challenges are related to different requirements for a robot to perform flexible work tasks. A basic requirement is that the robot knows its own position and heading in a local coordinate system. The localization need exists in indoor navigation but outdoor environment is more difficult.

Let us assume that the robot is brought to an outdoor work area and no map is available. The robot knows its roll and pitch angles relative to the gravity vector. By using a GPS receiver, the robot position can be defined in Earth fixed coordinates assuming that at least three satellites are on sight. At this stage, the robot does not know the working environment. It needs a pair of cameras or a laser range finder in order to map the environment.

Sensors that perceive the working environment are necessary when increasing the autonomy of a mobile robot. A mobile robot must detect obstacles in order to avoid them. The robot must know its own heading and distance to a work object in order to complete a task involving a contact, for example in a grasping task.

Bats use acoustic sonar in darkness for obstacle detection and navigation. Acoustic sonar has been widely used in indoor environments. The maximal range of acoustic sonar is not as great as that of laser range finders. However, acoustic sonar can be used below the laser measurement range, for example in grasping tasks. Acoustical navigation is more sensitive to error because of the large beam width of sonar [Harris and Recce, 1998]. Methods based on random distribution of the robot position are therefore more suitable for indoor acoustical navigation [Thrun et al., 1998b].

People and most animals use stereovision for pose estimation and obstacle detection. Inclination sensors near ears play an important role in animal vision. In spite of expectations, stereovision based on cameras has not become the primary sensor for mobile robots. However, single color cameras have been more commonly used in such cheap mobile robots as soccer robots [Stroupe et al., 2002] or in pet robots, e.g., in the Sony Aibo. Extraction of landmarks based on color is computationally easier than extracting geometrical features in 3D. A limitation is that a single color camera can measure the bearing to landmark but not the distance without movement between frames.

In outdoor environments, cameras and laser range finders can be used to define the position of objects. The accuracy and speed of laser range finders has made it an attractive alternative as laser technology has matured and prices become more reasonable. The laser range finder measures the distance to the obstacle directly. In this study, a horizontal scanning laser range finder has been selected as the primary sensor perceiving the environment.

The navigation problem is considered in with the context of a service robot intended mainly for outdoor use. The robot used in the tests included a color camera. The advantages of a laser range finder over a camera were improved accuracy in range measurements at wide ranges, a large horizontal viewing angle, and an easy output format. Outdoors, the illumination varies strongly and service robots using a laser range finder can operate in darkness. On the other

hand, a color camera is able to give 3D information from the environment and the sensor price is lower.

From camera pictures, the features must first be identified and then corresponding features at two different camera pictures must be compared to obtain the depth information. Feature recognition from a camera picture is not a simple task, particularly in real time, and a frame grabber is usually required [Murrieta-Cid et al., 2002].

The service robot is not useful if it lacks the flexibility to perform different kinds of task. One way to increase flexibility is to create every work task from smaller basic tasks. It is easier to maximize the number of possible combinations of basic tasks than to write a program code for each work task. Moving from point A to point B in local coordinates and bypassing obstacles can be one such basic task. This task requires that the robot knows its position in the coordinates where the points A and B are given. The obstacle avoidance task is active only when the obstacle exists in the way of the robot. Detecting a box in the vicinity of point B can be another basic task. By following an operator, the robot can move from point A to point B without knowing its own position. However, during the operator following task, the robot can use simultaneous localization and mapping (SLAM) techniques [Guivant et al., 2000b]. In simultaneous mapping and localization, the robot builds a map of the environment. The local coordinate system in SLAM can be freely selected. Coordinates fixed on the initial position and heading of the robot is another possibility.

When the robot returns to an area it has visited earlier, it may be useful to know the robot position relative to fixed landmarks such as the exterior corner of a building. In this case, the robot's goal can be given in the coordinates of the map made by using SLAM. The use of landmarks requires that the robot is able to detect and identify landmarks. In general, the detection of a tree is far easier than recognizing it as the same tree as previously seen.

When the service robot returns to a featureless open field it has visited earlier, there are no natural landmarks. The robot can use satellite navigation to find goal positions that have been visited previously. In this case, the robot can use Earth fixed coordinates. A GPS receiver does not give the robot's heading until it moves. An optional 3-D magnetometer could indicate the robot's magnetic heading. Unfortunately, it is sensitive to magnetic fields caused by currents of electric motors.

The localization accuracy of the mobile robot does not have to be as high as that required for a grasping task. A mobile robot's position and heading accuracy is satisfactory if it can find and identify the object to be grasped. Furthermore, the location of the unloading place must be found with the perception sensor. The mission route may be less accurate, and obstacles can be avoided with reactive navigation.

There are several different landmarks that can be used for pose estimate correction. These landmarks may change with time. When the robot is working on a construction site, the environment is continually changing. For example when a new building is constructed, the trees are harvested from the building site. The robot should adapt to the new situation and use the building's walls and corners as landmarks instead of tree trunks. A new building that was initiated in the neighborhood of the test site gave rise to this example.

In an outdoor environment, there hardly exist any maps in contrast to indoor environments where architects' drawings (blueprints) can be used. The simultaneous localization and

mapping problem has been considered difficult in outdoor environments. The challenge is that localization errors distort the map because the landmarks seen by the robot are put in the wrong places on the map.

Simultaneous localization and mapping using easily identifiable artificial landmarks has been found satisfactorily in outdoor environments [Guivant et al., 2000a], where there are feasible landmarks such as trees or cars. The extraction of such landmarks from a perception sensor view is not difficult. However, the real issue is the degree to which landmarks can be uniquely identified [Guivant et al., 2000b]. The most common solution until now has been the use of odometry. Based on wheel encoders and heading gyro, the robot position and heading has been predicted. By using the predicted position of the robot, the closest landmark in the reference map is identified as the same as in the current map. Indoors, the closest landmark, perhaps a wall, is usually correctly identified. Outdoors, the closest landmark, for example a tree trunk, may not be the correct one.

Outdoors, the environment inside the perception sensor maximum range may be devoid of objects or features. In such conditions, a mobile robot must continue to estimate its motion in the working task coordinates. Satellite navigation works well in open fields. Essentially, landmark based navigation and satellite navigation are complementary methods. In feature rich environments near buildings or inside thick forest, satellite navigation does not work because of occlusions. In the same environment, there are enough features for landmark-based navigation.

In outdoor robotics, all these challenges must be met reliably in real time. The fast increase in computing speed has given developers the opportunity to use CPU-intensive algorithms for feature extraction. However, 3D real time environmental mapping is not reality at the moment but will probably appear in the near future [Forsman, 2001].

The mobile robot uses different coordinates depending on the used navigation sensor and the work task. In this thesis a mobile service robot called as WorkPartner is used as the test platform. This centaur like robot is intended mainly for outdoor use. It is presented more detailed in Chapter 4.1. The main perception sensor is a horizontally scanning laser range finder. The laser range and bearing measurements of the WorkPartner robot are defined in laser fixed coordinates shown in Fig. 3.1.

The WorkPartner robot is able to grasp an object by using the two hands fixed on the manipulator body. The grasping task is defined in the coordinates fixed on the manipulator body. The object position and direction is measured in laser fixed coordinates. Because the laser range finder is installed symmetrically in the manipulator body, the transversal and directional coordinates are the same. The distance between longitudinal coordinates is constant. The front body coordinates are fixed symmetrically between the fixing points of the front legs.

The local navigation 2D coordinates are shown in Fig. 3.2. In order to determine the accuracy of different navigation methods, the local coordinates are fixed to static landmarks. However, the robot navigation does not need a map. If required for other purposes, a map can be built as a byproduct during navigation.

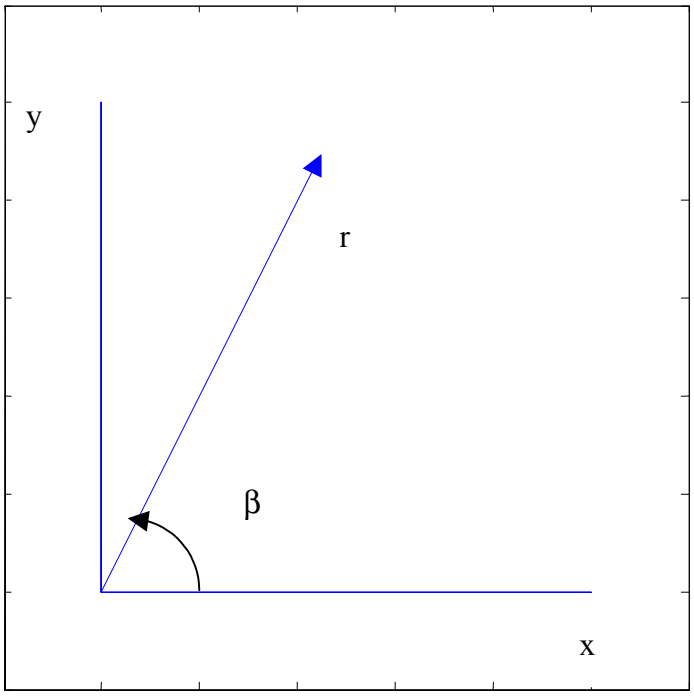

Figure 3.1 Robot laser range finder coordinates.

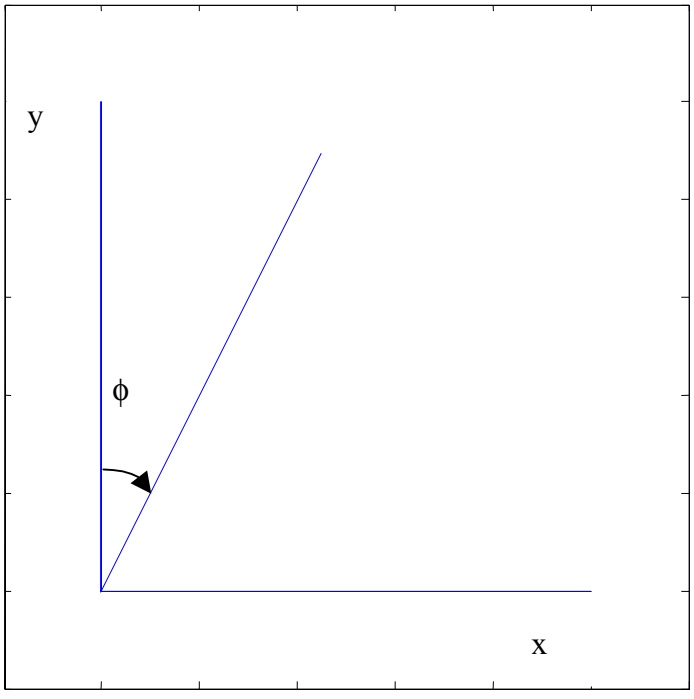

Figure 3.2 Local navigation coordinates.

The coordinates in Fig. 3.2 have been selected compatible to Earth fixed GPS coordinates on the eastern hemisphere. When the y-axis of the local coordinate system points to north, then the x-axis points to east, and the heading angle of the robot is equal to compass angle.

The robot coordinates are computed using the metric system. However, the GPS position coordinates are given in degrees and angular minutes. One angular minute in latitude direction is approximately 1852 m. In the longitude direction, one angular minute is equal to

$$1852\,m * \cos(latitude)$$

The latitude of the campus of Helsinki University of Technology is 60° and 11 minutes north and therefore one angular minute in longitude is equal to approximately 921 m.

Figure 3.3 shows the basic structure of WorkPartner. The joint angle between the front and rear body segment is controlled by a cross axle construction.

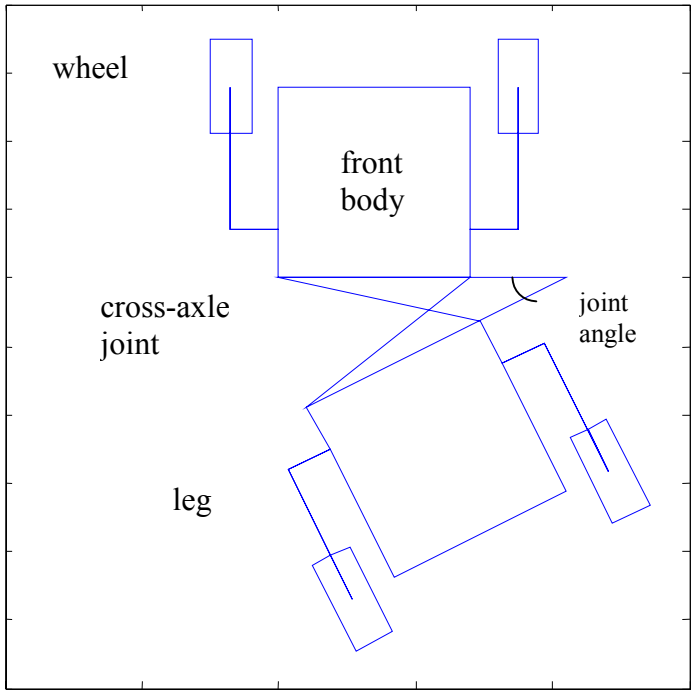

Figure 3.3 The main components of the WorkPartner platform.

3.2 Test arrangements

The navigation system is developed and verified on test trials conducted around the Computer Science Building of Helsinki University of Technology. The environment, consisting of a parking lot and surrounding trees, is shown in a camera picture in Fig. 3.4. The wall and the lift door of the process hall seen in the right part of Fig. 3.4 corresponds to the line and gap down in Fig. 3.6. The initial view of the robot during test trials can be seen in Fig. 3.5.

Under test trials, sensor readings were collected in two files. One file includes measured range values of the scanning laser. The second file includes GPS measurements as well as inclinometer and heading gyro values. The trials are identified by consecutive numbers. The street surrounding the faculty building is covered by asphalt but elsewhere the ground is covered by sand. The environment consists of trees, cars, and walls.

During the test trials, WorkPartner followed a predetermined route in local coordinates. The route consisted of waypoints, and the robot always moved to a target waypoint. The target waypoint was changed to the next waypoint when the robot's distance to the present waypoint was less than 1 m. Reactive control was used when the robot detected an obstacle on the route. An obstacle such as a car was bypassed when it was possible. Otherwise, a stop command was ordered to the robot. Obstacle detection was based on a scanning laser range finder.

Figure 3.4 The test site in the parking lot of the Computer Science Building.

The environment was modeled using a 3D laser range finder (Riegl LMS-Z210) in [Forsman, 2001]. In the following, this laser range finder is referred to as a mapping laser because it produces a consistent range scan from an area with 350 m radius. The modeled objects were the border lines of the walls of the building and some vertical cylinders (trees and a lamppost). One horizontal sub-scan was used as the reference map in test trials. The used laser range scan was taken at a place designated E. The position E is in front of the 3,8 m wide door opening, and 9 m from the process hall wall (Fig. 3.6). The letter E is used in the following

text when the map or objects in it are cited. A consistent map can be made based on a single range scan of this laser because its horizontal viewing angle is equal to 330°, and the maximum range is approximately 350 m. The standard deviation of the range measurement is approximately 25 mm. The 3D laser is clearly an off-line sensor because one horizontal scan takes typically 66 s.

Figure 3.5 Initial view of the robot during typical test trial.

The most obvious landmarks for definition of the initial position of the robot are the tree trunks seen in Fig. 3.5, where tree trunks are numbered, from left to right, 6, 5, 1, and 3. Numbering is the same in Table 3.1.

Tree trunk landmarks are not necessary for navigation. Landmarks are used to analyze the accuracy of the developed navigation method. Sometimes, landmarks can also be used to correct errors in position and heading estimates.

The map in Fig. 3.6 was used as the reference map in test trials. The origin of the map is the place where the mapping laser locates (point E). The position of cylinder objects was computed in [Forsman, 2001]. The coordinates of the centers of the cylinders at height 1 m above ground are shown in Table 3.1.

Table 3.1 The coordinates of the centers of cylinder object landmarks in map E.

Object no.	1	2	3	4	5	6	7	8
x (m)	2,16	-5,44	3,50	-5,11	2,02	2,04	-5,91	2,50
y (m)	2,73	1,81	3,90	2,26	4,90	7,22	2,16	1,29

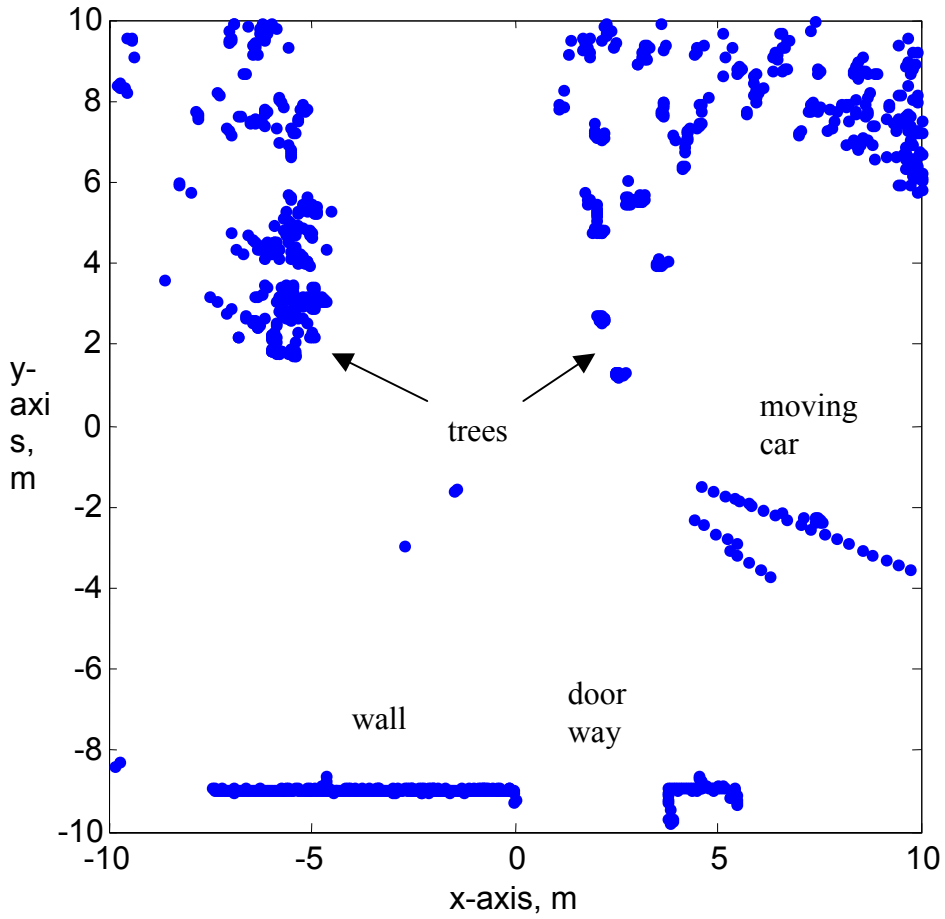

Figure 3.6 Map E computed from Riegl laser range finder values. The origin of the laser sensor is at (0,0) and the midline of the viewing angle points along the x-axis.

The error in coordinates of the cylinder objects is based on the circle fitting and laser range measurement errors. The error in the estimated cylinder radius by curve fitting was less than 3 cm. One cause of the error is that natural cylinder objects are slightly tilted. The robot laser range finder measures the distance from a height different to 1m because the robot is rolling and tilting. Therefore, rough estimate for the position error is more than 1 cm but less than 10 cm.

The two orthogonal walls of the building have the same direction as the coordinate axes. This makes it possible to compute one robot position coordinate when the laser range finder is able to measure the distance to one wall and the wall coordinate in the map is known.

There were 55 test trials with the WorkPartner robot between April 21, 2001 and July 11, 2002. The test route of the robot started typically near the NE corner of the Computer Science Building. The robot route was then directed to the parking area on the north side of the building. In some trials, the robot returned to its initial position. At initial pose, the robot was able to see trees. After turning 90° clockwise, it was able to see trees and parked cars. After turning a further 90° clockwise, it was able to see the wall of the building on the right side and parked cars on left side. After turning 90° anticlockwise, the robot was able to see parked cars on both sides. The map of the test area is shown in chapter 5 where the results are presented.

The laser range finder data was first logged at test trial no. 14. Table 3.2 shows the length of the different test trials. There are 361 range values in every sample row of MAP.TXT.

Table 3.2 List of recorded test trials with WorkPartner.

Trial nr	Trial date	Samples in LOG	Variables in sample of LOG	Samples in MAP
14	25.4.2001	616	12	624
16	9.5.2001	801	12	802
18	21.5.2001	801	12	803
19	21.5.2001	838	12	847
20	22.5.2001	431	12	435
21	22.5.2001	308	12	315
23	23.5.2001	716	13	718
24	15.6.2001	719	13	719
25	25.10.2001	433	15	442
26	25.10.2001	482	15	487
27	26.10.2001	433	15	437
28	1.11.2001	49	15	53
29	2.11.2001	177	15	181
30	2.11.2001	78	15	39
31	2.11.2001	78	15	43
32	3.11.2001	177	15	68
33	3.11.2001	177	15	68
34	4.11.2001	630	15	213
35	5.11.2001	630	15	213
36	5.11.2001	630	15	217
37	12.11.2001	512	15	476
38	12.11.2001	452	15	454
39	19.11.2001	196	15	201
40	11.2.2002	83	16	83
44	16.5.2002	403	15	404
52	11.6.2002	770	15	776

The variables in one row of LOG.TXT include sensor values such as GPS heading, GPS velocity, GPS position, horizontal dilution of precision, number of satellites used, gyro heading, and inclinometer values. There is also the estimated position and heading of the robot. In some trials, additional variables such as number of common points in matching, and number of lines have been included.

In the next chapter, the WorkPartner robot as well as the navigation sensors are presented in more detail. The collected navigation data is used to develop a flexible navigation system that can operate without a map. Furthermore, a predefined type of landmark is not required in navigation. However, the use of landmarks in pose initialization and pose error correction will be presented.

4 NAVIGATION SYSTEM OF THE WORKPARTNER ROBOT

4.1 WorkPartner

A robot with four legs and two hands has been built at the Automation Technology Laboratory of Helsinki University of Technology [Halme et al., 2001a]. The robot is designed to operate as a work partner for simple autonomous tasks. It is intended mainly for urban area outdoor use. Instead of having a foot, each leg has a wheel (Fig. 4.1). This construction allows the robot to move in three different ways. On level ground, the legs are locked in a fixed position so that the left and the right wheels are on the same virtual axle in both the front and rear. The robot moves by using active wheels. Turning motion is achieved by using the articulation joint of the body. On uneven terrain, the robot can walk by using the legs and it can step over obstacles. When the ground is uneven but contains no high obstacles, the robot can use the third way of moving, known as 'rolking', in which the robot slides its legs along the ground [Halme et al., 2001b].

Figure 4.1 The WorkPartner robot.

The micro-controller boards control articulation angle, leg joints, and wheel motors. The higher level commands to the actuators are computed at the main computer running the QNX operating system. The PC104 size main computer sends commands through the CAN bus to micro controllers. The CAN bus is also used to collect measurements from joint angle sensors (Fig 4.2).

The kinematic state of WorkPartner is formed by the various angular velocities between the leg joints and the angular velocities of the wheels. The articulation angle is part of the kinematic state.

The six degrees of freedom of the body are divided into linear and angular degrees. Surge, sway, and heave are the linear degrees of freedom. Respective angular degrees of freedom are roll, pitch, and heading. The angular degrees of freedom are defined around the axes of linear degrees of freedom.

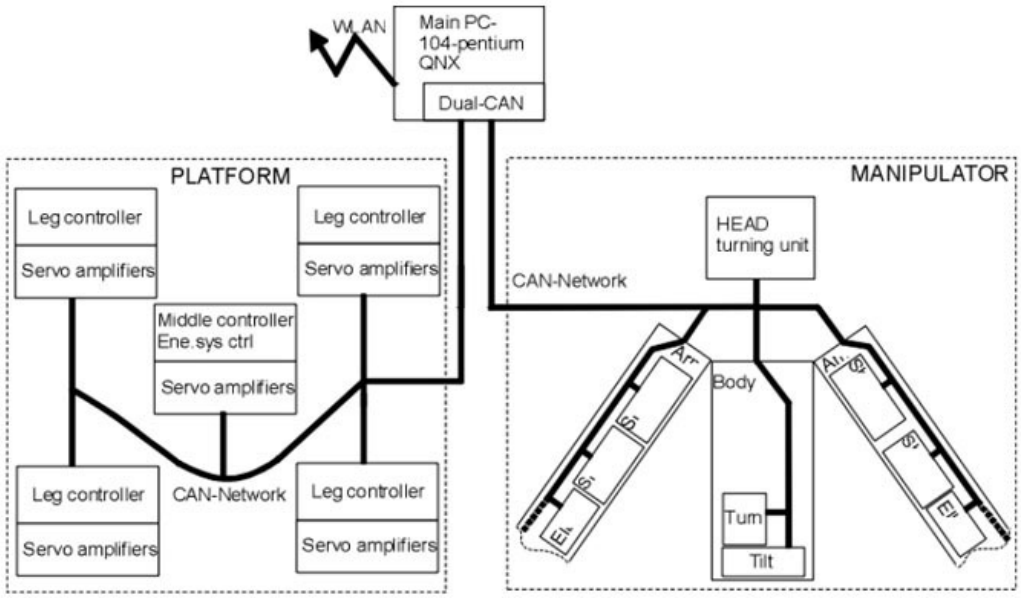

Figure 4.2 The CAN based distributed control system of WorkPartner.

The manipulator consists of a body with 2 degrees of freedom and two arms with 3 degrees of freedom. The camera head includes two additional degrees of freedom. Each joint is controlled by a single board micro controller. A 2D scanning laser range finder of type LMS-291 (by Sick Optic Electronic) was immersed in the front side of the manipulator body, as seen in Fig. 4.1. This laser range scanner model is a long range version and it is not sensitive to fog. In the following, it will be referred to as the robot laser.

Figure 4.3 defines the direction of robot inclination angles. Surge direction in robot fixed coordinates points to the heading direction in local coordinates.

The middle joint is based on cross-axle construction, and is shown in Fig. 4.4.

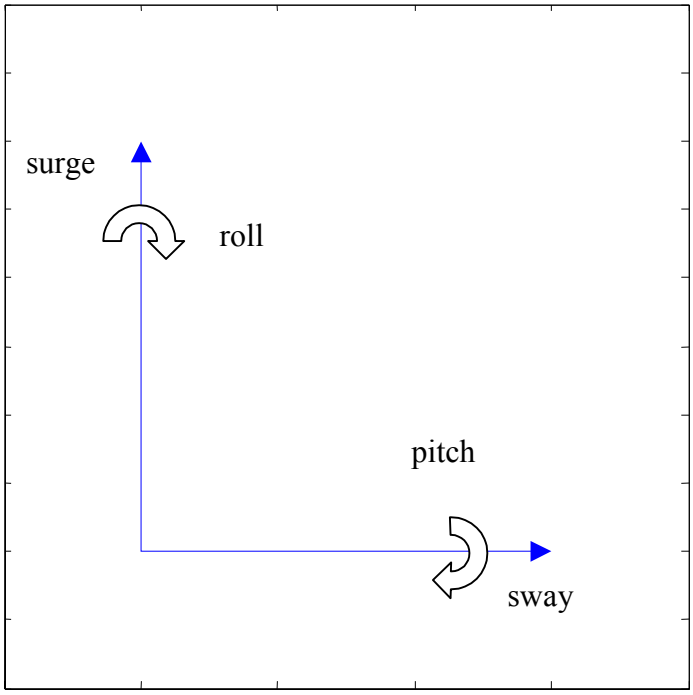

Figure 4.3 The four degrees of freedom of the front body segment of WorkPartner.

The computer system of the WorkPartner is designed to be modular. Each computer can operate independently from each other. The navigation system is easily transformed to another vehicle. The robot can be teleoperated without using a navigation system. The main computer and a navigation computer are installed on the front body segment of the robot. The navigation computer is a PC104 size dual card system with a 400 MHz AMD K6 processor and onboard Ethernet. The navigation computer runs on a real time QNX operating system.

The communication between the main computer and navigation computer is achieved by using QNX messages through twisted pair Ethernet cable. The navigation system hardware consists of the navigation computer, a 12 bit A/D-converter card, and several sensors. The sensors connected to AD-converter are read at 200 ms intervals.

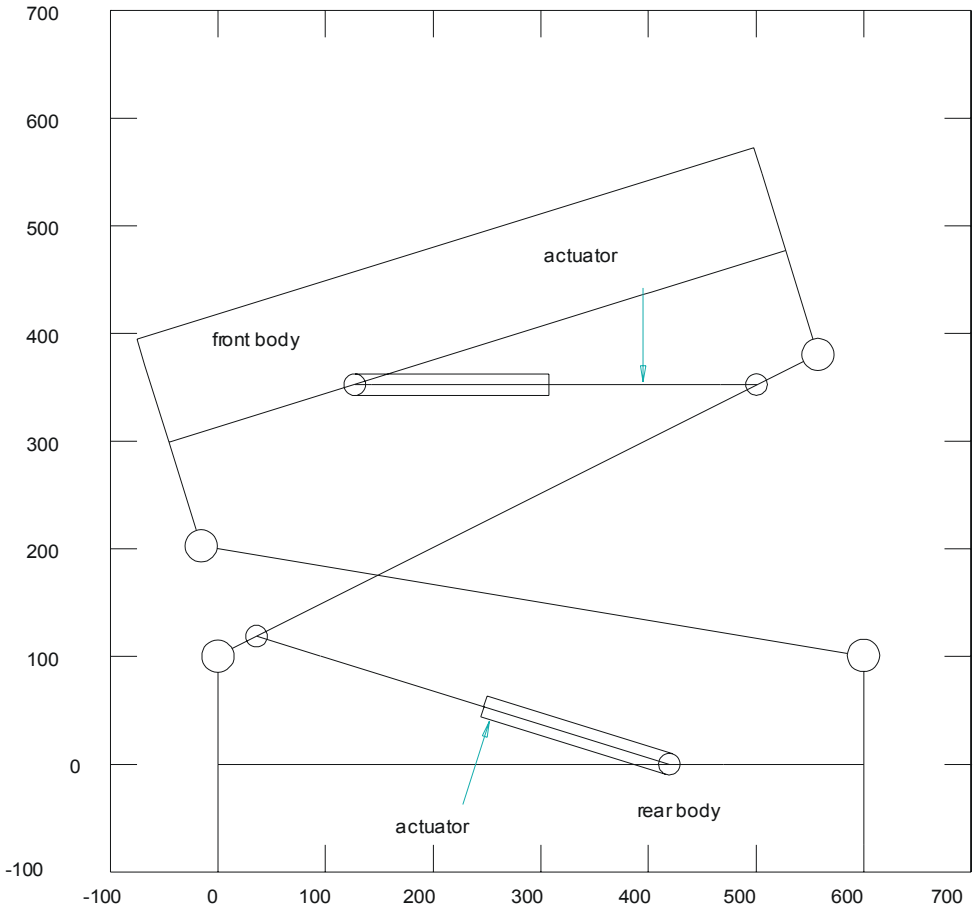

Figure 4.4 Schematic of the middle joint between the robot's front and rear body. The articulation angle is equal to –23 degrees in this case. Measurements are in mm.

4.2 Odometry of WorkPartner

The robot should be able to navigate also when external sensor readings are not available. Wheel angular velocities together with articulation angle measurement are commonly used for work machine navigation [Madhavan et al., 1998a] and [Mäkelä, 2001]. In an ordinary work machine with fixed front and rear axle, the turning radius can be considered almost the same for wheels on the same axle [Corke and Ridley, 2001]. This is not the case with WorkPartner, where every leg can move independently.

The WorkPartner robot has three different moving modes. Let us first consider wheeled locomotion. When the wheels are independently located on the ground, they have a different turning radius, and four drive mode could cause excessive slip of wheels. To avoid problems arising from too many degrees of freedom, the control model of the robot is based on its front body with two driving wheels and the rear body with two passive wheels. The turning radius can be computed approximately by fusing the front wheels as one virtual wheel located between the real ones. The same is done for the rear wheels. Then, we have a model (1)-(4) with a flexible joint between the front and rear virtual wheels.

$$\dot{x}(t) = v(t) * \sin(\phi(t)) \quad (1)$$

$$\dot{y}(t) = v(t) * \cos(\phi(t)) \quad (2)$$

$$\dot{\phi}(t) = \frac{-v(t) * \sin(\gamma(t)) + \dot{\gamma}(t) * L_B}{L_F * \cos(\gamma(t)) + L_B} \quad (3)$$

$$v(t) = R_W * (\omega_R(t) + \omega_L(t)) / 2 \quad (4)$$

where x, y, and ϕ are robot position and heading in local coordinates. The angle between the front and rear body segments is γ. L_F is the distance between the virtual articulation joint and the midpoint of the front wheels. L_B is the same for the rear wheels. Velocity v is computed from the angular velocities of the front body right and left wheels ω_R and ω_L, respectively. R_W is the effective wheel radius.

The articulation angle γ is positive when the forward going robot turns to the right. The midline distance of the front and rear bodies varies slightly according to the articulation angle. The midline distance between the body and the virtual articulation joint is 32 mm longer with the articulation angle equal to 25° compared to a straight position.

Eq. (1)-(4) are valid for wheeled locomotion. WorkPartner is also able to move by deploying "rolking" mode [Halme et al., 2001b]. In rolking mode, the wheels of three legs are locked and only the leg joints are active. The fourth leg uses leg joints and an active wheel simultaneously. In rollking mode, each leg moves in the longitudinal direction of its own body segment. The velocity vector of each leg attachment point to body segment relative to the ground can be computed based on leg joint movements and wheel rotation. The velocity vector of one body segment can be computed by taking the mean of the left and right legs to body attachment point velocities because the movement direction of the legs are inline with the body surge direction. Equations (1)-(4) can also be used for rollking odometry. The front body segment velocity is used as the robot velocity. The distances L_B and L_F are leg joint angle dependent variables in rollking motion.

The wheel revolutions are measured by Hall sensors that give 6 pulses/rev. Because of the gear (84,154), the total number of pulses/rev is approximately 505.

Wheel based odometry was not implemented in WorkPartner during the writing of this thesis. However, the implementation will be carried out in the near future. It could serve as a temporary backup system when other navigation sensors fail.

4.3 Navigation sensors

A manipulator body with two hands is fixed in the front body of WorkPartner. The scanning laser range finder is installed inside the manipulator body approximately 1 m above ground. It is able to measure distances to objects in front (180 degrees) of the manipulator. The inclination of the sensing plane is defined by the manipulator pitch and heading angles. Two inclinometers and one gyro are installed inside the same box as the navigation computer. This navigation box is fixed in the front body of the robot. A GPS antenna is installed on the top of the robot cover.

The main use of the color camera at the manipulator head was in measuring the bearing of colored objects. Thus, target recognition becomes easier during the operator following task.

The robot laser viewing angle can be controlled independently from the robot heading because the manipulator is able to turn. The ordinary viewing angle of the robot laser can thus be extended to 360° when the robot is not moving, which may be useful when searching for landmarks around the robot in feature poor environments.

Sensors that are either used or tested in WorkPartner are shown in Table 4.1.

Table 4.1 Sensors tested in the WorkPartner robot.

Sensor	Type	Position	Status
Sick LMS 291	2D laser range finder	Manipulator	In use
Murata ENV-05D	Piezoelectric gyro	Front body segment	In use
Ashtech 12-channel	GPS receiver	Front body segment	In use
Maxon HEDS 5540	Hall sensor	Wheels	In use
WPI LSRP-30	Inclinometer	Front body segment	Future use
Hitachi VK-C77E	Color camera	Manipulator head	Future use
Accurange 4000	1D laser range finder	Manipulator head	Future use
Schaewitz Accustar II	2D inclinometer		Not in use
TCM-2	3D magnetometer		Not in use

4.3.1 Inclination sensors

Pitch and roll angles of WorkPartner are important in controlling the inclination of the body segments in order to avoid falling down. They are also useful for discarding ground reflections of the horizontal scanning laser range finder. In 3D navigation, the knowledge of pitch and roll is necessary.

The pitch and roll angles of the front body are measured by using gravity based LSRP-30 inclinometers with WPI instruments. The maximal inclination is 30° corresponding to 5000 mV output. These inclinometers measure the Earth's gravity components in the surge (Fig. 4.5) and sway direction of the front body.
The maximum measurable gravity component is equal to 0.5 g, which corresponds to 30 degrees static inclination. The measured value in the surge direction consists of linear acceleration and a gravity component as follows

$$a_y = \ddot{y}_R + g * \sin(\alpha_P) \tag{5}$$

The same equation in the sway direction is

$$a_x = \ddot{x}_R + g * \sin(\alpha_R) \tag{6}$$

where y_R and x_R are robot surge and sway position in robot fixed coordinates, a_y and a_x are measured accelerations in robot fixed coordinates. The robot front body segment roll and pitch angles are marked by α_R and α_P respectively; g is the gravity constant.

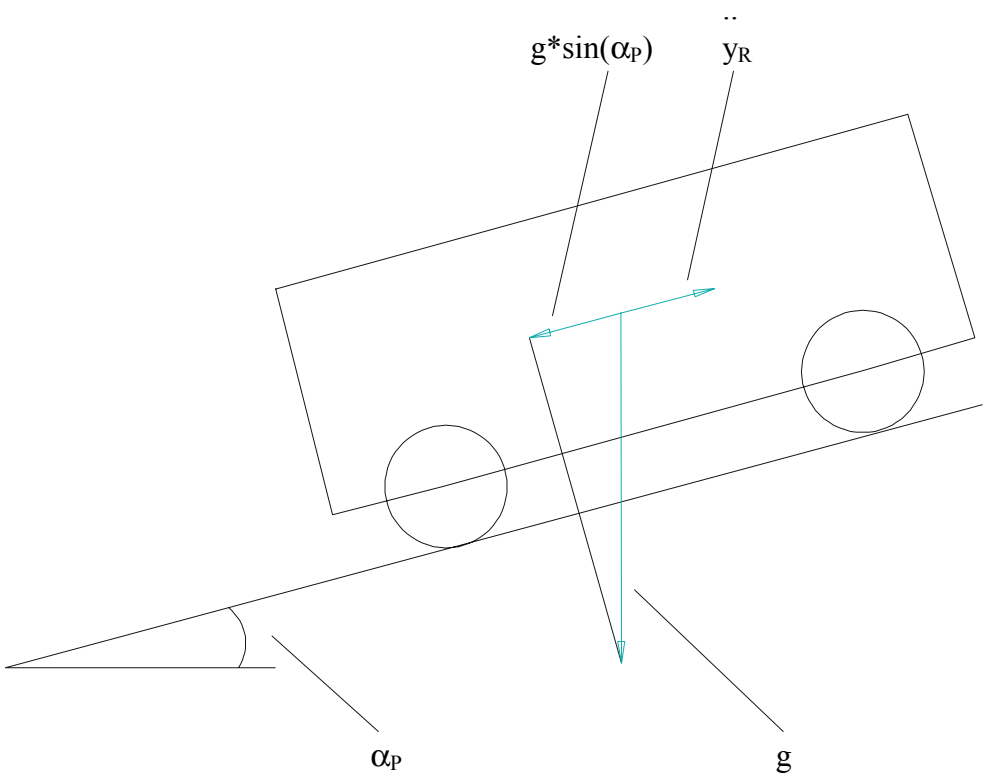

Figure 4.5 Gravity component in surge direction when the vehicle has a nonzero pitch angle α_P.

There is no straightforward way to distinguish between inclination and linear acceleration. Additional information must be obtained [Kim et al., 2001] in order to separate these acceleration components. When the acceleration is estimated based on odometry, and the inclination angle is estimated based on angular gyros, the robot linear acceleration and the gravity component acceleration can be separated by using the Kalman filter. Equations (5)-(6) can be used as measurement equations in the state correction phase. The state prediction can be computed from wheel odometry and gyro angular velocities.

The output offset of these inclinometers is less than 0,03 degrees, and a 10 degree change in sensor temperature produces an error of less than 0,03 degrees in output offset and a gain dependent error less than 0,018 degrees. The –3 dB damping of the sensor output occurs at a frequency equal to 20 Hz.

An affordable solution would be to use a dual axis sensor based on detecting the position of a bubble inside a liquid filled cone. An example is the Schaewitz Accustar II; its higher frequency limit is 0,5 Hz (-3dB), which limits its use to calibration of fast drifting angular gyros. The null output and scale factor accuracy is approximately 10%, which requires decent initial calibration. After calibration, the null point repeatability is equal to 0,1° and the error coming from non-linearity is less than 0,6° with inclinations less than 20°. A temperature change equal to 10°C increases the error by 0,1°.

The inclinometers are installed on the WorkPartner robot but they were not actively used in this thesis. However, inclinometer values of the front body segment are collected to LOG.TXT in every trial. Inclinometers will be used in the near future.

4.3.2 GPS receiver

The robot is equipped with a 12-channel GPS OEM receiver (by Ashtech) that estimates the 2D global position in WGS-84 coordinates when at least three satellites are on sight. The receiver computes velocity and heading by using instantaneous Doppler values from at least four satellites. The GPS receiver (manufactured in 1992) and the laser range finder communicate with the computer through a RS 232 serial line. The receiver sends one NMEA GPGGA and one NMEA GPVTG message at 1 s intervals. In the following text, shorter message names GGA and VTG are used respectively. The GGA message includes time, latitude, longitude, number of satellites used, horizontal dilution of precision, and altitude. The VTG message includes only direction of movement and velocity.

The Global Positioning System (GPS) is based on 24 satellites that are orbiting the Earth at a height of over 20.000 km. It is over three times the Earth's radius. The wavelength of the public 1575,42 MHz L1 carrier is equal to 0,19 m. The carrier wavelength gives the lower limit of the obtainable accuracy. The carrier is modulated by a 1023 bits long C/A code with a frequency equal to 1023 kHz. The GPS receiver computes its position by using distances from at least three satellites on known orbits. Ordinary receivers use the C/A code, and can obtain a position error typically less than 16 m. The more expensive real time kinematic (RTK) receivers use a static reference station locking to the carrier, and are able to compute the position with 0,02 meters accuracy.

The position accuracy of GPS navigation depends on the satellite geometry. The receiver computes a value called Horizontal Dilution of Precision (HDOP). The degraded position error is obtained by multiplying the position error in ideal conditions (HDOP=1) by the current value of HDOP.

4.3.3 Heading gyro

A Murata ENV-05D piezoelectric angular gyro was installed as a heading gyro on the WorkPartner robot. At zero angular velocity, the output of the gyro is approximately 2,5 V. At an angular velocity equal to 1°/s the output changes approximately 22 mV according to the technical data. In practice, the zero value and the gain value are slowly varying unknown variables. The heading angle can be integrated from the angular velocity. Without repeating calibration, the heading error grows beyond acceptable limits. The zero value can be determined whenever the gyro stands still. Assuming that the zero angular voltage is sufficiently accurately estimated, the gain can be calibrated by comparing the integrated angular velocity during a mission to the change of robot heading between the end and beginning of the mission. Once calibrated, the gain is relatively constant and daily recalibration is not required. However, outdoors large temperature changes may require recalibration. The zero output voltage drifts both randomly and according to temperature requiring recalibration typically at least at 10 minutes intervals. The –3 dB damping of the gyroscope output occurs at a frequency equal to 7 Hz. It is important to bear in mind that the

speed of the gyro is not sufficient for the fastest heading changes of the robot. Therefore, a faster heading gyro will be installed on the WorkPartner in the future.

The output corresponding to zero angular velocity is between 2300 mV and 2700 mV (-30°C<T<80°C), according to the manufacturer's technical data. The scale factor is between 20,4mV/(°/s) and 24,0mV/(°/s) from the same source. In ordinary temperatures between 0°C and 25°C, the zero angular velocity voltage is typically between 2465 mV and 2535 mV. The maximal error of the zero angular speed voltage equal to 200 mV given in the technical description corresponds to a drift equal to 9°/s. The drift in ordinary temperatures is less than 1,6°/s because the error in zero angular voltage is less than 35 mV. After real time calibration, the error of zero angular voltage typically remains below 0,2 bits or 0,49 mV (Table 4.2). The corresponding drift is less than 0,022°/s or 1,3°/min assuming that the scale factor is equal to 22,2mV/(°/s).

The model of the gyro measurement is as follows

$$u_g(t_k) = u_0 + g_g * \dot{\phi}(t_k) \tag{7}$$

where u_0 is the voltage of zero angular velocity and g_g is the gyro gain.

Let us consider how the heading value obtained from the GPS receiver is used for calibration. Before the robot starts moving from its initial position, the zero value u_0 is computed as the mean of all gyro measurement values associated with robot steady state. The robot heading was concluded to be constant if the gyro voltage fulfills the following conditions

$$\begin{aligned} &\left|u_g(t_k) - u_g(t_{k-1})\right| < 5mV \\ &2465mV < u_g(t_k) < 2535mV \end{aligned} \tag{8}$$

The values in Eq. (8) are specific to the piezoelectric gyro ENV-05D, and typical daytime temperatures at spring, summer, and autumn in southern Finland.

Table 4.2 Gyro voltage corresponding to zero angular velocity during trial no. 52. The time column shows the time periods when the robot is not moving. The gyro voltage estimates are computed as sample averages.

Time (s)	Voltage (mV)	Voltage in bits	Std in bits	Sample size
1-34	2513,67	1029,6	0,82	34
199-212	2514,65	1030,0	0,78	14
382-401	2514,16	1029,8	0,44	20
408-453	2513,18	1029,4	0,69	46
total	2513,67	1029,6	0,79	114

The zero angular voltage estimates shown in table 4.1 have random variation because of small sample size. Error in zero angular velocity voltage equal to 0,5 mV (=0,2 bit) causes a drift equal to 1,4°/min.

Fiber optic gyros are more expensive but they do not need calibration, and the drift is smaller. These laser light based gyros are used commonly as heading gyros, for example in Japanese

cars. The magnitude of drift is less than 10°/h or 0,17°/min. The Earth's rotation rate (0,25°/min) should be taken into account when using accurate gyros such as optic gyros. With piezoelectric gyros, the Earth's rotation rate is taken into account implicitly during the calibration.

The heading angle integrated from angular gyro can be used as a redundant measurement when absolute heading sensors such as GPS (NMEA GPVTG) or magnetic compass cannot be used. Even the most expensive angular gyros are drifting and calibration is required periodically.

In trial 16, the heading was changed between the start point and end point by 14,7° when integrating the angular velocity of the piezoelectric gyro. The actual heading change was equal to –4,4° based on matching the start point and end point laser range maps. Therefore, the drift was equal to 2,6°/min during the 448 s long mission. The used zero angular voltage was equal to 2488,0 mV (1019,1 bits), and gyro gain equal to 22,2 mV/(°/s). Some part of the drift may have been caused by dynamical slowness of the gyro.

Figure 4.6 shows how the averaged gyro measurement (in bits) behaves indoors after a cold start.

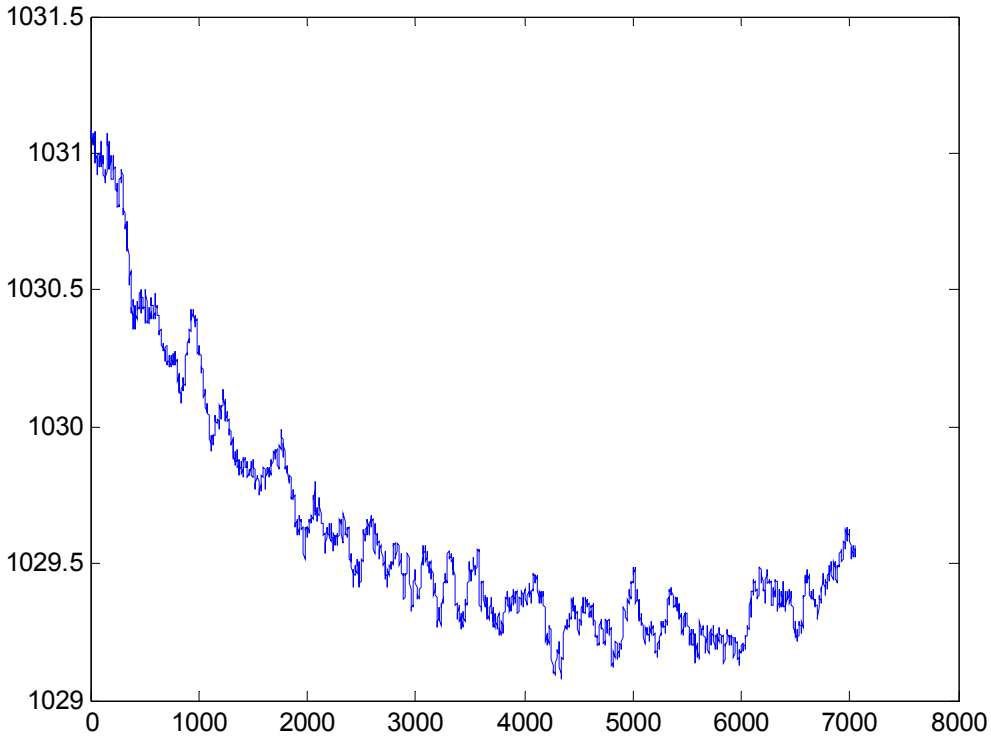

Figure 4.6 Moving average of gyro voltage in bits during static test after cold start. Moving average was taken from 101 successive values. The horizontal axis shows time in seconds.

Warming of the gyro after a cold start causes approximately a 1 h long transient. The trend upwards at t=6000 s in Fig. 4.6 is caused by lifting of the large door in the process hall making the air temperature decrease. The upward trend speed is approximately 0,1 mV/min corresponding to an accelerating heading error equal to 0,27°/(min)^2. In order to maintain the

gyro drift below 2°/min, the zero angular velocity voltage should be calibrated at least every 7 minutes. Generally speaking, it is a big problem that the position error originating from heading gyro is relative to third power of time [Nebot and Durrant-Whyte, 1999].

In [Kong et al., 1998], the temperature transient of the piezoelectric gyro in Watson Inertial Unit lasted approximately 2 hours. The temperature rose from 15 °C to 25 °C over the same time. The maximal drift after stabilization was approximately 0,15°/min in three-minute trials.

Faster piezo-electric gyros (Murata ENC-05E) exist with bandwidths of up to 50 Hz. After 20 minutes warming and estimating the zero level from 6 minute averages, the drift varied between 0,06°/min and 1,1°/min [Lillqvist and Åkerlund, 1993].

4.3.4 3-axial magnetometer

Accurate heading information is important in robot navigation because a small error in heading accumulates to a large position error. The heading estimate can be integrated from an angular gyro when the initial value of the heading is known. The heading initial value can be computed based on landmarks such as walls or trees in a well-known environment. A magnetic compass can be used as an alternative source of heading information when the positions of landmarks are not known.

The direction of The Earth's magnetic field deviates from the direction of rotation axis approximately 11°. At the campus area of Helsinki University of Technology (60.11 N, 24.49 E) the magnetic deviation was 6° 29 min (15.8.2001) based on IGRF 1995 model. The position of the magnetic North Pole was 79,0 N and 105,1 W in 1996. The magnetic North Pole has traveled to north after that. It is also possible to compute the magnetic deviation by comparing the compass heading to GPS heading when the robot is moving.

The ordinary magnetic compass based on floating needle is sensitive to ferrous material in the environment and to inclination. The compass technology stepped forward in 1980 when the magneto-resistive compass and in 1990 when magneto-inductive compass came to the markets. Both sensors are measuring the three orthogonal components of Earth's magnetic field. TCM-2 (by Precision navigation Inc.) is an example of a magneto-inductive magnetometer. An additional 2D inclination sensor is required in the calculations and it is included in the products. The natural frequency of an inclination sensor used in the model TCM-2 is equal to 20 Hz. However, the usable bandwidth is below that. A 3D magnetometer is able to distinguish between the Earth's magnetic field and the magnetic field errors bounded to chassis direction. The effects of ferrous chassis are calibrated by slowly alternating the yaw, pitch, and roll. The magnetometer works well on the back seat of a family car. The TCM-2 magnetometer was tested in various locations in a centaur robot but strong disturbances ruined the calibration. The most probable source of disturbances is the currents of the actuator motors.

4.3.5 Laser range finders

Laser range sensors based on triangulation are mainly restricted to indoor use because of short maximum range [Pears, 2000] and [Nilsson, 1997]. There exist two wide range measuring principles, namely time of flight (TOF) of a laser pulse and phase-shift of a continuous

modulated laser wave [Hancock, 1999]. Range is measured outdoors mainly based on time-of-flight (TOF). Sensors based on pulsed TOF are commonly in use. The continuous wave laser range finders are faster than the pulsed time-of-flight. The amplitude modulated continuous wave laser by Zoller & Fröhlich is able to operate at pixel rates up to 500.000/s, and the Riegl pulsed laser range finder is able to output at pixel rates of approximately 10.000/s.

The robot laser is based on time of flight measurement, and the shortest range is equal to 1 m according to technical data. In practice it can measure ranges down to 0,5 m. The longest range is 80 m when the object has 70% reflectivity according to technical data. In practice, ranges over 100 m have been obtained with highly reflective objects. According to the technical description, the range measuring error standard deviation is equal to 1 cm. The systematic error is less than 6 cm at shorter distances (1-4 m), and less than 3,5 cm at longer distances (4-20 m). The angular measuring range is equal to 180°, and the angular resolution is equal to 0,5°. Therefore, up to 361 range measurements were obtained over 26 ms. The laser beam initial spot diameter is equal to 2 cm, and the beam divergence is equal to 0,7°.

The robot laser was tested in a 3,79 m wide door opening, and the sum of the distance to the right and left door jamb was equal to 3,81 m. The error is inside the measuring error standard deviation. The result is better than the absolute accuracy (6 cm) given in technical data.

A cardboard box was placed at a distance of 75 cm from the manipulator body. The Hough transform algorithm was used to detect the front side of the 33 cm wide cardboard box. The algorithm found a line at 70 cm distance from the laser origin, and the length of the line was equal to 31 cm. The standard deviation of the reflection points around the line was 1 cm as stated in the technical description. There are two possible causes for the error in the line width. The technical description states that the systematic error in range measurement can be up to 6 cm. The true distance equal to 74 cm instead of 70 cm could explain the error in the box width. The angular resolution of the laser scanner is 0,5° which can cause an error equal to 0,6 cm in the box width. This experiment shows that the robot laser can be used to measure the distance and direction of a box for grasping tasks.

A metallic rack consisting of 10 metal bars in two rows was used as another test object. The diameter of bars is equal to 1,3 cm, the distance between bars is equal to 12,3 cm, and the distance between two rows is 8,8 cm. When the laser range finder is at 0,90 m distance to the first row of bars, two to three reflections are received from each bar. At that range, the distance between laser beams is equal to 0,8 cm, and the spot size is approximately 3 cm. From the distance equal to 2,55 m, only one reflection from each bar is detected. At that range, the laser beam spot size is approximately 5 cm and the LMS-291 detects erroneously reflected beams from the front and rear bar rows. This experiment shows that the robot laser can additionally detect thin sticks such as willow branches in the environment. Actually, the robot laser is able to measure range to a 4 mm wire fence with 100 mm gaps. This was verified from a distance equal to 6 m.

4.4 Initialization of the robot position and heading

In the initial state, the robot does not know its position and heading. If the environment is new for the robot, it can fix the local coordinates to the initial position and heading (Fig. 3.2). Navigation during a working task can be performed in such local coordinates. When

available, a magnetic compass may give an initial value for the heading, and a kinematical GPS receiver may give the value of the initial position.

When the view of the robot laser range finder includes a wall in initial position it can be used to define partially the local coordinate frame. The line extracted from the wall can be used as the x-axis, and the direction of the line normal as the heading pointing to the y-direction. It is useful to fix the coordinate frame to a wall line because measured distance to a wall gives the value of robot y-coordinate and the measured bearing gives the heading value.

In some circumstances, the initial robot view may include two orthogonal wall lines. It is especially useful to use for example the longer line as the x-axis and the shorter line as the y-axis. When distance and bearing to either of these walls is measured, then the heading and one position coordinate of the robot can be updated.

When the robot first comes to an area it has not visited before, it can write to a file the position or direction of extracted landmarks in local coordinates. A vertical cylinder landmark such as a tree trunk or barrel carries position information. A wall carries direction information and position information particular to the wall. When the robot returns to an area it has visited before, it can use these landmarks to estimate the position and heading in the same local coordinates. It is also easier to define a work task for the service robot in an environment where the positions of landmarks are known.

Figure 4.7 shows part of a single horizontal scan of the 3D mapping laser range finder placed in position E. The view is in front of the large door of the process hall (Fig.3.5).

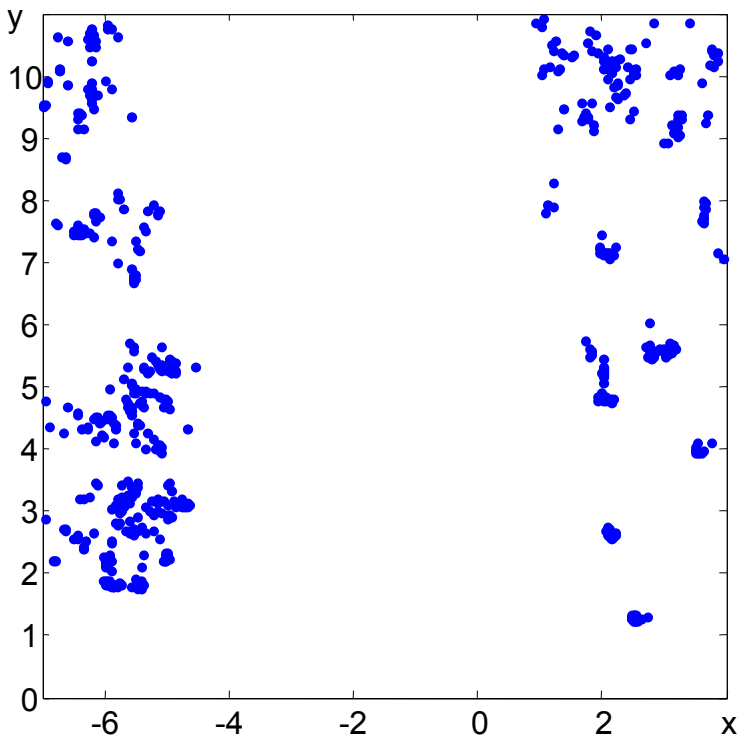

Figure 4.7 Part of a single horizontal scan of the 3D mapping laser range finder located at point (0,0). Measurements are in meters.

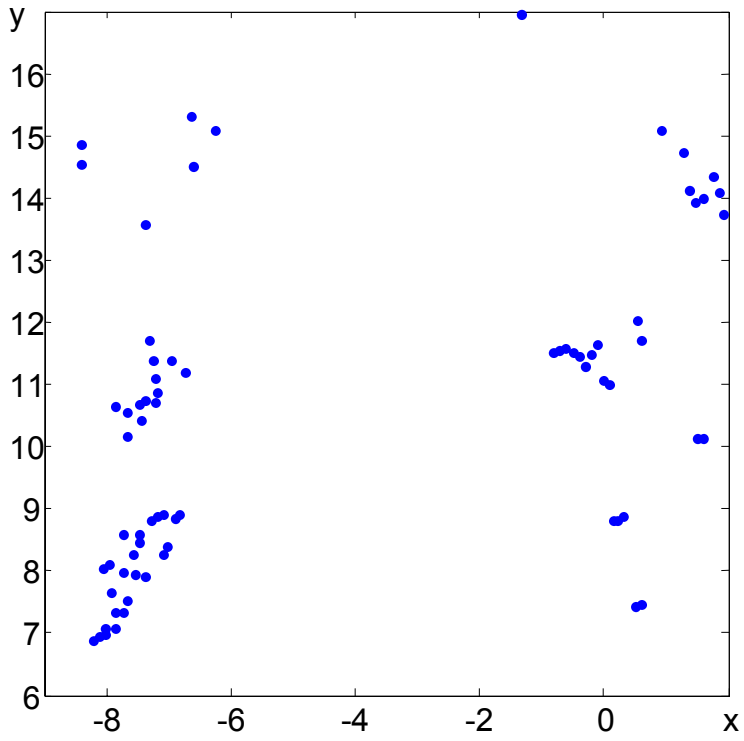

Figure 4.8 Raw map taken by the robot laser range finder approximately from the same area as in the previous figure. The laser is located at point (0,0), and the midline of the view is aligned along the y-axis.

The position and heading of the laser range scanners are different in Fig. 4.7 and 4.8. By solving the rotation and translation between them, the robot laser position and heading can be computed in the mapping laser coordinates fixed on position E, which was selected for reference coordinates.

The mapping laser coordinates were selected because they are inline with one wall in the process hall that could be used as a landmark for estimation of the robot's position. In addition, the tree trunk center positions are given in those coordinates.

[Forsman, 2001] used a 3D scanning laser range finder (Riegl LMS-Z210) for modeling tree trunks. The horizontal scanning range is equal to 324 degrees, and the angular resolution equal to 0,108 degrees was used. However, the laser beam divergence is equal to 0,17 degrees. The horizontal scan speed is limited to 15 deg/s but the actual limit is the measurement rate that is approximately 12.000 range measurements/s. Acquiring the entire 3000x720 pixel 3D range image takes over 3 minutes. Theoretically, a tree trunk with a diameter equal to 13 cm, and at 5 meters distance, reflects approximately 14 laser rays. Fig. 4.9 shows eight trees that have been detected when the mapping laser is in position E [Forsman, 2001].

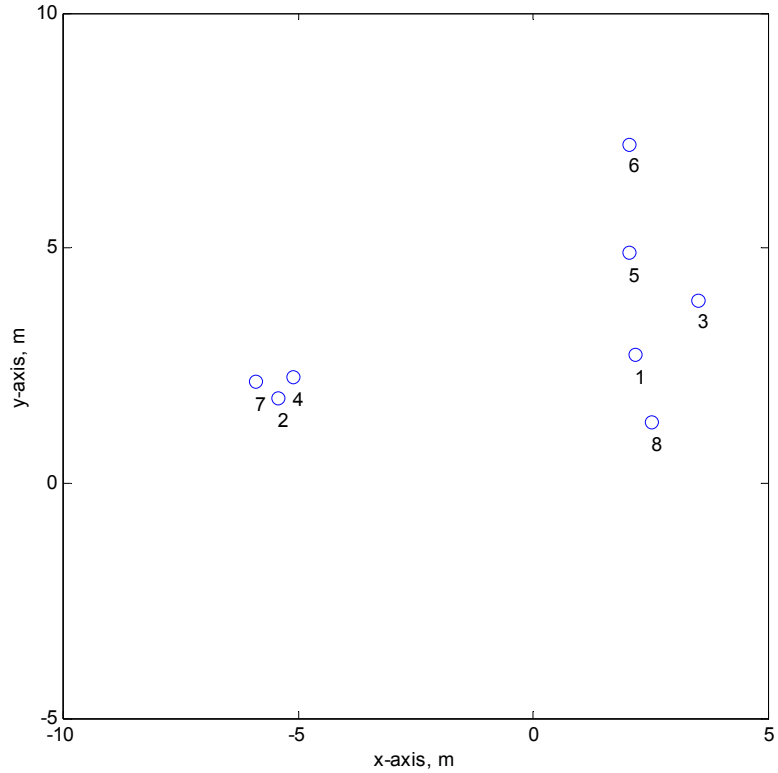

Figure 4.9 Positions of vertical cylinder centers that were modeled by using the mapping laser range finder placed in position (0,0). The respective raw data is shown in Fig. 4.7.

The numbered vertical cylinder centers in Fig. 4.9 were used as landmarks in estimating the robot position and heading at initial and final position during the test trials. The respective coordinate system is called E, following the documentation in [Forsman, 2001].

The robot laser range finder has a horizontal angular resolution equal to 0,5 degree. The laser beam initial spot diameter is equal to 2 cm, and additional laser beam divergence is equal to 0,7° [Technical description]. The robot scanning range finder suits better than expected for detecting tree trunks because of the wide beam width. The laser beam spot diameter is equal to 13 cm, and the beams overlap 5 cm at a distance equal to 8,9 m. In practice, a partial reflection is enough for a range measurement. Therefore, trees with a diameter of approximately 20 cm were given four reflections from a distance of approximately 9 meters. When three successive laser beams hit a tree trunk, then three range measurements were obtained. Two first order differences can be computed from two successive range measurements. Only one second order difference can be computed from three successive range measurements by using numerical derivative formulae. From four range measurements, three first order differences and two second order differences can be computed. Table 4.3 shows the first and second order differences computed from three to –four range measurements based on twelve successive laser scans in trial no. 18. Tree 1 E was recognized from every scan with four range measurements but lamppost 8 E only from 3 scans with three range measurements. The diameter of the metallic lamppost is equal to 109 mm, and the observation angle is equal to 0,84° at a distance equal to 7,5 m. The diameter of the birch tree is equal to 154 mm, and the observation is equal to 1,0° at a distance equal to 8,9 m. Obviously, the shiny metal surface is not such a dispersive reflector as the white birch tree.

The standard deviations of the distance measurements to tree 1 E were between 0,9 cm and 1,1 cm and to lamppost 8 E between 0,6 cm and 2,1 cm.

Table 4.3 Laser range values as well as first and second order differences in the case of two vertical cylinder landmarks.

	r (m)	Max Δr (m)	Max Δ^2r (m)	Min Δ^2r (m)
Tree 1 E	8,9	0,06	0,08	0,02
lamppost 8 E	7,5	0,07	0,08	0,06

The rules for tree extraction were as follows

$$\Delta r < 0{,}095m$$
$$0{,}0002/m < (\Delta^2 r / r^2) < 0{,}0015/m \quad (9)$$

In trial no. 16, the robot remained in the same place for the first 116 scans. Tree 4 E gave all the time four reflections but tree 1 E only three times. Table 4.4 shows the first and the second order difference computed from the laser distance measurements to these trees.

Table 4.4 Laser range values and their first and second order difference in the case of two trees shown in Fig. 4.9.

	r (m)	Max Δr (m)	Max Δ^2r (m)	Min Δ^2r (m)
Tree 1 E	8,9	0,12	0,12	0,10
Tree 4 E	10,7	0,13	0,19	0,09

When a tree was narrow or at a longer distance, the laser was able to obtain only 2 range measurements from the tree. These range measurements are almost equal. Usually, the first order difference in range reading is between 0 and 2 cm (Table 4.5).

Table 4.5 Distance, diameter, and first order difference of range measurements to two vertical cylinder objects shown in Fig. 4.9.

	r (m)	D (m)	Mean Δr (m)	Max Δr (m)
Tree 3 E	10,27	0,089	0,021	0,050
Lamppost 8 E	7,49	0,065	0,010	0,040

In practice, it is very seldom that any object other than a narrow cylinder gives two almost equal range readings from any direction, but not three or more. The tree extraction rule for two range readings is as follows

$$\Delta r < 0{,}025 \text{ m} \quad (10)$$

Usually, the maximum step in a tree diameter estimate occurs when one laser beam less than usual is reflected from a tree trunk. The error in range estimate and in radius estimate is equal. The error depends on the range and is computed as follows

$$e_r = r * \sin(\Delta\beta) / 2 \quad (11)$$

where $\Delta\beta$ is the laser bearing resolution.

The error originating from laser bearing resolution in radial and tangential directions is less than 5 cm when the range to the tree is less than 11,46 m. A tree is not usually detected from longer ranges than this.

Figure 4.10 shows trees that are detected by the robot laser range finder when the robot is at approximate position (2,-6) in the mapping laser coordinates.

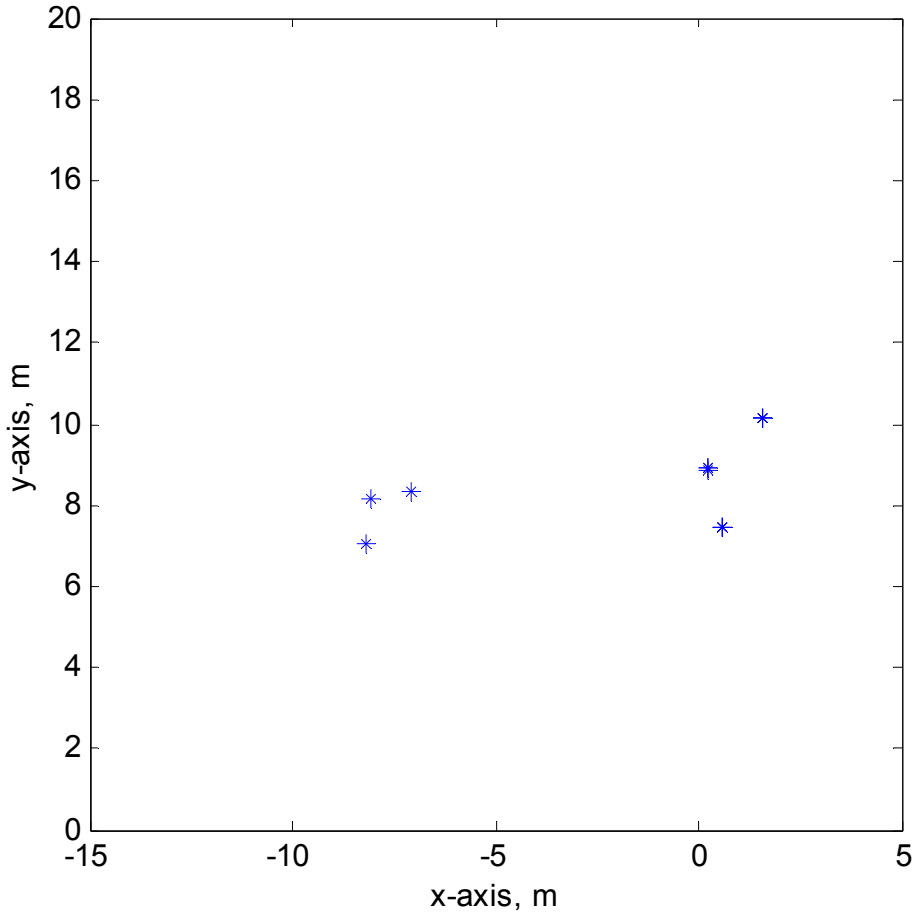

Figure 4.10 Positions of extracted trees by using the robot laser range finder. The coordinates are in meters, and are fixed on the laser.

By computing the rotation and translation between Fig. 4.10 and Fig. 4.9, the robot position and heading can be estimated in the E-coordinates.

The conventional GPS measurement has a large variance, and therefore a single position fix cannot be used for robot position initialization. However, the robot initial position can be determined by summing up position measurements when the robot is in its initial position. The mean value converges slowly because the GPS position error is correlated in time. When

the robot moves, the position fixes can be transformed to initial position by using the estimated robot position and heading in local coordinates. However, the direction of local coordinates must be known. The direction of local coordinates in Earth fixed coordinates can be estimated by taking the mean value of the difference between the GPS heading and robot heading in local coordinates during a mission. The error of a single heading measurement from a conventional GPS receiver was up to 40° during the test trials. However, the GPS heading error is statistically zero mean. When the GPS receiver is moving slower than approximately 0,1 m/s the heading is set to zero.

4.5 Position and heading estimation by laser range data matching

In outdoor environments, the objects are not necessarily circular or linear. Matching of dense laser range data requires no extracted features [Konolige et Chou, 1999]. Actually, every obstacle point that reflects the laser beam can be considered as a low level feature. Matching of laser range data cannot be used in open areas where the obstacles are beyond the maximal measurement range. The maximal range is between 30 m and 80 m depending on obstacle reflectivity when LMS291 is used.

The range values obtained from the 2D scanning laser can also be presented in terms of xy-coordinates. The resulting 2D map shows objects as point groups. After the measurement interval, the next map can be computed. The robot's rotation and translation during the measurement interval (< 1 s) is relatively small, and therefore most of the obstacle points can also be seen in the new map. If the new map is rotated and translated so that the corresponding obstacle points in successive maps coincide, the robot rotation and translation can be solved.

In principle, the xyz-coordinates of the object points in two successive range maps can also be matched by using a 3D scanning laser range finder. However, direct use of correlation type methods is not possible with current computer technology in real time.

The maximum angular and linear velocity of the robot defines the 3DOF search space for the rotation and translation. The function that is maximized during the map fitting can be constructed in many ways. When using occupancy grids, the corresponding grid probabilities are multiplied and summed over the grid [Moravec et Elfes, 1985]. [Schultz et Adams, 1998] used a binary match function that obtained a value equal to 1 if the corresponding cells were both occupied or both empty. The match functions were then summed over all cells.

Structured landmarks are not guaranteed in outdoor environments. Therefore, a mobile robot should be able to determine its incremental position and heading from raw laser range measurements. Lu [Lu, 1995] presented two methods to determine robot position and heading from raw laser range measurements. The approximate rotation and translation between two successive laser range scans is defined by using odometry. The accurate matching of successive laser scans is carried out separately for the position and heading by using modified ICP.

Successive laser range scan matching can be done also without odometry. Selkäinaho et al. [Selkäinaho et al., 2001] presented a method based on 3DOF correlation of raw laser range data. The method presented in the following is far more reliable and faster. Bailey and Nebot

[Bailey et Nebot, 2001] independently developed a method known as laser odometry, based on matching line or point features in successive range scans.

The coordinates of an object point are written in the local coordinate system as follows

$$\begin{aligned} x_j &= r_j * \cos(\beta_j - \phi_i) + x_i \\ y_j &= r_j * \sin(\beta_j - \phi_i) + y_i \end{aligned} \tag{12}$$

where r_j is the range to an object point and β_j is the corresponding bearing in laser coordinates. The robot pose is (x_i, y_i, ϕ_i), and the coordinates of the obstacle point in local coordinates are (x_j, y_j). The map built by using points (x_j, y_j) is known as a reference map.

When the next laser range scan is taken, the robot position and the heading have changed equal to $(\Delta x, \Delta y)$ and $\Delta\phi$, respectively.

$$\begin{aligned} x_k &= r_k * \cos(\beta_k - \phi_i - \Delta\phi) + x_i + \Delta x \\ y_k &= r_k * \sin(\beta_k - \phi_i - \Delta\phi) + y_i + \Delta y \end{aligned} \tag{13}$$

where r_k is the range to an object point, and β_k is the corresponding bearing in laser coordinates. The coordinates of the object point in local coordinates are (x_k, y_k). The map built by using points (x_k, y_k) is known as a current map.

When the indexes j and k of corresponding points are known, the rotation and translation can be solved from Eq. (12)-(13). In practice, the solution is found by going through all possible rotation and translation values for the robot and then computing the number of corresponding points for each combination.

The best match is found by maximizing the number of corresponding points N relative to translation $(\Delta x, \Delta y)$ and rotation $\Delta\phi$:

$$\begin{aligned} &N(\Delta x, \Delta y, \Delta\phi) = \sum_{k=1}^{361} n_k \\ &n_k = 1, \quad if\ \exists j \left((x_k - x_j)^2 + (y_k - y_j)^2 < d_k^2 \right) \\ &n_k = 0, otherwise \end{aligned} \tag{14}$$

The obstacle points are assumed tentatively corresponding if the distance between them is less than d_k.

$$d_k = 0{,}6 * \Delta s + 0{,}6 * \Delta b * r_k \tag{15}$$

where Δb is the bearing search resolution in radians, and Δs is the position search resolution. The values in Eq. (15) yielded the most accurate results in trial no. 16 but they are actually the same as concluded from the position and bearing search resolution. When the robot position is searched in 10 cm steps, the maximum error in robot position is equal to 5 cm. The range measurement noise standard deviation is equal to 1 cm. The first term in Eq. (15) is the sum of these two values. When the heading is searched in Δb steps, the maximum error in heading is equal to $0{,}5 * \Delta b$. The laser may rotate during the 26 ms long laser range scan. A rotation

speed equal to 4°/s causes a heading difference equal to 0,1° between the first and last laser beams. The difference relative to the middle laser beam is 0,05°, which is considered as error. The error caused by the heading search resolution and moderate laser sensor rotation is therefore the same as the second term in Eq. (15). The position error is obtained by multiplying the heading error by the range measurement. It was assumed that the heading search resolution Δb is equal to 0,5°. A smaller value for heading search resolution was not adequate because the laser beam width was equal to 0,7°.

The radius d_k in Eq. (15)corresponds somewhat to half of the cell size in occupancy grid based methods. At small object distances, the diameter of a circular cell is approximately 12 cm. The object distance defines mainly the cell size when the distance is greater than 11,5 m.

The search space in position and heading is constrained according to the robot's motion range during the measurement update period. When the robot uses wheeled locomotion, it is sufficient to search the translation in front of the body surge direction. The maximum velocity of the robot defines the search space in the surge direction. The search space in heading is determined by the angular speed of the articulation angle as well as robot velocity and articulation angle.

Organizing object coordinate pairs (x_i,y_i) in ascending order along x_i, and using binary search make the computation faster. Only points that fulfill $r_i<r_{max}$ are taken into account.

The search space in position and heading is selected according to the motion range coming from the vehicle dynamics. Figure 4.11 shows the robot's front body segment (arrow) in two successive positions.

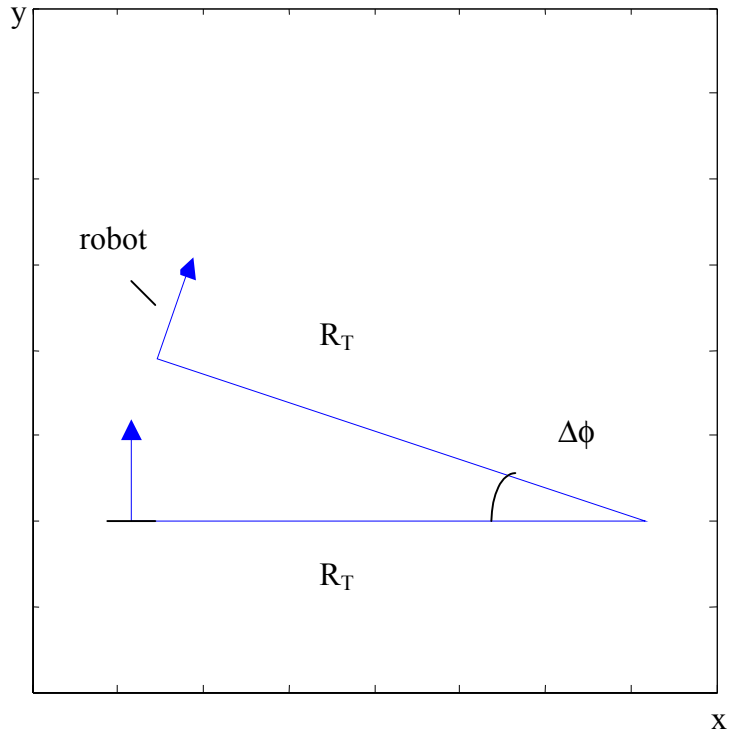

Figure 4.11 Robot front body (arrow) in two successive positions while in turning motion.

When the robot moves on wheels, the one step heading difference, surge difference, and sway difference are not independent of each other. It can be seen from the above figure that when surge difference is Δy and heading difference is $\Delta\phi$, then the sway difference must be as follows

$$\begin{aligned} \Delta x &= R_T - R_T \cos(\Delta\phi) \\ \Delta y &= R_T \sin(\Delta\phi) \end{aligned} \tag{16}$$

where R_T is the turning radius.

By using the second order approximation of trigonometric functions, we get

$$\begin{aligned} \Delta x &= R_T - R_T (1 - \Delta\phi^2 / 2) \\ \Delta y &= R_T * \Delta\phi \end{aligned} \tag{17}$$

Substituting the Δy equation to Δx equation, we get

$$\Delta x = \Delta y * \Delta\phi / 2 \tag{18}$$

Thus, the new position and heading can be searched in 2DOF space, namely in Δy and $\Delta\phi$. Sway value Δx is computed according to the last equation.

Figure 4.12 shows the pair wise scan match of the lowest number of common points in trial 16. The surface that shows the number of common points in matching is maximized. It has sometimes twin peaks with almost equal heights. The lower peak shows the situation where the error in rotation is compensated by the translation.

Figure 4.13 shows the pair wise scan match of the highest number of common points in trial no. 16. When the number of common points is high, then the optimized surface has only a single peak.

There is no guarantee that in partially structured environments, the matching solution is always unique. Erroneous matching results have been occasionally obtained when using a constant acceptation square of size equal to 20 cm. The acceptation circle (Eq. 15) that depends on laser range measurement works reliably. However, other sensors such as heading gyro and wheel based odometry can be used to verify the correct match in future work.

In [Olson, 2000], a method was presented to match two maps in an unstructured environment. The divide-and-conquer method is effective when the robot pose search space is large. In [Forsman, 2001], this method was used for matching 3D-maps. Computing of one match with 20 cm accuracy took several hours. By using discrete features instead of occupancy grids, the algorithm could show a comparable, but not a faster, performance in 2D as in the method presented in this thesis.

The biggest difference from other methods is that robot navigation is successful without extracting landmark features. In addition, wheel-based odometry is not required in successive laser range scan matching. In [Madhavan et al., 2002], maximum curvature features in laser range values were used as landmarks. The corner of a car chassis was a typical such feature. The landmarks were detected by using a 2D laser range finder and wheel-based odometry.

The results were obtained with the same utility car as in [Bailey et Nebot, 2001]. Bailey and Nebot used discontinuities in laser range values as landmarks.

The successive laser range scan matching method was tested in numerous trials presented in Chapter 3. Because the presented navigation method behaves similarly with all the collected data, trial no. 16 was selected as representative of all trials.

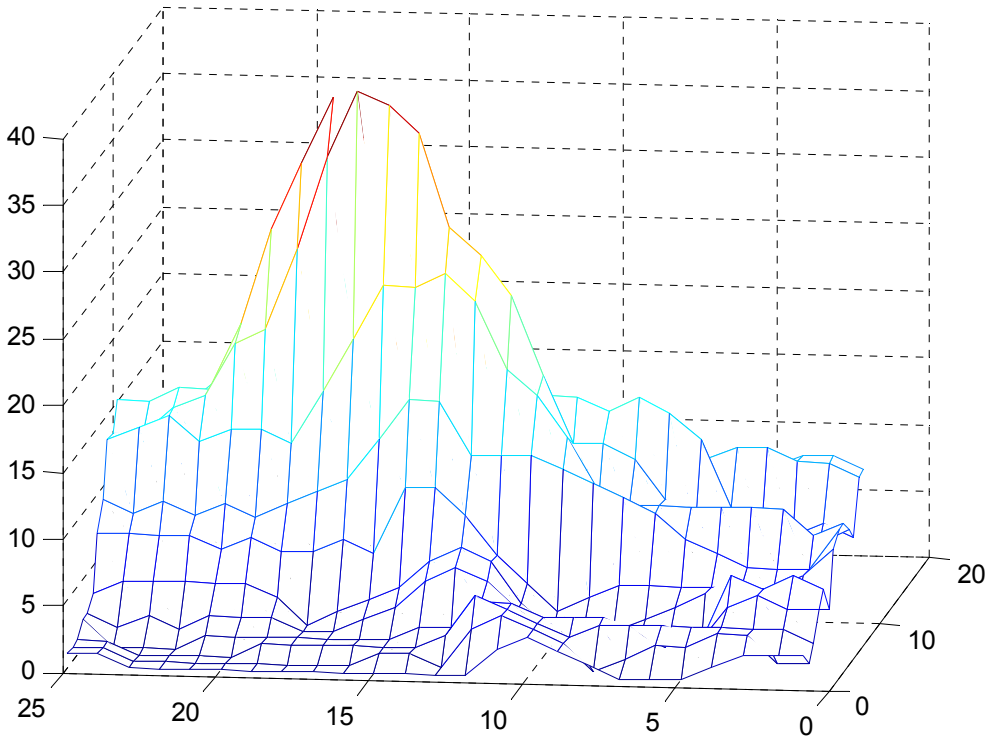

Figure 4.12 Number of common points in successive scan matching. Laser range scans from time instants 176 and 177 from trial no. 16 have been matched. The axis in front shows the rotational search index, and the axis on the right the longitudinal translation search index.

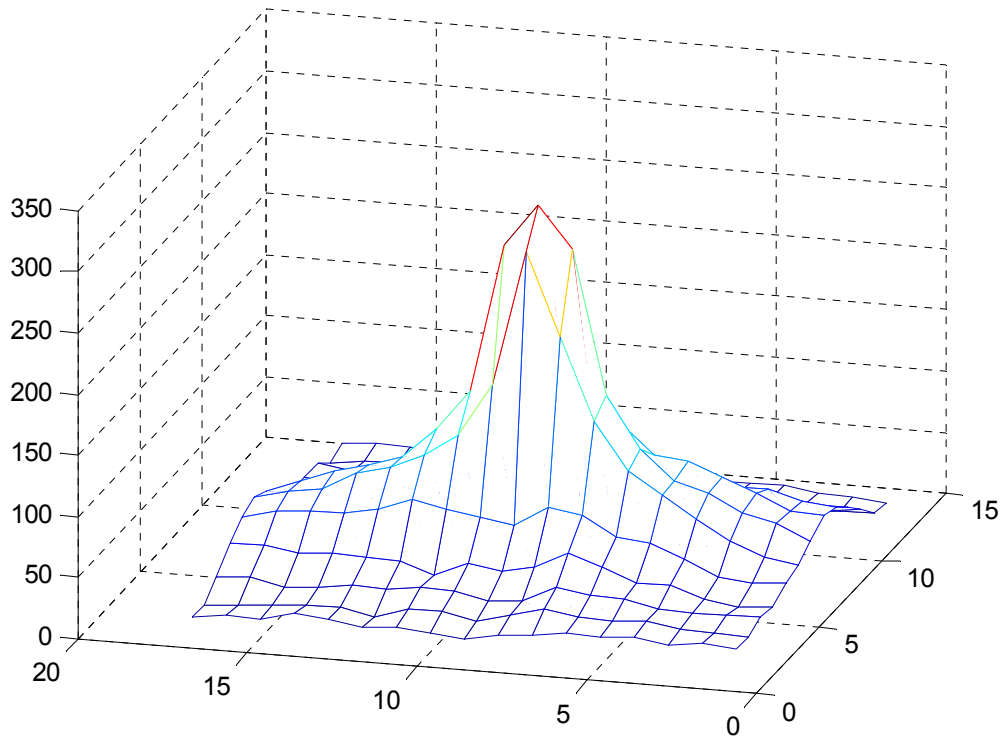

Figure 4.13 Number of common points in successive scan matching. Laser range scans from time instants 388 and 389 from trial no. 16 have been matched. The axis in front shows the rotational search index and the axis on the right the longitudinal translation search index.

4.6 Correction of the robot position and heading

In the sequential laser range data matching, the position and heading errors grow without limit in a similar way as in ordinary odometry although usually at a slower speed. Therefore, pose errors should be removed at certain intervals. Recognized landmarks such as tree trunks, fences, and walls can be used for the calibration, which will be shown in this chapter.

Laser range data matching can also be used in pose correction. The correlation method is not as sensitive as the iterative closest point method to the initial guess for the translation and rotation. When the robot returns to approximately a previous position and heading, the corresponding laser range scans can be matched by the method presented in the previous chapter, Eq. (12)-(15). The search space in position and heading should be selected according to the maximum accumulated error; the search is done in 3DOF.

The Hough transform was used to search a cloud of points around a line. With Sick LMS 291, the standard deviation of points around a line is typically 1 cm. When the number of points with predetermined accuracy around the line exceeds a certain limit, a line feature is found. The Hough transform is not able to define the length of a line; this is estimated separately by checking the continuity of the line. The Hough transform can also be used to find geometric primitives other than lines.

The ability to detect a wall by using a 2D vertically scanning laser range finder and the Hough transform was tested around the Computer Science Building. Faulty detections were made from bushes of young trees up to 10 points on a line. The Hough space was discretized with Δr=0,02 m and $\Delta\alpha$=0,2°. A wall that is 20 m long is never seen as complete because the laser beam is reflected only less than 60° around the direction of the wall normal. The reason is that

the metal plates used on the cover of the wall are poor diffuse reflectors. The maximal viewing angle of a wall was only 51° during the test trials because the heading of the laser range finder was usually pointing partly in the wrong direction.

Line candidates are found by seeking the local maximum in the discrete Hough space. Additionally, the local maximum must be at least a certain number of points in order to avoid false line features. The Hough transform finds nearby flat objects easier because the number of reflections is inversely proportional to distance. This feature can be utilized when the robot seeks a box that should be grasped by a robotic manipulator.

The range weighted Hough transform was used successfully indoors [Jensfelt, 1999]. The walls that are behind furniture can be easily detected in this way. In outdoor environments, the range weighted Hough transform appears to give false alarms because the maximum range is much higher than indoors.

A line that is found by using vertically scanning laser range finder and the Hough transform is most often a wall in an outdoor environment. A delivery van looks very similar to a wall because of its box like shape. Therefore, a long line feature in an outdoor environment is not automatically perceived as wall. Trees or people may occlude a wall, and therefore it is reasonable to accept one to three missing reflection points when checking the continuity of a wall.

According to the Hough transform, the nearest distance from origin to a line going through a point in rectangular coordinates is shown as a function of angle and distance from the origin. By using the Hough transform, a point (x_i, y_i) in the Cartesian coordinates is shown as the nearest distance d to a line that is going through that point. Because a line going through a point can have any value, the nearest distance is shown as a function of the direction of the line normal. The nearest distance from the origin is computed as follows

$$d = x_i * \cos(\alpha) + y_i * \sin(\alpha) \tag{19}$$

In the Hough space, the distance d and the angle α of line normal are discretized and a point is shown as a sinusoidal wave. A proper choice for a laser range finder implies that Δd=0.02 m and $\Delta\alpha$=0.2°. The resulting discrete Hough space has 1800x5000 elements when d_{max}=100 m and $\alpha_{\max}$=360°. The Sick laser scan produces a maximal 361 points that will transform to 1800x361 points in discrete Hough space. Points that belong to the same line have the same arguments in discrete Hough space.

Because the storage space is quite high, it is better to search the maximum density separately for every discrete angle value in Hough space. The local maximum is compared with the neighboring angle values in Hough space. Thus, only 15,000 density values are in the memory at the same time.

The maximal angular misalignment between the true line direction and the estimated line direction is half of the angular search step. If the length of the row of points is equal to ll, then the line width Δd must be at least

$$\Delta d = ll * \sin(\Delta\alpha / 2) \tag{20}$$

The used values Δd=0,02 m and $\Delta\alpha$=0.2° correspond to the longest line length of approximately 11,5 m.

Table 4.6 shows the number of points in the longest line in trial no. 16 with a different line acceptation width. Figure 4.15 shows the respective points belonging to the wall in map E.

Table 4.6 Points on a line presenting a wall with different values of line width (Δd).

Points on line	56	79	95	101	104	104
Line width	1 cm	2 cm	3 cm	4 cm	5 cm	6 cm

Sometimes, a thick group of small trees can produce reflections that are on the same line with defined accuracy (2 cm). However, the line points are not continuous, in contrast to the points reflected from a wall. In this study, two points are considered to belong to the same physical line when the distance between two consecutive points in a line candidate is less than 0,04*d_i . The distance between two consecutive points along a line in laser range data is equal to

$$d_P = \sin(\Delta\beta) * d_i / \sin^2(\beta_I) \qquad (21)$$

where β_I is the laser beam angle of incidence and d_i is the shortest distance between the line and laser.

Figure 4.14 explains the situation graphically. It was assumed during the derivation of Eq. (21) that $\Delta\beta$ is negligibly small.

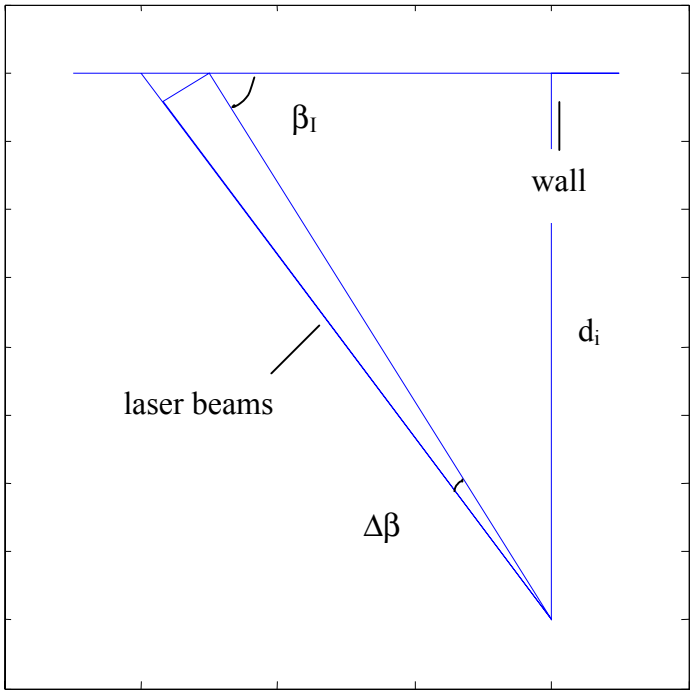

Figure 4.14 Two successive laser beams hitting a wall.

The rejection rule means that when the laser ray hits a wall perpendicularly, 3 consecutive occlusion points are accepted in the physical line, and when the angle of incidence β_I is equal to 42°, only one occlusion point is accepted.

The position of end points of a continuous line can be used to identify a new line if the line has been modeled previously. In [Forsman, 2001], the neighborhood of the Computer Science Building was modeled using a Riegl 3D laser range finder. Both the walls and trees were modeled in the same coordinates.

The robot laser range finder does not usually see the entire wall but only part of it. Especially smooth walls that are made of sheet of metal or glass cause problems. The cause is poor reflectance with a small value of angle of incidence. Therefore, the endpoint of an extracted line is not a reliable feature.

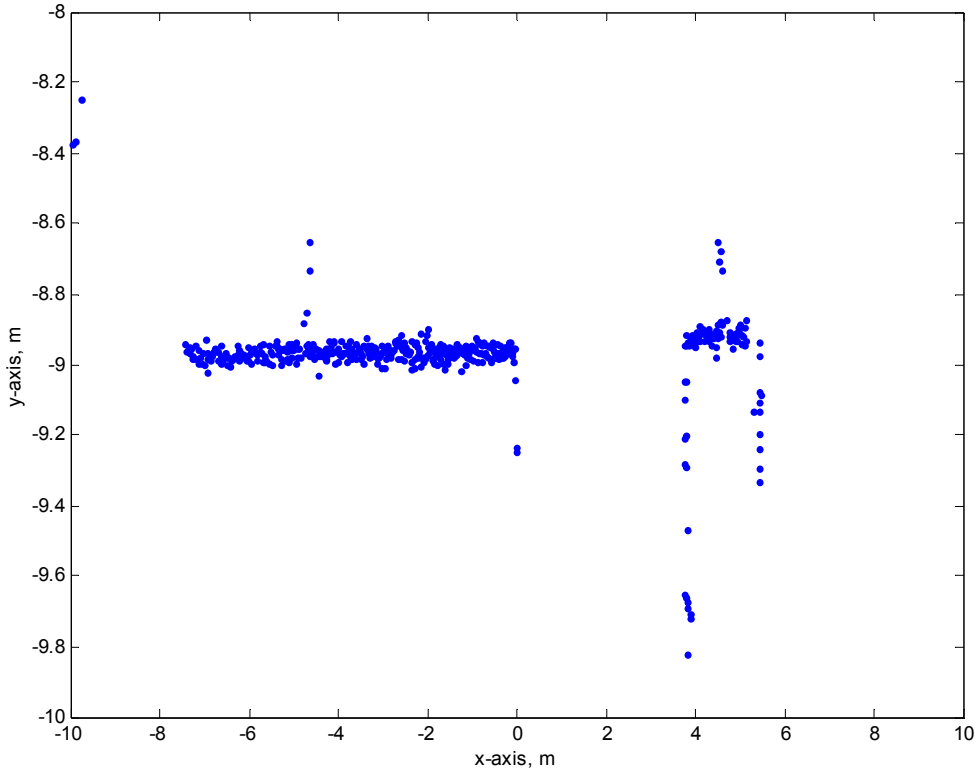

Figure 4.15 The resulting 2D map of a single horizontal range scan of a mapping laser placed at (0,0). The line in the figure shows the wall and the doorway of the process hall.

Figure 4.15 is a part of Fig. 3.5. The large noise associated with the mapping laser range measurements is clearly seen. A line must be fitted to points belonging to the wall shown in Fig. 4.15 in order to use it as an accurate landmark.

Inside a room, the robot is able to find up to 4 walls for landmark positioning. Outdoors, two walls can be found only in the vicinity of corners, and most of the time the robot must rely on a single wall or no walls at all. The robot heading can be estimated based on a single line landmark. The robot position can only be defined on a line that is at constant distance to a

wall. An additional point type landmark such as a tree trunk center can be used to uniquely determine the robot's position (Fig. 4.16).

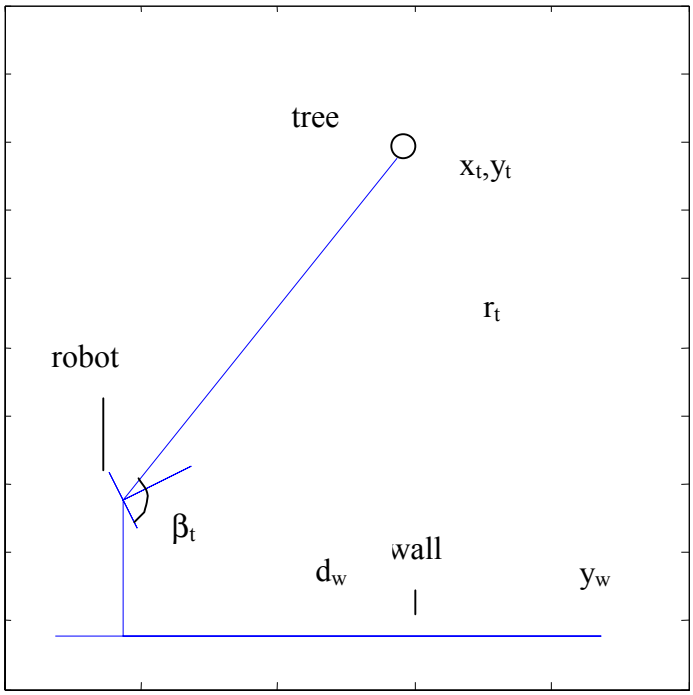

Figure 4.16 Robot's position and heading based on a wall and tree landmarks. The coordinates of a tree are (x_t,y_t) and the those of the wall y_w. The robot's distance to the wall is d_w, and range to the tree is r_t.

The shortest distance between a tree candidate and the line that defines all the possible robot locations is computed by using the Hough line equation. From all of the modeled tree candidates, the one that is on the measured distance with some predefined accuracy is selected for landmark positioning. If more than one tree is found at the same distance, then the distances to other trees can be used for identifying.

4.7 Satellite based navigation with gyro aiding

Radio navigation based on satellite vehicles (SV) is a complementary way to estimate the position and heading of a mobile robot. The laser range finder based navigation works well in feature rich environments. Obstacles such as buildings and trees prevent the receiver from seeing satellites. On the other hand, satellite navigation works best on a featureless field.

In open areas where the laser range finder receives few laser beam reflections, the number of GPS satellites is usually high. A conventional GPS receiver computes the velocity and heading at 1 s intervals. The measured heading includes relative large time correlated error but the error is bounded. The measured speed is sufficiently accurate for navigation purposes. GPS heading can be used for navigation if the time-correlated error is first removed by using a heading gyro, for example.

The Doppler based velocity measurement of a GPS receiver is relatively accurate. The standard deviation of velocity error of the Ashtech GPS receiver is equal to 0,01 m/s [tech manual]. The standard deviation of WorkPartner's velocity was verified to be 0,02 m/s including variations in the robot velocity.

The error of the GPS heading information is strongly colored, and its variance is approximately 8° when HDOP is less than 4. However, a useful property is that the GPS heading error is zero mean.

An extended the Kalman filter using a noise shaping filter is sometimes used first to make the error white and then to filter it out [Cooper and Durrant-Whyte, 1994].

The computed heading has a standard deviation of approximately 2-10°. However, the heading seems to be unbiased. The heading standard deviation is a function of the HDOP value. The position error of the Ashtech GPS receiver is less than 16 m (SEP) when PDOP is less than 4 [tech manual]. An extended Kalman filter is ideal for estimating the position and velocity of the robot based on considerably large position error and very small velocity error.

The satellite navigation receiver measures the robot position and heading in WGS-84 coordinates. The navigation system of the robot needs to know the relation between the coordinates before the robot switches from laser based navigation to satellite navigation.

4.7.1 The Kalman filter for heading estimation using GPS and gyro

The Kalman filter is used to fuse gyro angular speed and GPS heading. The system equations are written as follows:

$$\dot{\phi} = (u_g - u_0)/g_g + w_g \tag{22}$$

$$y_{GPS} = \phi_i + v_s \tag{23}$$

where ϕ is the heading of the robot front body, u_g is the gyro angular speed measurement, w_g is the gyro error, y_{GPS} is the GPS heading measurement, and v_s is the corresponding measurement error.

The constant gain discrete Kalman filter is written as follows:

$$\begin{aligned} \phi(i \mid i-1) &= \phi(i-1 \mid i-1) + \Delta t * (u_g(i) - u_0)/g_g \\ \phi(i \mid i) &= \phi(i \mid i-1) + G * (\phi_{gps}(i) - \phi_0 - \phi(i \mid i-1)) \end{aligned} \tag{24}$$

where $\phi(i|i)$ is the heading estimate in local coordinates, and ϕ_0 is the direction of local coordinates in global GPS based coordinates.

Parameter ϕ_0 should be estimated before GPS based navigation is used. Estimation is possible during the mission whenever the laser-based navigation is used and GPS receiver is operational at the same time.

4.8 Adaptive navigation system

Most navigation systems until now have been able to navigate in a certain type of environment. Navigation systems that require certain type of landmarks do not work without them. A versatile service robot that operates outdoors should be able to navigate without landmarks. In this thesis, robot adaptivity to environment is accomplished by using three alternative navigation methods. Satellite navigation and laser odometry are complementary navigation methods. Satellite navigation works best in open featureless fields outdoors. On the other hand, laser odometry is most accurate in an environment rich in vertical objects.

Sensor fusion has not been used to combine all the measurement information. The adaptive navigation system is partly based on logical decisions. Satellite navigation based on poor geometry and laser range finder operating in featureless environments have not been taken into account. This is effectively the same as rejecting erroneous measurements in optimal filtering.

The flowchart of the adaptive navigation system is shown in the Fig. 4.17. The basic navigation method is based on the matching of successive perception maps. This has also been referred to as laser odometry when using recognized features [Bailey et Nebot, 2001]. However, laser odometry is an explanative term in the matching of successive perception maps. It is used when the number of common points in successive perception maps is greater than approximately 36 points. It was found in practice that below 36 points, the probability of wrong matches increases rapidly.

Laser odometry is not usable in open fields. On the other hand, the visibility of navigation satellites is better in such cases. The primary information used from the GPS receiver is the NMEA GPVTG message including velocity and heading. The value of the heading is usable when the velocity of the robot is greater than approximately 0,2 m/s. The receiver sets the heading to zero when the velocity is almost zero. An additional requirement is that the satellite geometry is sufficiently good. This is assured when HDOP is typically less than 4. The gyro is the primary source for alternative heading information. The GPVTG heading is used to restrict the gyro to drift without limits. The gyro heading is corrected by using constant gain Kalman filter (Eq. 24).

When the robot exits a building, it takes some time before the GPS is working. If the laser range finder view does not include enough objects, then conventional odometry is required momentarily. The robot position is computed by using heading gyro and wheel revolutions.

Laser odometry drifts slowly but without limits. Therefore, it is useful to correct the estimated heading by using the GPVTG heading whenever reliable measurements are available. A constant gain Kalman filter [Maybeck, 1979] is used for heading estimate correction.

If a consistent map of landmarks is available, it is possible to initialize the robot position and heading. If no landmarks are on laser range finder view, the initial position and heading of the robot can be used as local coordinates. During the robot's mission, occasionally seen landmarks can be used to remove the errors in robot position and heading.

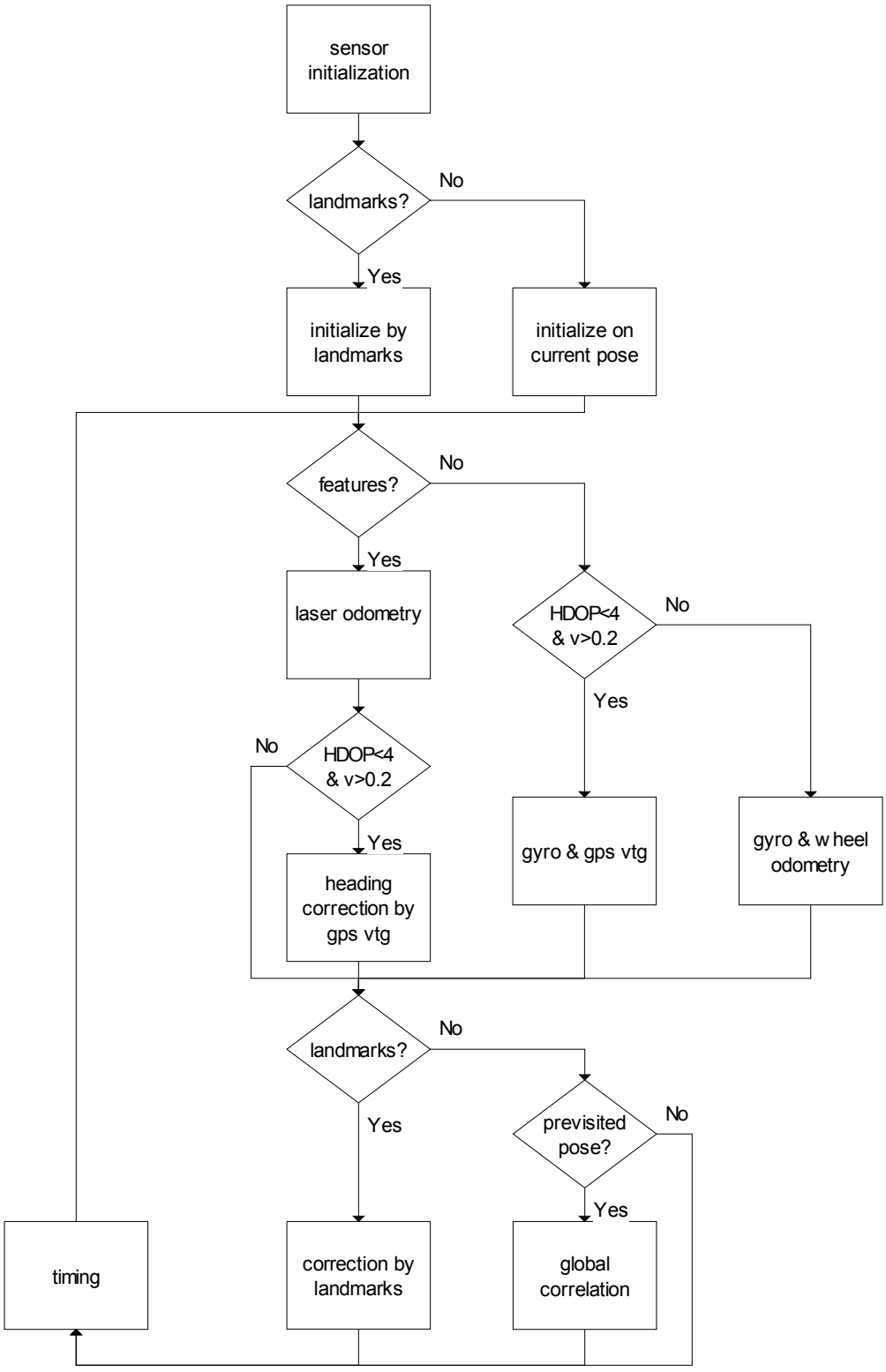

Figure 4.17 Diagram of the adaptive navigation system.

Computationally heavy methods exist for correcting position and heading errors. This is referred to as global correlation in Fig. 4.17. When a robot comes to a position and heading it

has previously visited, the accumulated error after the previous visit can be effectively corrected. If the old perception map from the previous visit is in memory, correlation matching (Eq. 12-15) can be used to find the rotation and translation between the current perception map and the perception map from the previous visit. The search space in position and heading must be up to maximal accumulated error, and is therefore computationally heavy. Search time can be reduced by using the divide-and-conquer method presented in [Olson, 2000].

In the next chapter, every branch in the system shown in Fig. 4.17 is verified with real time experiments. Only the conventional wheel based odometry has not been verified because its typical properties are generally known. However, WorkPartner odometry will be tested in the near future.

5 RESULTS WITH EXPERIMENTAL VERIFICATION

5.1 Vertical cylinder objects as landmarks

The navigation system that was presented in the previous chapter was tested in a university campus environment. The environment includes trees, lampposts, bushes, parked cars, and a university building. The robot starts outside the building, shown earlier in Fig. 3.4, and the viewing angle of the laser range finder includes only trees at initial position (Fig. 3.5). Some of the tree trunks will be used as landmarks.

A single horizontal laser range scan shown in Fig. 3.6 will be used as the reference truth. The reference coordinates are fixed on the position and direction where the 3D laser scanner was when the scan was recorded. The position is marked with E and all landmarks extracted from this scan are also marked with E. The centerlines of the vertical cylinder landmarks have been computed in [Forsman, 2001]. Centerlines are sampled at a height of 1 m, and the resulting positions are shown in Fig. 4.9. The tree trunk centers are computed by fitting horizontal ellipsoid models on range values in Cartesian coordinates.

The landmarks form a consistent map of the environment because the 3D laser was static when the scan was taken. In the following, a method for finding these landmarks by using the robot laser range finder is presented.

The 2D robot laser range finder is able to sample a 3D object at a certain height. If the landmark object is vertical or almost vertical, as with trees, the measurement height is not important. The robot can estimate its position and heading based on two vertical cylinder landmarks. The positions of the cylinder landmark centers must be known, and the robot position can be defined using the same coordinates as those of the landmarks. The inclination of the moving robot body and the inclination of the manipulator affect the height at which the robot laser beam reflects from an object.

There are two main reasons why the robot laser scan plane touches the ground. Either the robot laser is tilted relative to the flat ground under the robot, or the robot laser scan plane is coplanar with the ground below the robot, but there is sloping ground around the robot. A ground reflection should be avoided because a robot position change may be wrongly deduced when two successive ground reflections hit different places on the ground.

Ground reflection is avoided on flat ground if the following equations are true.

$$\begin{aligned} &\alpha_R\left(r_i * \cos(\beta_i)\right) \le h_L, \quad \forall i \\ &\left(\alpha_P + \alpha_M\right)\left(r_i * \sin(\beta_i)\right) \le h_L, \quad \forall i \end{aligned} \tag{25}$$

where α_R and α_P are the rolling and pitching angles of the front body segment. α_M is the manipulator body pitching angle and h_L is the robot laser distance from the ground. Laser range and bearing values of beam i are r_i and β_i respectively.

On hilly terrain, the successive laser-scan planes usually hit the uphill terrain at different heights. In this case, the distance to successive ground reflections gives erroneous information

about robot motion. The subsequent laser range scan matching result must therefore be verified with the wheel-based odometry on hilly terrain. In general, navigation on hilly terrain prefers the use of a 3D laser scan finder and a powerful computer.

The robot laser measures at most 361 laser range values to any reflecting objects. Next, the focus will be on extracting tree features from the laser range data. Characteristic of a tree is that it is circular in section, and the difference in ranges hitting a single tree is less than the tree radius. In the campus area, the maximal tree radius is equal to 15 cm. The tests conducted in the campus area of Helsinki University of Technology showed that it is sufficient that the tree feature candidates are recognized when at least three consecutive range values are inside 12 cm. Because the width of the laser beam is equal to 0,5 degrees, no more than 4 hits from a single tree were found since the distance to the trees was greater than 5 m. In addition, it was impossible to find at least three hits from distances over 13 m because the width of the laser beam is greater than 11 cm at that distance.

An additional requirement for a tree feature candidate is that the laser range hit points should appear convex from the laser side.

Let us consider a case of three successive laser beams hitting a tree trunk. The coordinates of the reflecting points are

$$\begin{aligned} x_1 &= d_1 * \sin(\Delta\beta) \\ y_1 &= d_1 * \cos(\Delta\beta) - d_2 \\ x_2 &= 0 \\ y_2 &= 0 \\ x_3 &= -d_3 * \sin(\Delta\beta) \\ y_3 &= d_3 * \cos(\Delta\beta) - d_2 \end{aligned} \tag{26}$$

where d_1, d_2, and d_3 are successive laser range measurements to the tree trunk surface, and $\Delta\beta$ is the angular resolution of the scanning laser range finder.

The coordinate origin was selected as the middle reflecting point. The direction of the middle ray defines the direction of the y-axis.

Assuming that d_1*(1-cos($\Delta\ \beta$)) and d_3*(1-cos($\Delta\ \beta$)) are negligibly small (typically less than 0,5 mm), we get the circle equation going through the three reflecting points as follows

$$\begin{aligned} &(x_c - \Delta\beta * d_1)^2 + (y_0 - d_1 + d_2)^2 = r_c^2 \\ &(x_c + \Delta\beta * d_3)^2 + (y_0 - d_3 + d_2)^2 = r_c^2 \\ &x_c^{\ 2} + y_c^{\ 2} = r_c^2 \end{aligned} \tag{27}$$

where x_c, y_c, and r_c are the coordinates and radius of the tree trunk center. Substituting the last equation into the first and second equation, we get

$$
\begin{aligned}
&2*\Delta\beta*d_1*x_c 2*(d_1-d_2)*y_c=(\Delta\beta*d_1)^2+(d_1-d_2)^2\\
&-2*\Delta\beta*d_3*x_c+2*(d_3-d_2)*y_c=(\Delta\beta*d_3)^2+(d_3-d_2)^2\\
&x_c{}^2+y_c{}^2=r_c^2
\end{aligned}
\tag{28}
$$

From the first two linear equations, the circle center coordinates x_c and y_c can be easily solved, and the circle radius r_c is computed from the last equation.

The robot laser range finder receives only 3-4 reflections at 6 meters distance from a tree trunk with a diameter of 15-20 cm. This is because at 6 meters distance, the width of the laser ray is equal to 5 cm. When a tree is sampled by three equally spaced (0.5 degrees) laser rays, the intersection points of the laser ray center and the tree trunk present only a sector equal to 84 degrees of the entire circle. In addition, practical tests have shown that side rays measure only the nearest distance inside the laser tray rather than the distance of the laser ray center (Fig. 5.1). The fact that the side tray measurements are biased and taken only from a narrow sector of the circle makes the least squares curve fitting overestimate the tree diameter (Table 5.1).

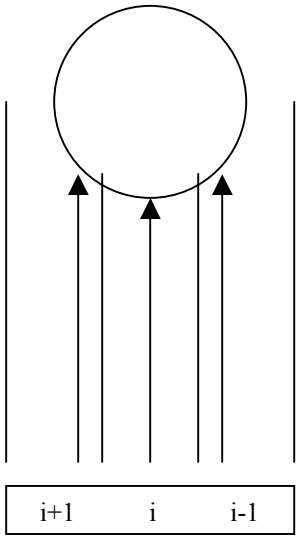

Figure 5.1 Three laser beams (lines as beam border) hitting a circular object such as a tree. The measured distance (arrowed lines) is the shortest distance inside each beam.

Table 5.1 Radius of five vertical cylinders (four trees and one lamppost) in mm measured manually and estimated with circle fitting using two different laser range finders.

Cylinder no.	1	3	5	6	8
Measuring tape	77	67	101	139	54
Mapping laser	69	54	97	104	46
Robot laser	96-138	99-115	126	124	59

Values in Table 5.1 give an impression of the accuracy of the landmark in the reference map. The error in estimated cylinder radius gives an equal error in the landmark position, and it is typically less than 4 cm. The bearing resolution of the mapping laser is as low as 0,17°, and therefore the respective position error is less than 2 cm at distances of less than 10 m. Errors in landmark positions on the reference map increase the pose error of the robot. The accepted

difference between the distance of detected landmarks and the corresponding distance of landmarks on the reference map should be increased accordingly.

A robust way to estimate the tree diameter is to use the distance between the side laser rays hitting the tree trunk as an estimate. Bailey and Nebot [Bailey and Nebot, 2001] have also used this method. The tree trunk radius estimate is computed as a function of the range of the first (d_1) and last beams (d_n) hitting the tree trunk.

$$\hat{r}_C = (n-1) * \Delta\beta * (d_1 + d_n) / 4 \tag{29}$$

where n is the number of laser beams hitting the tree surface.

The tree center is assumed to be in the direction of the middle laser beam and at the distance

$$d_m + \hat{r}_C \tag{30}$$

where d_m is the range of the middle beam in odd cases, or the mean of two middle rays in even cases.

Table 5.2 shows tree radius estimates based on methods using measuring tape, circle fitting, and the viewing angle. The method based on Eq. (28) is known as “circle fitting”, and the method based on Eq. (29) is known as “viewing angle”.

Table 5.2 Radius of four trees measured manually and with two methods based on the robot laser.

Tree no.	1	3	5	6
Measuring tape	77 mm	67 mm	101 mm	139 mm
Circle fitting	96-138 mm	99-115 mm	126 mm	124 mm
Viewing angle	77-104 mm	78-106 mm	105-110 mm	123 mm

It can be seen from Table 5.2 that the viewing angle method is more accurate than the circle fitting method. Therefore, the method based on Eq. 29 and 30 will be used in computing the vertical cylinder landmark position. The position error in the viewing angle direction is typically less than 4 cm, as can be seen in Table 5.2. The average value of the position error orthogonal to the viewing angle is half the laser bearing resolution. When a tree is at 10 m distance, the error corresponding to 0,25° is equal to 5 cm. This is the accuracy of position that can be achieved by using trees as landmarks. If the viewing angles of trees are orthogonal, optimal position accuracy can be achieved. Otherwise, bad geometry of trees further decreases the robot position accuracy.

Distances between tree pairs can be used to identify trees. One distance is not necessarily enough for unique tree pair recognition. Three or more distances computed between all tree pairs are usually enough for unique tree recognition. The pair wise distances between trees in the reference map are compared to pair wise distances between trees that are found from a single 2D range scan taken by the robot.

5.2 Initialization of robot position and heading

The initialization of the robot pose is easy when the environment is totally unknown. The local coordinate system can be fixed to the initial position and heading of the robot. In this case, the robot initial position is (0,0) and the initial heading is equal to zero. This trivial case does not require further consideration, and in the following we consider how new landmarks or landmarks with known coordinates can be used in robot pose initialization.

Position and heading initialization is usually based on a known map of the environment. The robot must assume that it is inside the map but does not know exactly where. In [Thrun et al., 1998b], it was assumed that the robot could be initially in any place inside the map, and probabilities were assigned to all alternative robot positions. The robot gathered information about its environment, and the probability mass of possible locations concentrated on a few specific places depending on the symmetry of the environment. The robot position and heading could uniquely be solved with increasing information if the environment was not fully symmetrical.

In outdoor environments, obstacles that are small in the horizontal direction but tall in the vertical direction are ideal landmarks for pose determination. Tree trunks are examples of such landmarks that have been used [Bailey and Nebot, 2001], but pillars and lampposts are also feasible. Let us consider detecting tree trunks by a scanning 2D laser range finder. Let us assume further that the robot has measured distances to two tree trunks, that both can be recognized, and their position is known beforehand (Fig. 5.2). Then, the robot's position and heading can be determined based on triangulation. In general, there exist two solutions for the position, but the viewing angle to the identified tree trunk determines the correct one. The solution for laser range finder position and heading is computed as follows.

$$
\begin{aligned}
x_1^R &= d_1 * \cos(\beta_1) \\
y_1^R &= d_1 * \sin(\beta_1) \\
x_2^R &= d_2 * \cos(\beta_2) \\
y_2^R &= d_2 * \sin(\beta_2) \\
\alpha_1 &= \arctan((y_2^R - y_1^R)/(x_2^R - x_1^R)) \\
\alpha_2 &= \arctan((y_2 - y_1)/(x_2 - x_1)) \\
\hat{\phi} &= \alpha_1 - \alpha_2 \\
\hat{x}_0 &= x_1 - d_1 * \cos(\beta_1 - \hat{\phi}) \\
\hat{y}_0 &= y_1 - d_1 * \sin(\beta_1 - \hat{\phi})
\end{aligned}
\qquad (31)
$$

where x_i and y_i are the map coordinates of trunk i. The scanning laser viewing angle and range to trunk i are β_i and d_i respectively. The approximate estimates of the robot's heading ϕ and position (x_0, y_0) are denoted by hats. α_1 is the directional angle of the line between the vertical cylinder objects in robot laser coordinates, and α_2 is the directional angle of the same line in map coordinates.

During the trials, the robot coordinates were fixed to the laser position. Therefore, the robot's position is actually the position of the robot laser range finder. Because the midpoint of the

front wheels is typically below the robot laser, this coordinate point is adequate. The position of the midpoint of the front wheels does not move when the robot velocity is zero and the articulation angle changes.

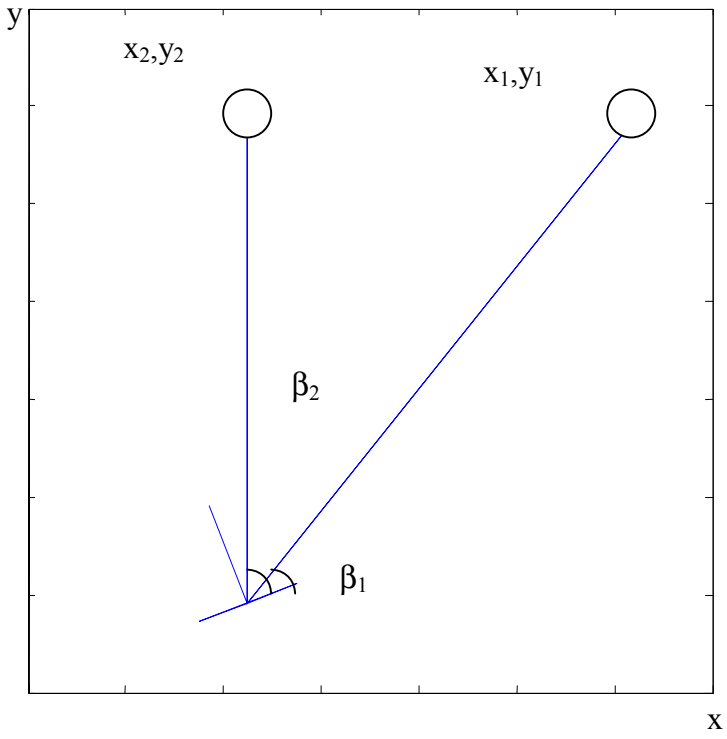

Figure 5.2 Computing robot pose using two vertical cylinder landmarks.

The above problem is over-determined, and includes another solution where the last two rows in Eq. (31) are written to trunk 2. An optimal solution for the robot's position and heading can be computed by using all recognized vertical cylinder landmarks and an optimization method.

Errors in landmark position, viewing angle, and range have an effect on the robot position accuracy.

Eq. (31) requires that both trees have been identified. The value of the distance between a tree trunk pair can be used for identification. The value of the distance between every tree trunk pair in map E, shown earlier in Fig. 4.9, has been computed. When the robot laser range finder detects tree trunks, distances between tree trunks can be computed and compared to reference values based on map E.

In trial no. 18, the robot was not moving during the first 12 laser scanning measurements and several trees were found. The distances between the detected trees in first 12 laser scans were computed and compared to reference values. Table 5.3 shows the results

Table 5.3 Recognizing individual trees by using estimated distances between them. The reference distances are computed from map E.

Tree	Tree	Distance (cm)	Reference (cm)	Tree pair
A	B	146	148	1 and 8
A	C	792	796	2 and 8
B	C	759	766	1 and 2

From the above table, it is easy to conclude that A=8E, B=1E, and C=2E. The bearing and range as well the position of tree trunk centers in robot laser coordinates are shown in Table 5.4.

Table 5.4 The bearing, range, and position of trees in laser coordinates at robot initial position during trial 18.

Tree	Bearing (deg)	Range (m)	x (m)	y (m)
1 E	90.75	8.88	-0.12	8.88
2 E	134.0	11.01	-7.65	7.92
8 E	88.0	7.47	0.26	7.47

The 2D laser pose was computed in table 5.5 by using Eq. (31) and the detected tree pairs.

Table 5.5 Robot position and heading estimates based on three different pairs of tree trunk landmarks.

Tree pair	x (m)	y (m)	ϕ (deg)
1E and 2E	2.17	-6.15	0.5
2E and 8E	2.14	-6.17	0.6
1E and 8E	1.72	-6.14	3.8

The estimated heading based on trees 1E and 8E includes large error due to bad geometry. The fact that tree trunk 2 has large curvature in the vertical direction additionally causes position error.

The difference in bearing values to trees 1E and 4E is more than 40°. Figure 5.3 shows the robot initial heading based on these tree landmarks. The robot was not moving during the first 117 time instants. Because the geometry is not optimal, the repeatability of the heading estimate is approximately 0,5° as can be seen from Fig. 5.3. The variance of the heading estimate is larger when the angular distance between landmarks is less.

Based on the same landmarks, the robot's position is also computed in map E coordinates. As can be seen from Fig. 5.4, the variance in position is larger in x-direction than in y-direction because the landmarks are not in orthogonal directions. The most accurate position is obtained when the difference in landmarks bearing values is 90°. However, the position repeatability in this case is approximately 7 cm.

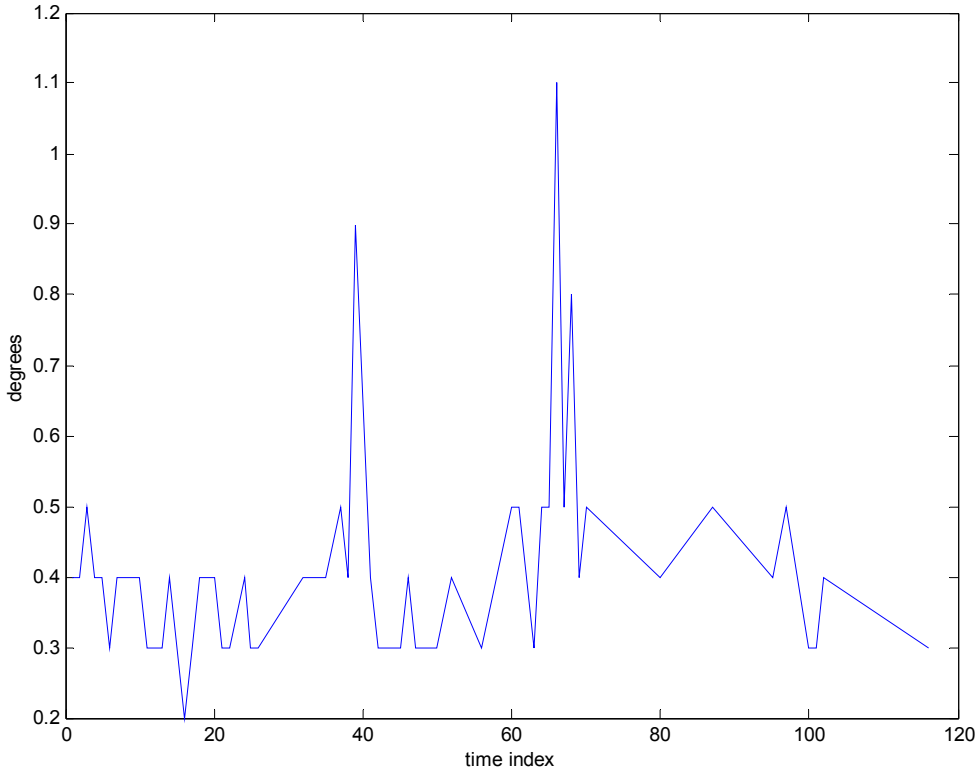

Figure 5.3 Estimated heading of the robot at initial position during trial no. 16. Heading estimation is based on estimated range and bearing values to trees E1 and E4. The robot is not moving.

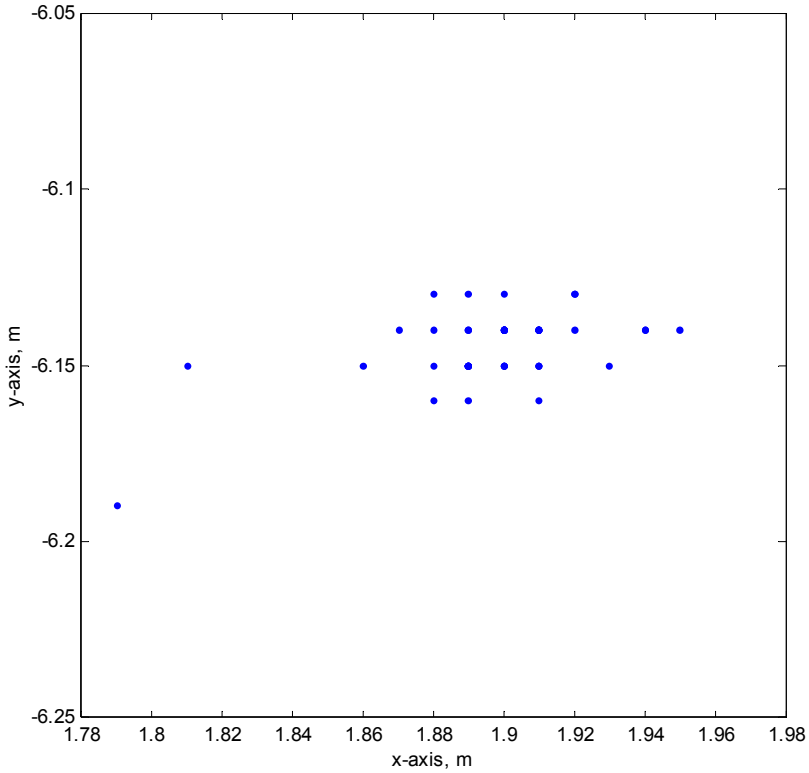

Figure 5.4 Estimated initial position of robot during trial no. 16. Position estimation is based on estimated range and bearing values to trees 1E and 4E at 58 different time instants.

5.3 Pose estimation based on a tree trunk and a wall

A wall and a tree trunk carry enough information for robot heading and position estimation. Let us assume that in the working environment, the 2D coordinates of a wall and several tree trunk centers are known. The robot is able to measure the distance to the wall and at least to one tree. It is assumed that the wall is identified but the tree is not. The robot can compute its heading from the wall heading, and additionally the robot knows its distance to the wall. The distance between the observed tree and the wall can be computed as follows:

$$d_{tw} = d_w - d_t * \cos(\beta_t - \alpha_w) \tag{32}$$

where d_w is distance between the robot and the wall, d_t is distance between the robot and the observed tree, α_w is the angle of the wall normal obtained from the Hough transform and β_t is the viewing angle of the observed tree trunk center.

Table 5.6 shows distances between modeled tree trunk centers (map E) and the west wall of the Computer Science Building Process Hall. The geometry can be seen from Fig. 4.16. Table 5.6 is used to recognize individual trees.

Table 5.6 Distances of trees to the west-side wall of the Process Hall based on the mapping laser range finder.

Tree	1	2	3	4	5	6	7	8
Distance(m)	11,68	10,76	12,93	11,21	13,85	16,17	11,11	10,24

In trial no. 27 (26.10.2001), the robot detected a wall at a distance of 4,57 m and a bearing of –2,5°. A tree was observed at a range of 8,70 m and a laser bearing of 161,5°. Using Eq. (32), the distance between the observed tree and the wall was estimated to be 12,93 m. The observed tree was identified to be 3 E because the estimated range was same as the value in Table 5.6 for tree nr 3. In this case, the distance measured by the mapping laser and the robot laser were equal with 1 cm accuracy. The smallest difference between tree and wall distances is equal to 10 cm (trees 4 and 7). Therefore, a unique solution can be found from Table 5.6 when the distance error between tree and wall is less than 4 cm.

The robot initial position in trial no. 27 can now be computed. In map E, the wall of the process hall is modeled as y=-8,95 m. Therefore, the robot position is equal to –4,38 m (-8,95+4,57). The robot heading is 90°-2,5°=87,5° according to Eq. (33).

$$\hat{\phi} = 90^\circ + \alpha_w \tag{33}$$

where α_w is the direction of the normal axis of the wall.

Figure 5.5.a shows one horizontal scan made by the mapping laser range finder from tree 3 E. Figure 5.5.b shows the range measurements made by the robot laser range finder from the same tree.

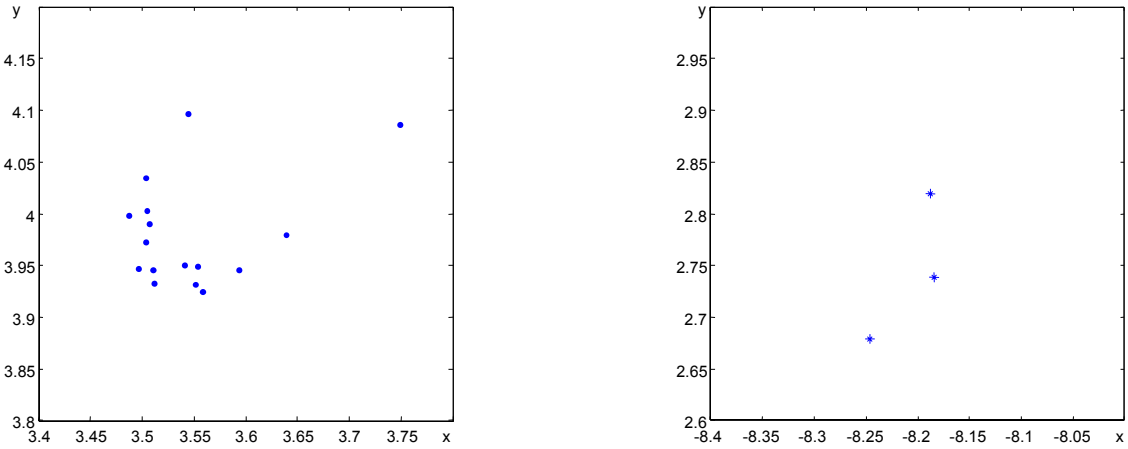

Figure 5.5 The horizontal position of reflection points on the surface of tree trunk 3 E by using the mapping laser range finder (Fig. 5.5.a) and robot laser range finder (Fig. 5.5.b) in laser fixed coordinates. In both figures, the laser views the tree from the coordinate origin.

The robot laser range finder is more accurate in range measurement, and the form of the circular arc can be seen more clearly (Fig. 5.5.b). However, the bearing resolution is smaller in the robot laser range finder. The mapping laser range finder noise in range measurement is 3,5 cm (standard deviation), and the extraction of circular arc requires curve fitting.

5.4 Matching successive laser range scans

A series of laser range measurements taken within a short period is known as a laser scan. Because of the short period, the robot does not have time to change significantly the heading or the position.

The raw range measurements together with the respective bearings can be transformed from polar coordinates to the Cartesian coordinates. The reflection points form a 2D map of the objects.

The laser range finder fixed on a robot and connected to a computer is able to form such maps. When the subsequent pair of maps are taken within a short period, they include partly the same objects. By rotating and translating the later map with the amount equal to robot movement, the common objects in the maps match each other. Respectively, the best match of two maps can be searched by rotating and translating the later map relative to the earlier. If the objects in the maps form a unique pattern, then the solution is the same as robot rotation and translation. The number of common points in matching reduces when the movement of the robot between two successive laser range scans increases. Change in heading affects more than change in position.

The maximal angular and linear velocity of the robot can be used to limit the rotation and translation search space, which is extremely important because too large a search space can generate multiple local optima in correlation. In the following test trials, the search space is limited to surge and yaw direction. Because of the relatively large turning radius (4 m), low speed (<0,6 m/s), and short measurement period (<1 s), the movement in sway direction is

negligible. Therefore, the motion in sway direction is computed as a function of the surge motion and yaw angular motion (Eq. 18).

The angular rate of the centaur robot heading was observed to be less than 26°/s, and the robot's velocity was less than 0,7 m/s. The onboard navigation computer (400 MHz) is able to search in real time the rotation from –18° to 18° in 0,5° steps, and the translation in surge direction from –0,7 m to 0,7 m in 0,1 m steps. However, such a large search space in rotation has occasionally caused wrong matches. Therefore, the rotation search space is restricted around the rotation predicted by using the heading gyro. The correct robot heading is usually within 5° of the gyro heading, and maximally within 18°. As the gain of the Murata piezoelectric gyro, a value of 22 mV/(°/s) was used. The zero level of the gyro was almost constant within a trial, and it was equal to 2488 mV in trial no. 16, and 2500 mV in trial no. 18. Figure 5.6 shows the matched rotation angle relative to gyro angle change (trial no. 16).

The step size in location search was equal to 10 cm and in rotation 0,5°. If the matching error is uniformly distributed, the standard deviation of the location error is equal to 2,9 cm/match, and the standard deviation of the rotation error is equal to 0,14°/match. Assuming these errors were independent, the standard deviations of these errors were after 720 matches (in trial 18) 0,8 m and 4°. These values give the lowest limit obtainable in accuracy. In practice, the heading error is the main cause of position error, as is shown in Eq. (34)-(35).

The search space in surge direction was selected as (-0.7 m, 0.7 m) in 0.1 m steps. The search space in the yaw direction is around the heading predicted from the previous heading. Table 5.7 shows the search space around the heading predicted by the gyro. If a narrower search space is chosen, then some correct matches are missed; and if a wider search space is chosen, then the matching problem becomes an optimization problem where there are more than one almost equally good match.

Table 5.7 The required heading search space in successive laser range scan matching as a function of gyro angular speed.

Gyro speed	Search space
<2°/s	5°
<7°/s	10°
>7°/s	18°

In Figure 5.6, the robot heading angle increments are computed by matching two successive laser maps.

Computing one estimation cycle takes about 700 ms with the present hardware. Additionally, the serial communication of the laser scan measurements takes over 200 ms. Therefore, the computed robot pose is actually about 1 s old. Wheel based odometry can be used to predict the robot pose to current time.

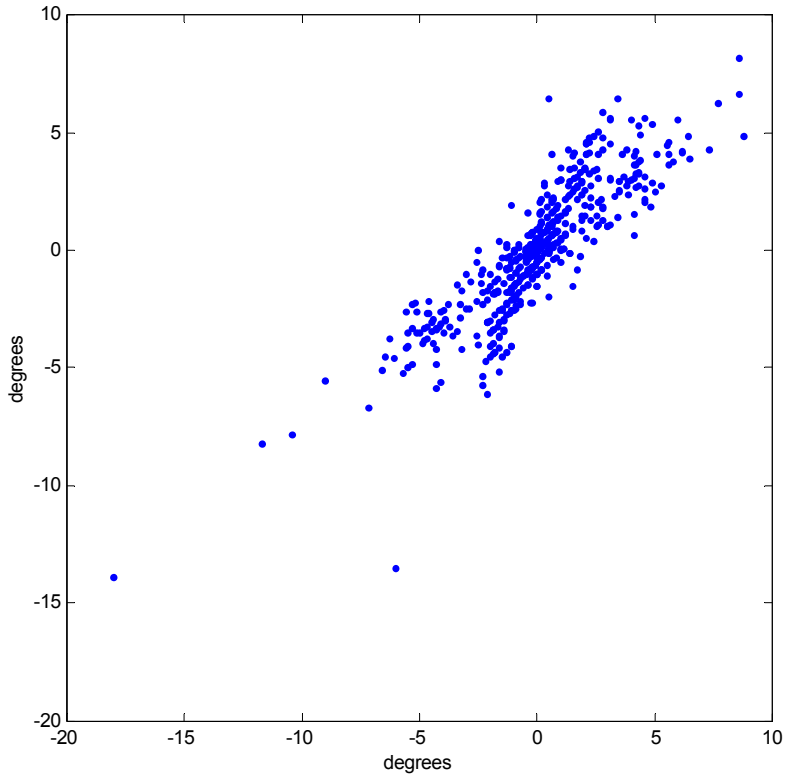

Figure 5.6 Heading angle difference between two successive laser range scans as a function of respective gyro angle difference. Measurement update period is approximately 0,7s and the units are in degrees.

The error in position and heading is accumulated in every laser scan match. The error in position chiefly originates from the wrong heading value. An error in heading angle accumulates to position mainly in the direction orthogonal to the direction of movement, as can be seen from Eq. (33)-(34). When the robot has been moving for a period equal to T, with a velocity equal to v, and a heading error equal to $\Delta\phi$, then the position error in direction of motion is

$$v * T * (1 - \cos(\Delta\phi)) \approx v * T * (\Delta\phi)^2 / 2 \tag{34}$$

Position error orthogonal to moving direction is

$$v * T * \sin(\Delta\phi) \approx v * T * \Delta\phi \tag{35}$$

The approximations in the above equations were obtained by assuming heading error to be typically less than 0,1 radians or 5,7°.

5.5 Accuracy of matching laser range maps

Test trial 16 was conducted on May 9, 2001 and lasted approximately 8 minutes. The measurement update period was approximately 0,7 s. The environment included cars in parking places, trees, bushes, and a university building. Human moving objects were removed automatically from the raw laser data before successive scan match. Detection of human targets will be presented in Chapter 6. The local coordinate system was adopted from laser map E shown in Fig. 3.6. The main coordinates of this system are in the direction of the outer

walls of the building. These walls have been used as landmarks when evaluating the error in position and heading of the robot originating from the matching of successive laser range scans. The robot is able to see the wall only occasionally. The error in heading estimate can be computed only when the robot can see a wall (Fig. 5.7). The accuracy in wall direction is approximately 0,25° and in distance approximately 1,5 cm.

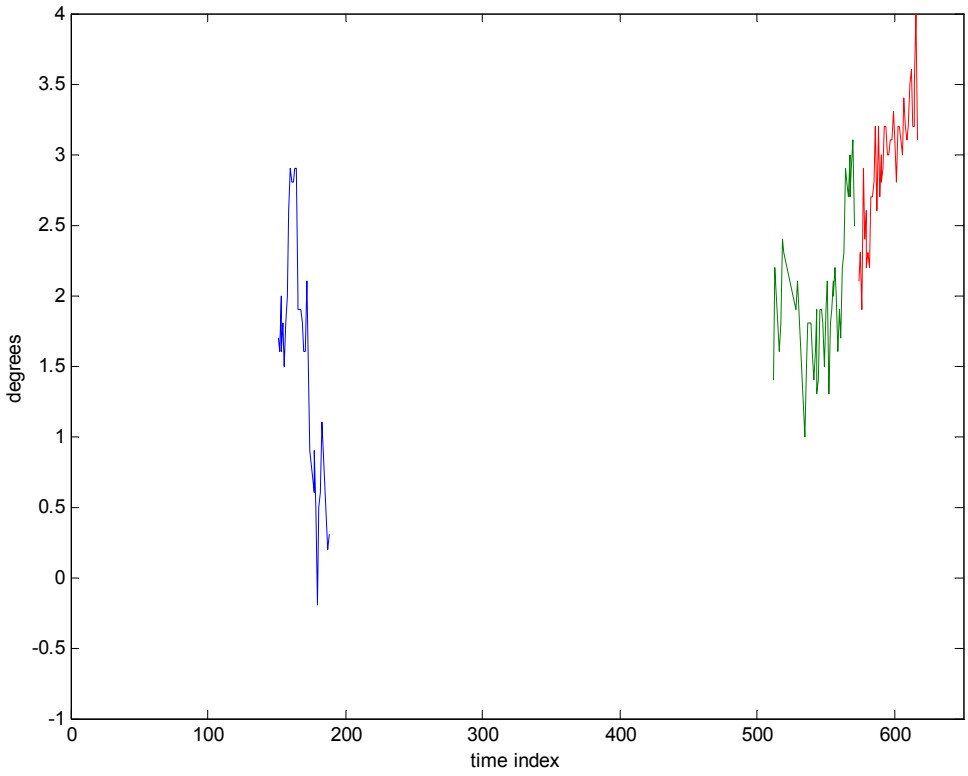

Figure 5.7 Heading error as a function time of index in trial 16. Wall lines extracted using the Hough transform has been used as the heading reference.

Let us assume that the heading error is modeled as a random walk. Then, the error variance grows linearly, and the standard deviation in square root. With curve fitting in the above figure, the standard deviation of the heading error is approximately as follows

$$s_\phi = 0{,}12^\circ \sqrt{i} \tag{36}$$

where i is the time index after initialization, and s_ϕ is the standard deviation of the heading error.

It is not a surprise that the heading error for each match is less than half of the heading resolution in matching. The laser beam width is equal to 0,7° and the heading search step size was equal to 0,5°. The standard deviation of the matching error in heading (Eq. 36) is approximately same as the theoretical standard deviation 0,14°.

Fig. 5.8 shows the values of the time index when the robot could see a wall during trial no. 16, and the position error normal to the detected wall.

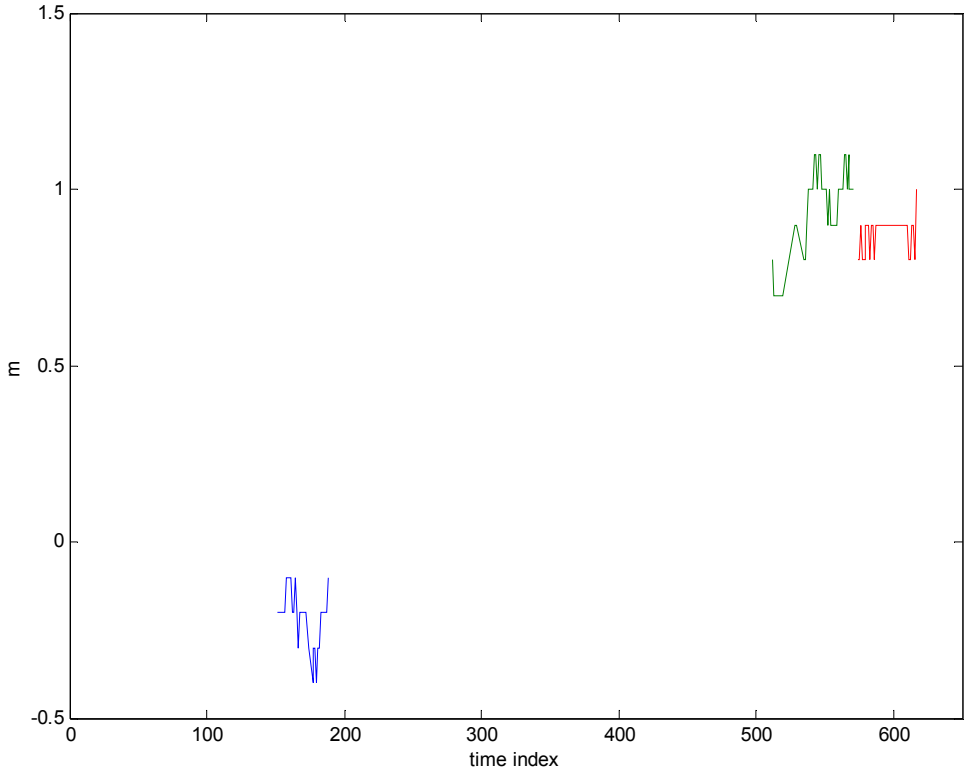

Figure 5.8 Position error based on successive laser range map matching in the x-direction (first two curves) and in the y-direction (last curve). Data is based on trial 16, and wall lines of map E have been used as position reference.

Table 5.8a shows the accumulated errors at seven time instants during trial no. 16. The initial position was computed by using trees 1 E and 4 E shown in Fig. 4.9 as landmarks. The errors were computed at six different time instants based on wall landmarks. The final pose error was computed based on pair wise matching of the first and last laser range scan.

Table 5.8a Accumulated error in successive scan matching in trial no. 16 computed by using walls as reference truth. The first map was used as reference at the final pose.

Time index	Reference	Heading error	Error in position x	Error in position y
0-151	Wall	1,7°	-0,2 m	
0-188	Wall	0,3°	-0,1 m	
0-512	Wall	1,4°	0,8 m	
0-571	Wall	2,5°	1,0 m	
0-574	Wall	2,1°		0,8 m
0-617	Wall	3,1°		1,0 m
0-639	First map	4,0°	0,29 m	1,1 m

The maximal angular speed of heading computed using the gyro occurs between time instants 171 and 172. The gyro estimate for the subsequent heading angle difference is equal to –13°,

and the best match is found with an angle difference of –6°. Reason for the difference between these estimates is the different sampling time instant. The total laser scan, consisting of 361 range readings, takes only 26 ms but the data transfer through serial line takes approximately 200 ms.

When the human targets were not removed from the laser scan data, the final error in heading was equal to 11,5°. Respective position error was equal to 4,66 m in y-direction and 0,52 m in x-direction. When moving targets are included in the laser range data, the estimation method may occasionally match moving targets instead of static features.

In trial no. 52, the laser scan matching period was equal to 1 s. The robot initial and final positions were estimated using the inner and outer walls of the Process Hall. The coordinates were fixed to an inner corner of the process hall.

Table 5.8b Accumulated error in successive scan matching during trial nr 52 computed by using the walls as reference truth.

Time index	Reference	Heading error	Error in x-axis	Error in y-axis
0-71	Wall	-1,8°	-0,98 m	
0-617	Wall	3,7°	-0,74 m	
0-725	Wall	1,7°	-0,64 m	3,25 m

Accumulated error does not essentially vary between the trials, as can be seen from Tables 5.8a and 5.8b. The error in the y-axis is remarkably higher than in the x-axis because heading error shows mostly as position error in the sideward direction of robot motion.

Because the error in heading and position grows without limit, the estimated position and heading should be corrected by using landmarks or satellite navigation during the mission.

5.6 Pose estimate correction

Structured landmarks such as walls, fences, corners, and tree trunks can be used to correct the errors in position and heading of the robot. In outdoor environments, the structured landmarks are not so common that pose can be estimated using structured landmarks alone. However, these landmarks can be used for correcting the position and heading drift.

It is a common situation in outdoor environments that there are no structured landmarks in view. Occasionally imperfect landmarks such as walls can be detected. When a wall is detected, the heading of the robot can be corrected. In addition, the position error in the direction of the wall normal can be corrected. Since the drift accumulates slowly in the pose, the estimated pose error should not be used to update only one pose but all the pose history.

When a robot makes a trip and returns to the start position, the accumulated drift can be corrected by matching the first and last laser range scan. This is usually a time- consuming task because of the large search space in map matching.

Table 5.9 The final position and heading error in successive scan matching when correcting with wall landmarks during the mission.

Time index	Reference	Heading error	Error in position x	Error in position y
0-639	First map	0,5°	-0,52 m	0,26 m

The estimated robot route during trial no. 16 is shown in Fig. 5.9. The robot's position and heading have been initialized using trees 1 E and 4 E as landmarks. The position and heading during the mission were estimated by using the method of successive laser scan matching. The accumulated position and heading errors have been corrected by using walls as landmarks. The time instants when the heading and one position coordinate are corrected can be seen in Fig. 5.7 and 5.8.

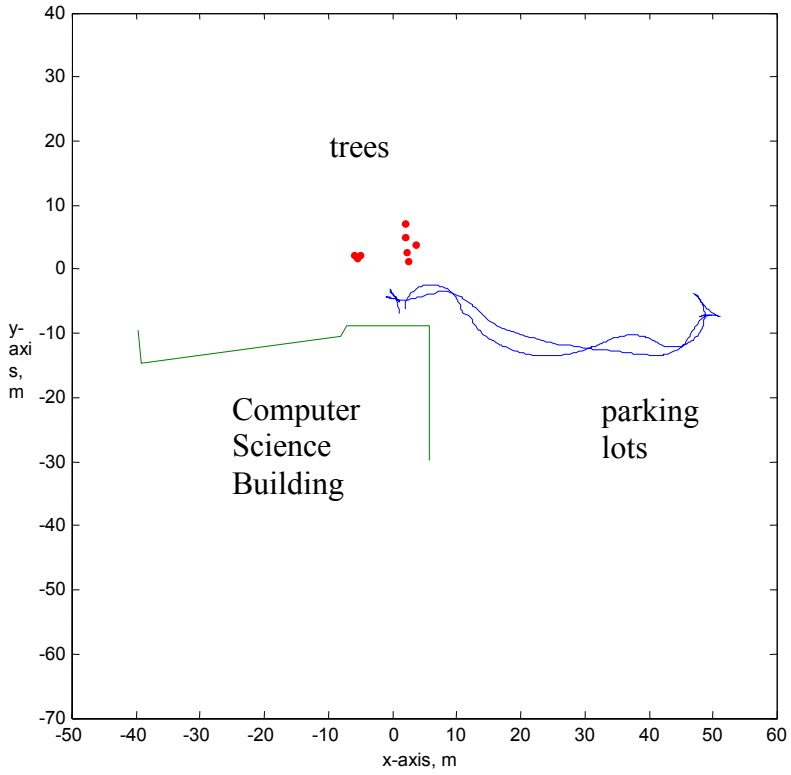

Figure 5.9 The estimated mission route in trial 16 based on the method of successive scan matching and correcting with walls and tree trunks as landmarks.

The initial and final position of the robot is between the trees and the building. The traveled distance is over 100 m.

5.7 Consistent matching of random outdoor features

In the method of successive laser range map matching the current map is compared to the previous map, which serves as a temporary reference map. The position and heading errors accumulate slowly in every laser range map matching because the temporary reference map is updated on every estimation cycle. As long as the temporary reference map is not changed, the position error does not accumulate. The initial position represents the reference truth when

computing the position error. Therefore, the temporary reference map made at initial position includes no accumulated position error. This can be utilized when the robot returns to its initial position [Gutmann and Konolige, 1999].

The search space in the method of non-successive range map matching is defined by the maximal accumulated position and heading error between the maps. The matching of two range scans is time consuming when a long time has elapsed between scans and the accumulated error is large. The common points in the range scans are maximized by choosing scans taken from approximately same place and viewing angle. Almost the same viewing angle is more important than the same estimated position because of maximal number of common points.

In order to make consistent maps of the environment, the accumulated error should be avoided. The accumulated position and heading errors at the final position can be removed by matching the initial and final laser range map. The entire mission can further be divided into shorter sub-missions where the reference map of the new sub-mission is built at the ending point of the last sub-mission. When the reference map does not change, the position error does not increase. A new sub-mission is started when the number of common points in the current map and the reference map falls under a certain limit. The initial map should be selected as the first reference map.

Table 5.10 shows the accumulated error at final position during trial no. 16, when the matching is based on a reference map that is changed infrequently. The reference map index is not increased until the number of common points in matching declines below 90. Fig. 5.10 shows the reference map index as the function of the current map index. Because the robot is not moving until the time index reaches 117, the error free initial map can be used as reference map for 125 matching cycles.

Table 5.10 The final heading and position in trial no. 16 when using same reference map as long as possible in matching. The penultimate line shows the heading and position computed by matching the initial and final map.

Map indexes	heading	x-position	y-position
0-639	-1,8°	1,85 m	-7,12 m
0 and 639	-4,3°	1,65 m	-7,13 m
error	2,5°	0,20 m	0,01 m

The reference truth was computed by matching the initial laser range map (i=0) and the final laser range map (i=639). The number of common points in initial and final maps was equal to 121. Therefore, the matching result can be considered as reliable. The position and heading error were accumulated less than in method of successive matching because the temporary reference map is not changed for each estimation cycle.

The increase in navigation accuracy when updating the temporary reference map less frequently is not always as good as shown in Table 5.10. The reason is that when using an older temporary reference map, the number of common points in map matching decreases. This increases the probability of erroneous matching results.

Position and heading estimation errors do not accumulate when the robot is not moving. However, the sensitivity to estimate change in position or heading is defined by the step size

in the matching algorithm. For example, a slow drift in heading is not detected if it is smaller than half of the step size in heading. The smallest possible value in the heading step value is limited by the laser beam width and bearing resolution.

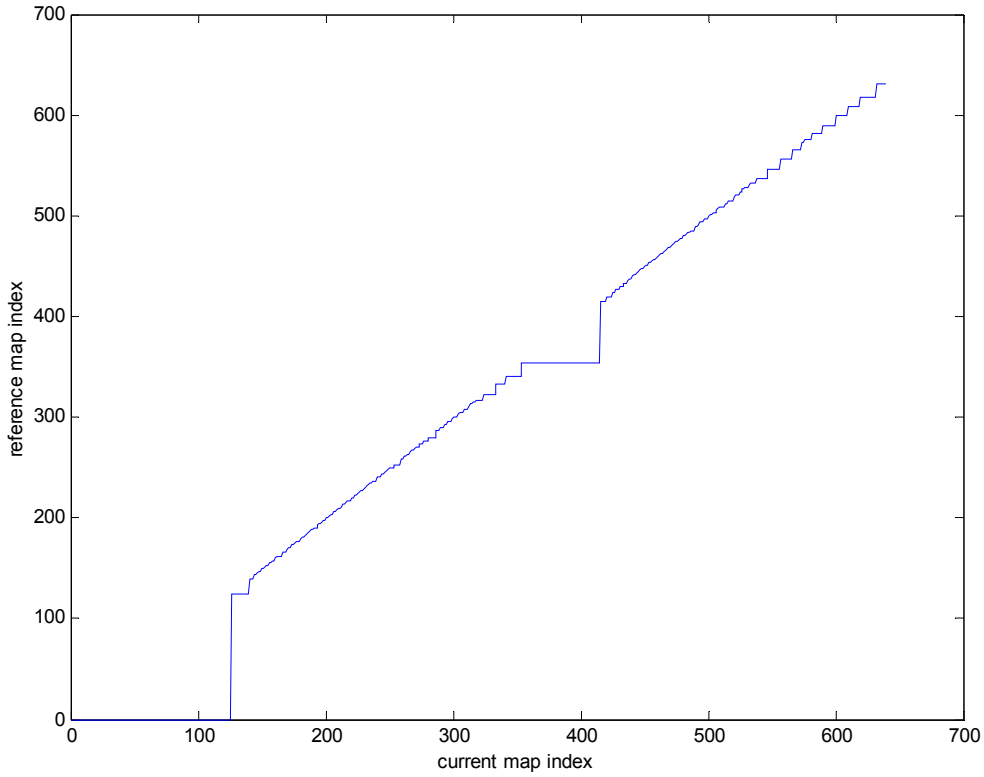

Figure 5.10 The horizontal axis shows the current map index; the vertical axis shows the reference map index in matching during trial no. 16.

5.8 Satellite based navigation

The WorkPartner robot uses a GPS receiver as an optional navigation device. The position accuracy of this receiver is equal to 16 m (Spherical Error Probability 50%) when position dilution of precision (PDOP) is less than 4. The velocity computation is based on the Doppler effect, and its accuracy is equal to 1 cm/s. These values are based on the manufacturer's operating manual. The velocity accuracy was also verified in practice (Table 5.11). The latitude degrees and minutes to north (N) and longitude degrees and minutes to east (E) in the GGA message are translated into meters from origin that is located at 60° 11 min N and 24° 49 min E.

At low velocities, the GPS receiver sets the value of the heading to zero. Therefore, the heading information is not reliable when the velocity goes below 0,2 m/s. Table 5.11 shows the measured velocity of the robot in trial no. 16.

Table 5.11 The mean and standard deviation of the robot velocity measured with a GPS receiver.

Time (s)	Velocity (m/s)	Std (m/s)	HDOP	No. of satellites
217-241	0,380	0,033	18,0-18,2	3
288-373	0,364	0,024	2,2-2,4	5
444-556	0,508	0,025	2,4	5

The standard deviation of velocity includes variation originating from robot speed control, and therefore measurement accuracy is better than the standard deviation. It is important to note that the horizontal dilution of precision (HDOP) has almost no effect at all on the accuracy of velocity measurement.

The heading value obtained from the GPS VTG message is compared to the wall direction obtained using the Hough transform. Table 5.12 shows results from trial no. 16 and 19.

Table 5.12 Standard deviation of GPS heading measurement by using a wall landmark as reference.

Time (s)	Std of hdg	Trial	HDOP	Nr of satellites
217-240	8,7°	16	18,0-18,2	3
531-544	3,2°	19	1,2	5

The accuracy of heading measurement clearly deteriorates when the value of HDOP increases. Therefore, the GPS heading measurement was used when the value of HDOP was less than 4.

Figure 5.11 shows the GPS heading error between time indices 441 and 600 in trial no. 16. The reference truth is computed using the consistency optimization method presented in Chapter 5.7. The heading error reaches values of up to 40°, and strong time correlation is evident. The large time correlated heading error was unknown for a long time. Finally, it was discovered that the heading error correlated strongly with the angular speed of the heading gyro. An obvious reason is that the GPS receiver computes the heading by averaging. When the robot turns, the averaged value lags.

The lag in GPS heading measurement can be corrected by using the following filter:

$$f(i) = 0{,}8 * f(i-1) + \Delta T * \left(u_g(i) - u_o\right) / g_g \tag{37}$$

where *f(i)* is the correction added to the GPS heading measurement, and ΔT is the measurement update period.

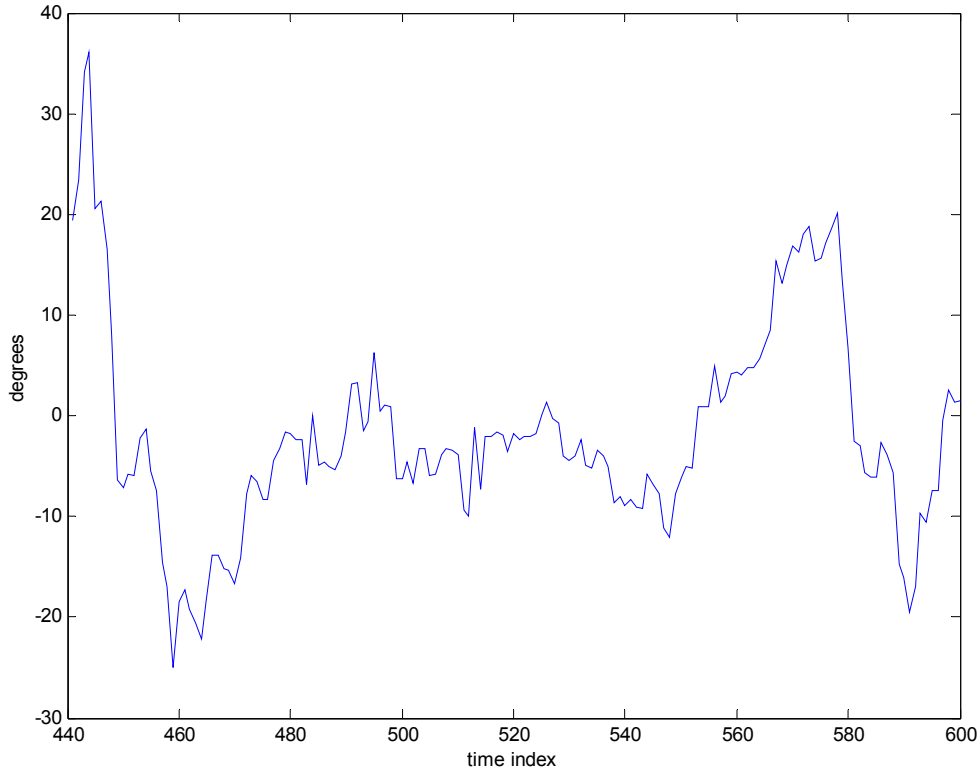

Figure 5.11 GPS heading error in trial no. 16. The vertical axis is in degrees and the horizontal axis shows the time index.

Figure 5.12 shows the GPS heading error after using the filter in Eq. (37). The error is significantly smaller after lag compensation. The standard deviation of the error of the filtered GPS heading in Fig. 5.12 is equal to 4°.

The lag compensated GPS heading can be used to reduce drift in odometry or in laser scan matching. Drift reduction is best done using a Kalman filter. The Kalman filter requires white measurement noise. Therefore, a noise shaping filter should be used [Maybeck, 1979]. The parameters of the linear first order heading error model were estimated (Eq. 38) using the expectation maximization algorithm (EM) [Shumway and Stoffer, 1982]. Heading estimated by the laser scan matching algorithm was used as the true heading.

$$\begin{aligned} e_\phi(i+1) &= 0{,}74 * e_\phi(i) + 2{,}43^\circ * w_u(.) \\ e_{GPS} &= e_\phi(i) + 1{,}21^\circ * w_u(.) \end{aligned} \tag{38}$$

where e_{GPS} is the GPS heading error after lag compensation, and e_ϕ is the part of the error that can be modeled.

It can be seen from Eq. (38) that the GPS heading error correlates with time, and is therefore colored noise. Model (Eq. 37) could be used to develop a noise shaping filter [Maybeck, 1979], which could reduce the heading error variance further. However, this time a constant gain Kalman filter was used to estimate the robot heading from gyro and GPS heading measurements. If GPS heading is used as the only heading measurement, then it is more important to use a Kalman filter extended with a noise shaping filter.

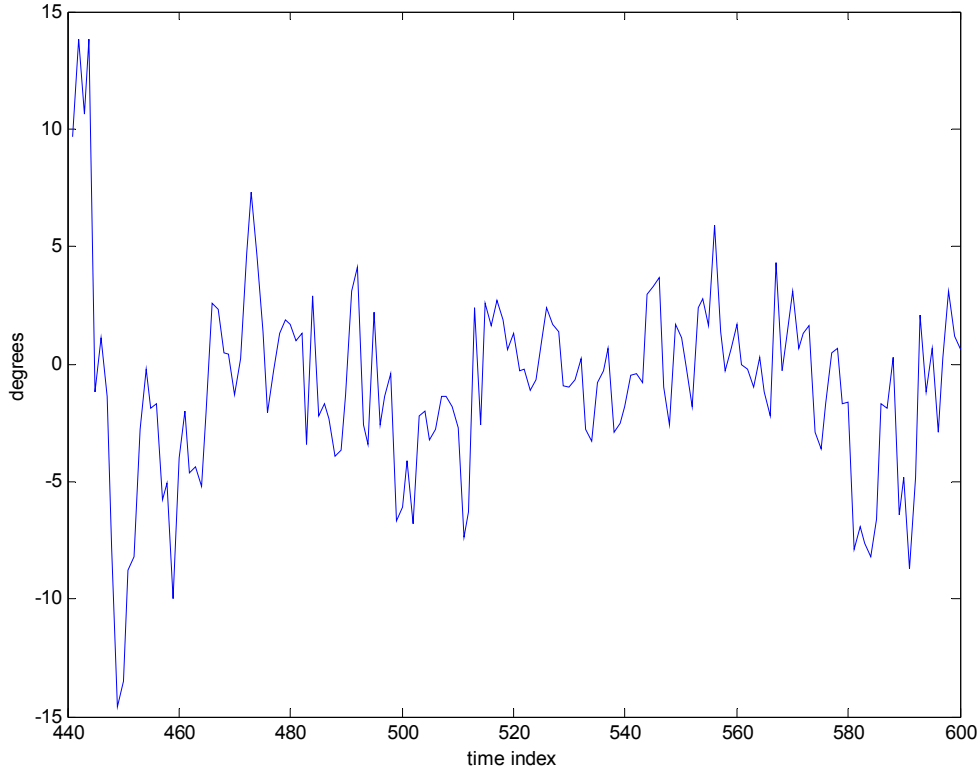

Figure 5.12 GPS heading error in degrees after lag compensation with cumulative gyro filter.

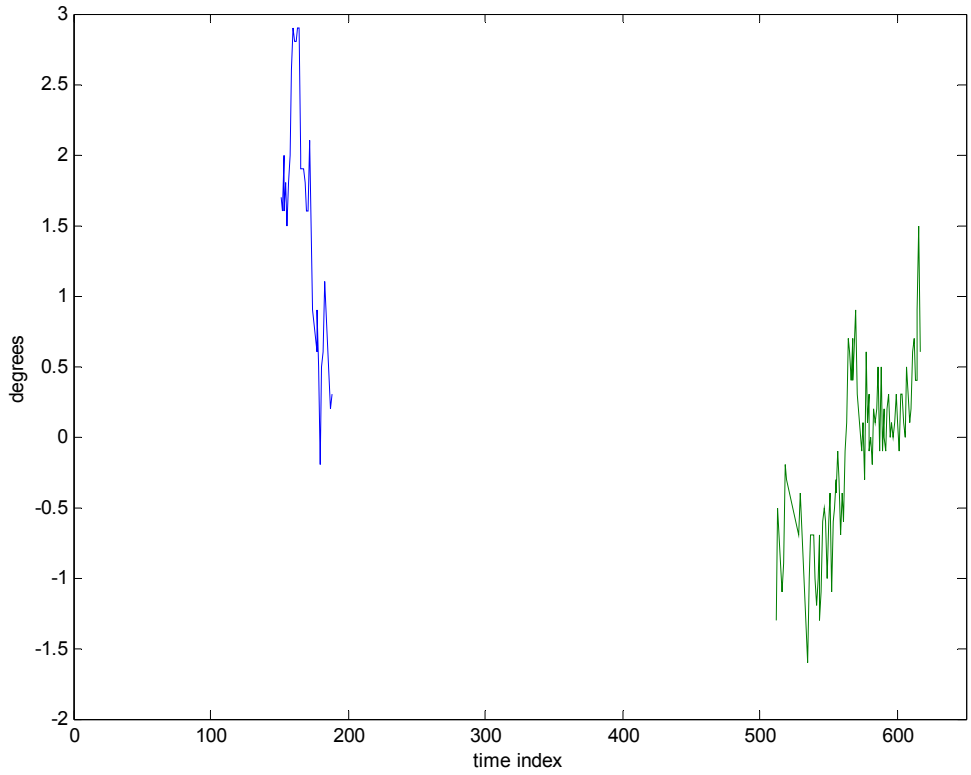

Figure 5.13 Heading error in laser scan matching when using walls as reference. The heading was corrected using GPS heading when available.

When the robot heading is estimated by the method of successive scan matching the filtered GPS heading is used to reduce the slow drifting of the heading. The used estimation gain was typically 0,01. Figure 5.13 shows the heading error, and Fig. 5.14 the position error components when using the method of successive laser scan matching and drift correction using GPS heading. When the robot occasionally sees a wall, this is used as a landmark. The position and heading error can be computed only when the robot sees the wall.

The estimation gain for the GPS heading measurement was equal to 0,01. The value was obtained by trial and error. The heading error with the drift reduction using GPS heading was smaller than without drift reduction (Fig. 5.7). However, the value of the estimation gain was too great because the error variance is larger than without drift reduction. The heading error between time indices 140 and 180 was not affected because the first satellite fix occurred at time index 217.

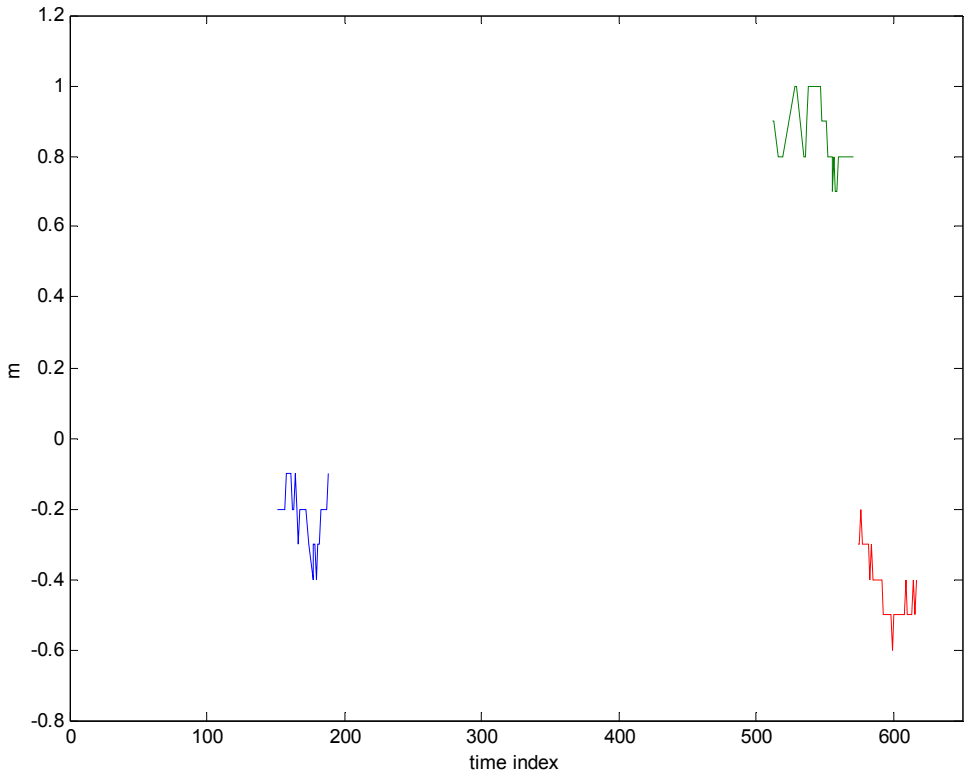

Figure 5.14 Position error in the x-direction (first two curves) and in the y-direction (last curve). The heading obtained by laser scan matching was corrected using GPS heading when available. The estimation gain for the GPS heading measurement was equal to 0,01.

The position error is clearly smaller when using drift correction using GPS heading. Figure 5.8 shows the position error without drift correction.

5.9 Adaptive navigation results

Matching of laser range scans requires features in the environment. In object free environments, satellite navigation should be used instead. The decision to change from laser

navigation to satellite navigation is based on the maximal number of common points in matching, and the quality of satellite navigation information.

GPS velocity and heading are used when the velocity is at least 0,3 m/s in two successive VTG messages, and HDOP is less than 4. Matching of laser range scans should be avoided when the number of common points in matching is less than 30-50.

The data acquired from trial 16 was used to verify the method. The data included 640 time instants. During time instants 287-372 and 443-600, the navigation was based only on gyro heading, GPS heading, and GPS velocity. At other time instants, navigation was based on laser scan matching. The estimation cycle is approximately 0,7s, and the gyro heading is corrected using the GPS heading with an estimation gain of 0,1. The gyro zero angular voltage is updated whenever the robot is not moving. The gyro gain was equal to 22,2 mV/(°/s). There were enough objects in the test trial, but they were not used when the GPS quality was satisfactory for testing the accuracy of the GPS heading and velocity. Figure 5.15 shows the heading estimation error of the robot when a wall can be seen.

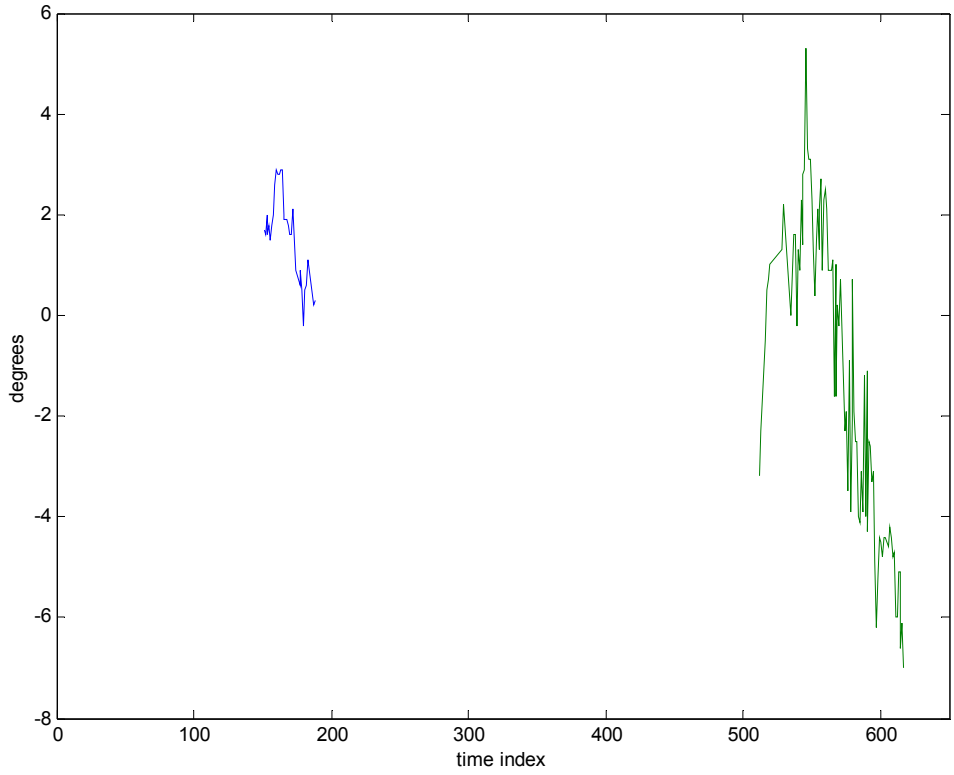

Figure 5.15 Heading error in GPS odometry. Walls were used as reference. Laser scan matching was used when fewer than three satellites were visible.

Heading error is essentially larger than with pure laser scan matching (Fig. 5.7). The route of the robot is shown in Fig. 5.9. Figure 5.16 shows the time index values when the GPS heading was used in estimation.

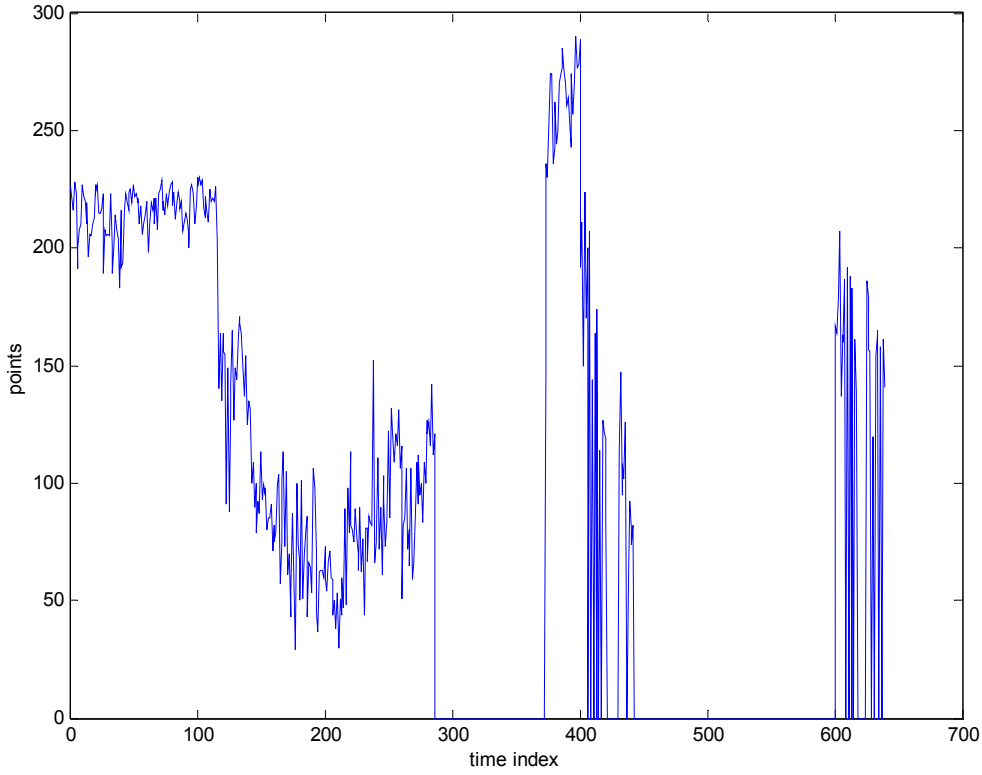

Figure 5.16 Number of common points in successive laser scan matching. A zero value shows the time index values when GPS velocity and heading were used.

Gyro and GPS based odometry is less accurate than the method of laser scan matching. Table 5.13 shows the heading and position error at time index value 639. In global matching, the first map was used as reference.

Table 5.13 The final heading and position in trial 16 estimated using GPS velocity and heading when available, and alternatively using the method of successive laser range scan matching. Reference is computed by matching the first and last range scan.

	Heading (deg)	x-position (m)	y-position (m)
GPS odometry	-5,4	-1,93	-5,64
global matching	-4,4	1,62	-7,11
Error	-1,0	-3,55	1,47

The above table shows clearly that the accuracy is not satisfactory in odometry based on GPS velocity and heading supplemented with gyro angular velocity. Maximal error in the heading was equal to 7° as can be seen from Fig. 5.15. This is partly because the used gyro is slow (7 Hz –3dB) and cannot respond to rapid heading changes. Although the heading is not very accurate, the GPS heading is non-biased, and therefore the long time position accuracy is satisfactory.

The rotation between the local coordinates and the NE coordinates can be estimated by computing the mean value between the robot heading in local coordinates and the GPS heading. The rotation parameter cannot be computed at the same time when the GPS heading

is used in heading estimation. In the above trial, the local coordinate direction equal to -70° from North was obtained from earlier experiments.

Figure 5.17 shows cumulative mean of the difference between robot heading in local coordinates and GPS heading during trial 16. The robot heading was computed by using successive scan matching. Additionally, robot heading was corrected by using walls as landmarks. GPS heading was corrected by using Eq. (37).

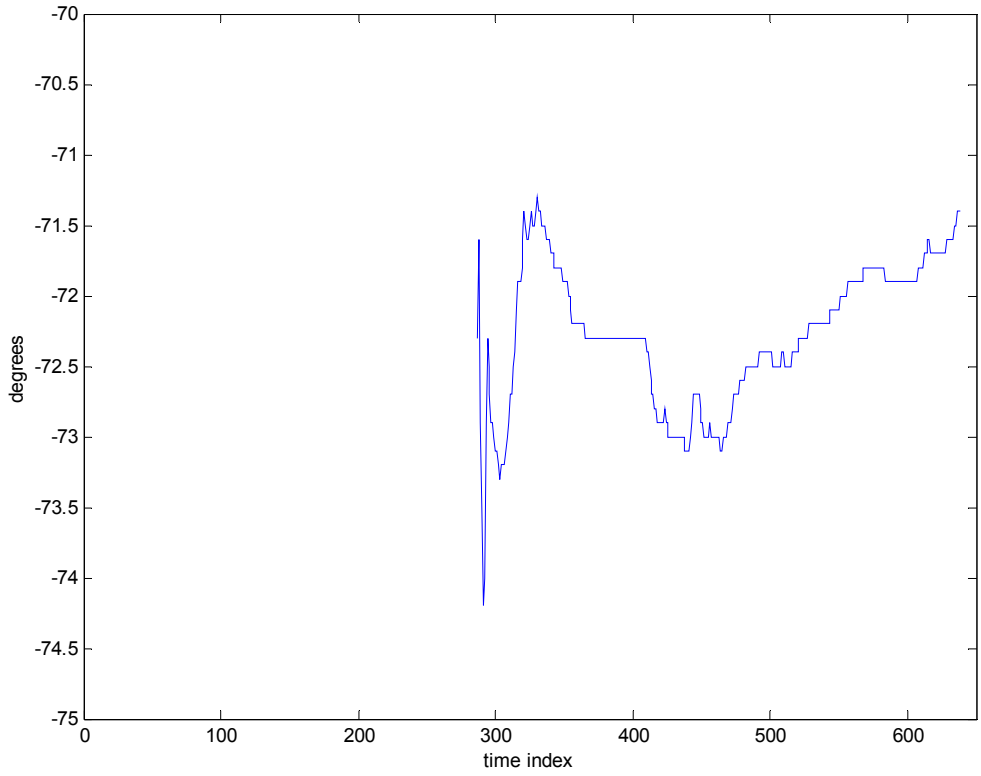

Figure 5.17 The estimated difference between robot heading and GPS heading.

The convergence is slow because the lag compensation (Eq. 37) is not able to remove all the colored error in GPS heading.

6 SLAM IN DYNAMIC ENVIRONMENT

A map of the environment is useful when an operator is defining a work task for a service robot. In previously unknown environments, simultaneous localization and mapping seems attractive [Guivant et al., 2000b]. A scanning laser range finder is an appropriate sensor for building maps. The resulting map is consistent if the scanning laser range finder is not moving during the scan. Consistency is lost when the map is based on several scans taken at different poses and there are errors in the poses. An inaccurate map may still be useful as a common concept for the service robot and human operator. For example, sailing on the sea has been based on inaccurate maps for several hundred years.

People walking cause undesirable traces on a map if they are not detected and removed in the mapping process. Detected human targets can further be used in operator following task. In unknown environment, the robot can learn a path by following an operator.

6.1 Detecting and tracking of moving targets

This chapter concentrates on detecting people moving at the same time as the robot is moving. The movement of the tracked people is estimated relative to the ground. Schulz et al [Schulz et al., 2001] have shown that it is possible to identify and track moving targets. Different targets usually give different responses when scanned with a laser range finder. The human target was assumed to resemble a continuous line with a typical length. Additionally, the target must have a slight curvature to distinguish people from walls and cars. The following rules were used to detect a human target:

$$\begin{aligned} &\Delta r < 0{,}13m \\ &0{,}35m < o_w < 0{,}85m \\ &0{,}06m < \Delta^2 r \end{aligned} \tag{39}$$

where o_w is the computed target width and Δr is the first order difference between two sequential range measurements to the target.

These values are based on statistics found when students and research scientist moved around the campus area. Because the angular resolution of the laser scanner is equal to 0,5°, a group of thin trees with the same width may give a similar response. Human targets have been detected by requiring that potential human size targets move relative to ground. In test trial nr 16, target candidates were detected by checking that the range measurements of one target were under 17 cm. A new position for a human target was assumed to be at a distance less than 1,2 m from the predicted position. The predicted position was computed by using last position and velocity estimates. A target was detected to be moving if the target position changed more than 0,25 m. In Table 6.1, the percentage of human targets from all potential candidates that have been detected to move a certain number of times at least 0,25 m is shown. Only 5% of potential candidates were human targets when there was no evidence of motion relative to ground. From potential candidates that have been detected to move one step, 43% were human targets.

Table 6.1 The percentage of human targets from all human like targets that have moved at least 0-4 times.

No. of moves	0	1	2	3	4
Human targets	5%	43%	77%	90%	100%

False target detections occur when there exist at least two human like targets and the distance between them is less than 1,2 m. Targets that did not move for 10 s were removed from the memory. The computations were done in the Earth fixed local coordinates. The target evaluation was based on the probability that the human like target was in fact a human one. The following model for probability that a target is human was assumed based on the above table:

$$p(o_i \mid m_i) = p(o_i \mid m_i - 1) + 0{,}4 * (1 - p(o_i \mid m_i - 1))$$
$$p(o_i \mid 0) = 0{,}05 \tag{40}$$

where $p(o_i|m_i)$ is the probability that target o_i that has moved m_i times is a human one.

Figure 6.1 shows the tracked positions of two persons in map E during trial nr 16.

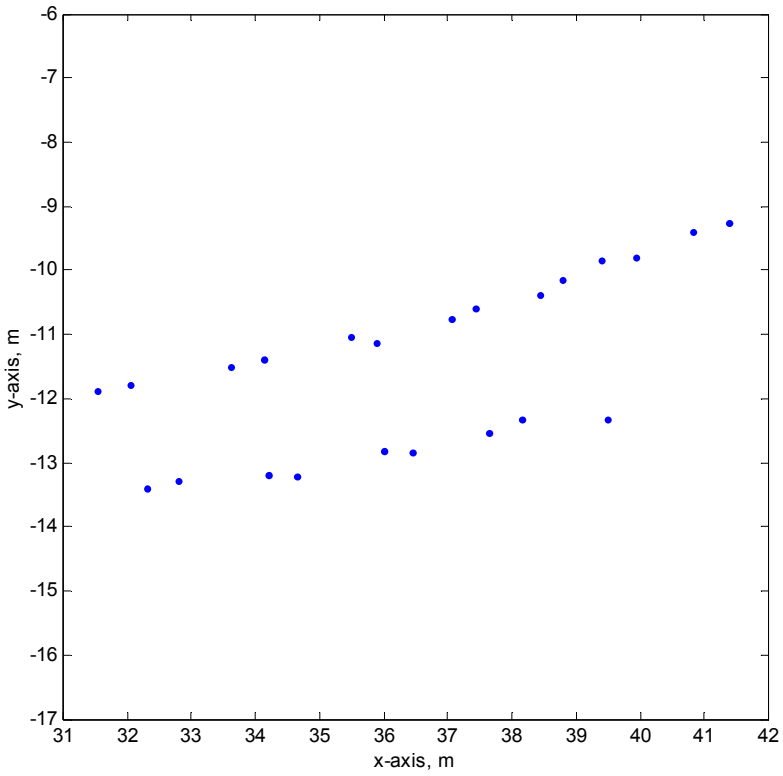

Figure 6.1 Positions of two tracked human targets moving to right in trial no. 16.

Figure 6.2 shows the direction of motion of the upper target. Estimation is based on sequential position values only. Figure 6.3 shows the estimated velocity of the target.

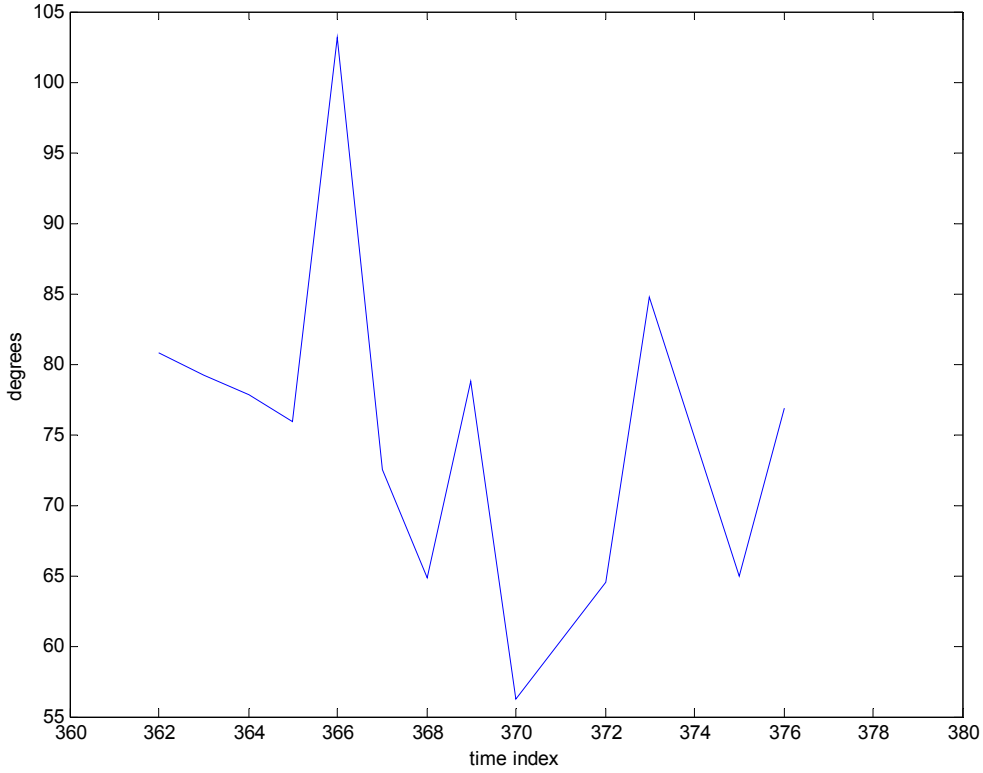

Figure 6.2 The estimated direction of motion of the upper target as a function of time index.

The traveled distance of the target oscillates in Fig. 6.3 because the estimation period oscillates approximately between 0.5 s and 1 s. The estimation period was set to 1 s but the delay function of QNX operated in a different way to that expected. The tracked human targets were only briefly inside the view angle of the laser range finder. However, the robot was able to follow a moving human target for a long period of time if such a task is set. Figure 6.4 shows the estimated position of the tracked human target in trial 52. Position is shown in the coordinates fixed on the inner corner of the Process Hall in the Computer Science Building. The zero heading is the same as in the coordinates fixed on pose E. The position of the inner corner is (5.31,-9.31) in the coordinates fixed on position E. The target has been assumed to move at most 0,7 m/s. However, if the target cannot be found within 4,9 m for 10 s, the target is cleared from memory.

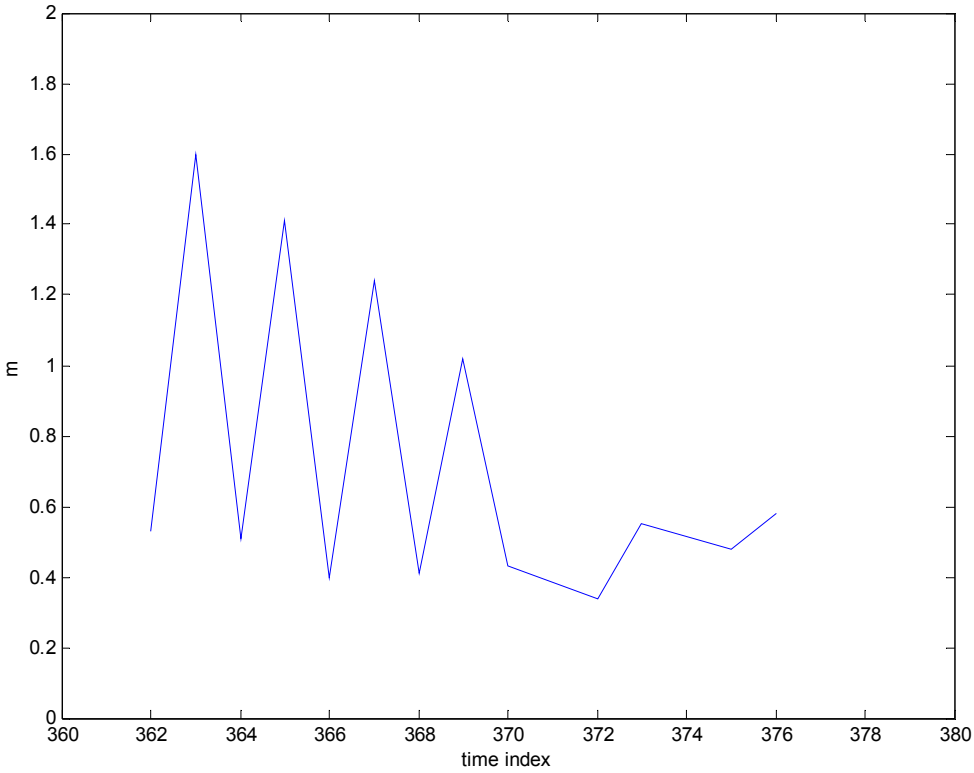

Figure 6.3 The increment of traveled distance of the upper target as a function of time.

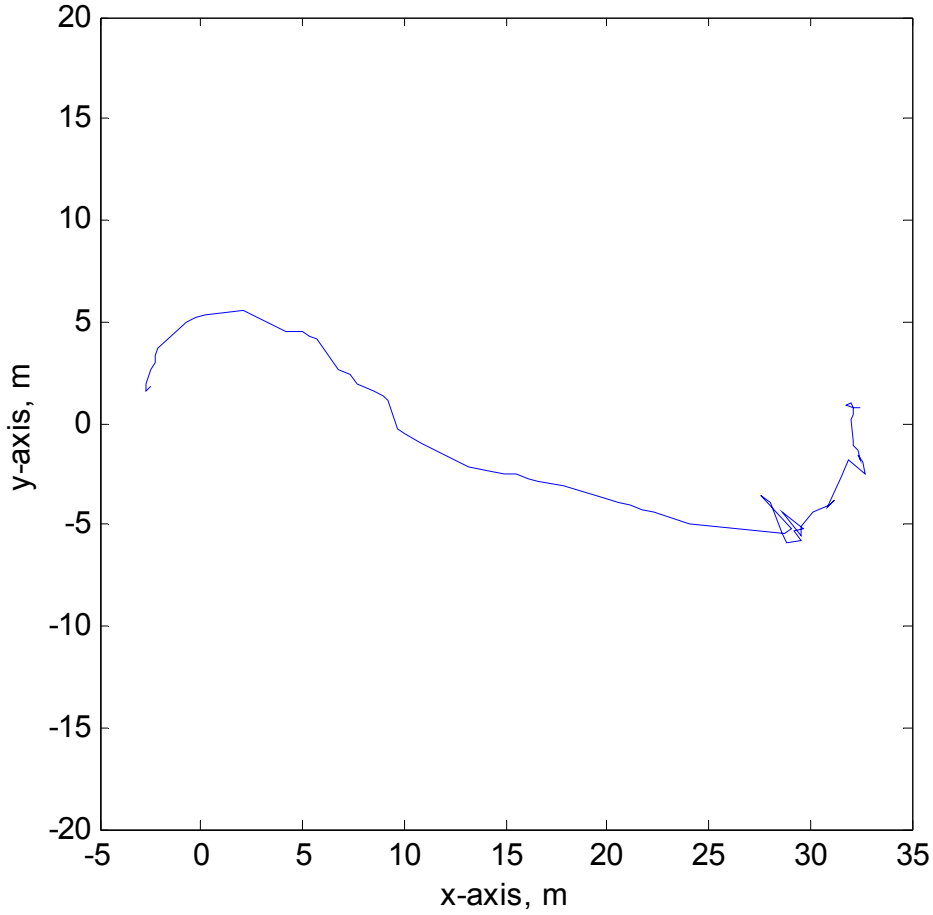

Figure 6.4 Route of a tracked human object in trial no. 52.

Figure 6.5 shows the direction of motion of a tracked human target in trial no. 52. The coordinate system fixed to pose E defines the zero direction.

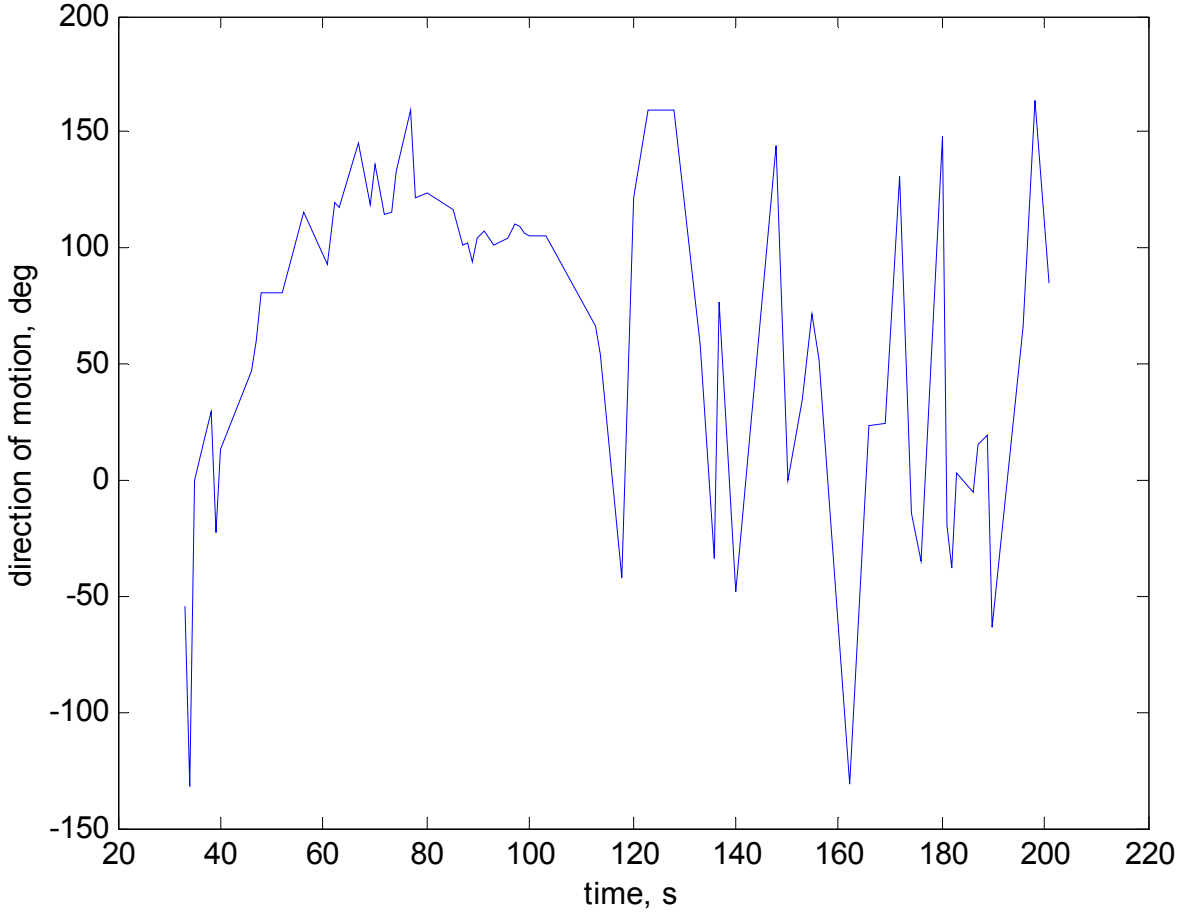

Figure 6.5 Estimated direction of motion of tracked human target in trial 52.

Figure 6.6 shows the estimated velocity of a human target relative to ground in trial no. 52. The velocity estimate deteriorates when the target is not seen every second. The target has not been inside the viewing angle of the laser scanner between 104 s and 112 s.

Parameters such as human target width and maximal velocity were applied in a typical trial situation. For more common use, these parameters should be checked against particular situations.

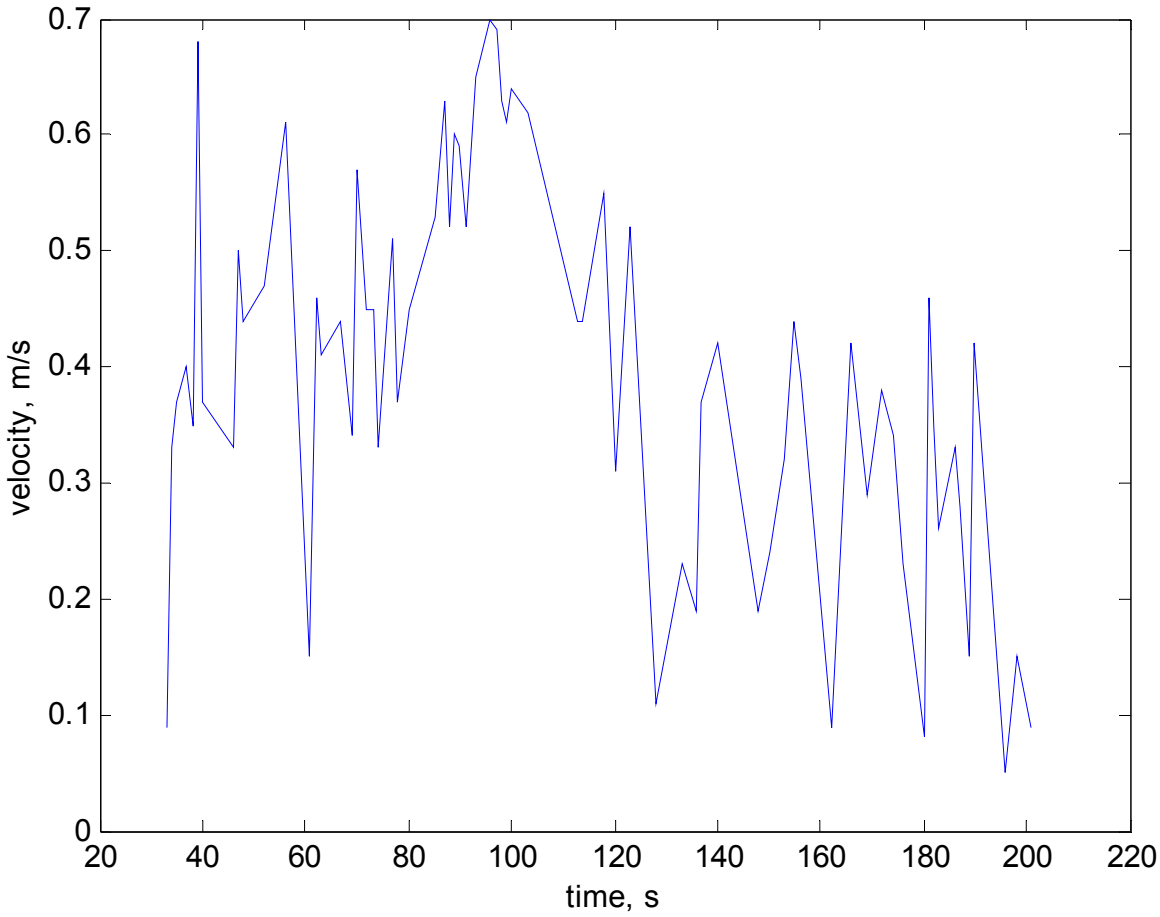

Figure 6.6 Estimated velocity of a tracked human target in trial no. 52.

6.2 Simultaneous localization and mapping

When a mobile robot operates in the working environment, a map is needed so that the work tasks can be defined. In certain cases such as autonomous cars driving on motorways, there is usually a map available. With mobile robots, it is usually too restrictive to assume that there exists a map of the working environment. Therefore, the only possibility left for an autonomous robot is that the robot itself builds a map when it first operates in the working environment. The mapping task requires that the robot knows its position relative to objects in the environment. Simultaneous localization and mapping has been extensively studied, for example in [Guivant et al., 2000b].

A mapping laser range finder that is able to see up to 350 m and to view 330° is ideal for making a consistent map of the environment. Figure 6.7 shows such map made by using a mapping laser range finder in the university campus area.

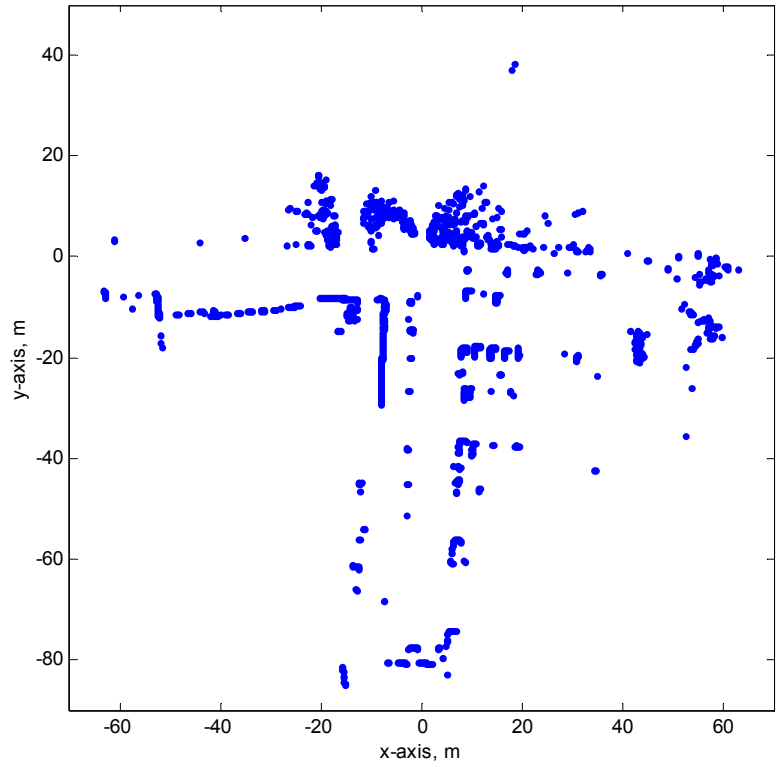

Figure 6.7 Map F based on one horizontal laser range scan (mapping laser). Coordinates are fixed on the laser position.

When the viewing angle of the laser is smaller, a map cannot be made based on a single laser range scan. However, a series of smaller laser range maps can be fused together to obtain a bigger map. A serious problem in fusing maps is the lack of consistency. Perfect consistency requires that all laser range finder positions and heading values are known at the time of scanning time. In practice, when the robot is moving, some error in position and heading accumulates that compromises the map's consistency. Thus, the same object is written many times to slightly different positions. If the position error is known, then multiple objects can be rejected from the map by checking the distance between the old object and a new candidate. The new object candidate is assumed to be identical to the old one if the distance between them is smaller than the position error. By rejecting objects in this way, some true objects are missed from the map. The consistency of the fused map is kept high by using the method presented in Chapter 5.7. Figure 6.8 shows a map that is based on fusing 720 laser range maps in trial 18. The final position error in the direction of the x-axis was equal to -0,53 m and in the direction of the y-axis it was equal to –0,13 m. Moving targets such as people were rejected from the map.

The error in position and heading estimates of the robot during mission causes distortion in the map shown in Fig. 6.8. However, the accuracy of the map may be sufficient for some service robot tasks. For example, the target position accuracy equal to 1 m is sufficient to find a box that should be grasped.

Figure 6.9 shows a map that is based on fusing 640 laser range maps in trial 16. A point was written to the map when it exists in two consecutive sub-maps and the distance between points is less than 0,2 m. The robot trajectory was computed by using the method presented in Chapter 5.7. The maximal position error during the trial was equal to 0,4 m when using walls as the reference.

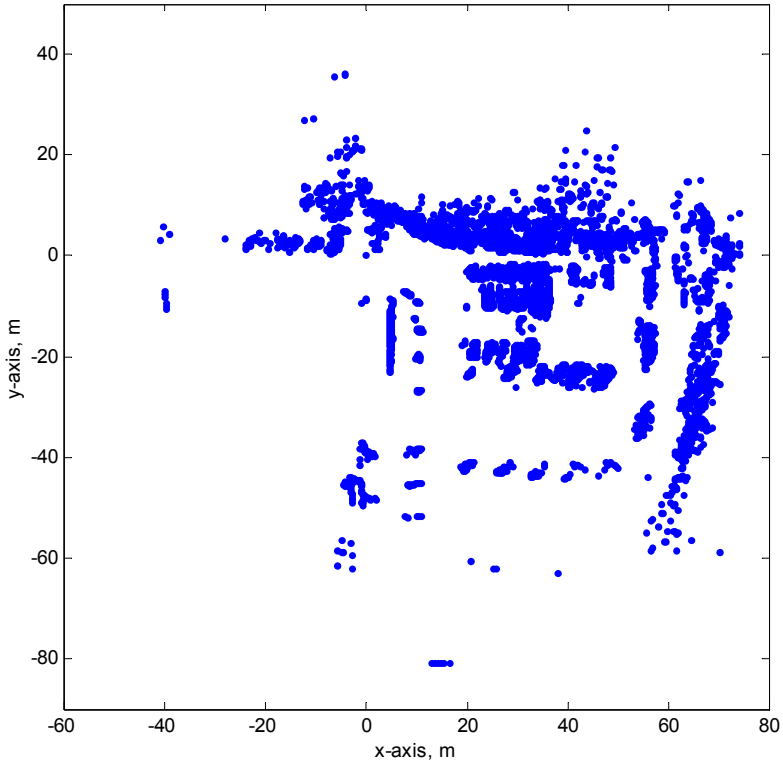

Figure 6.8 Map based on 720 successive sub maps in trial no. 18.

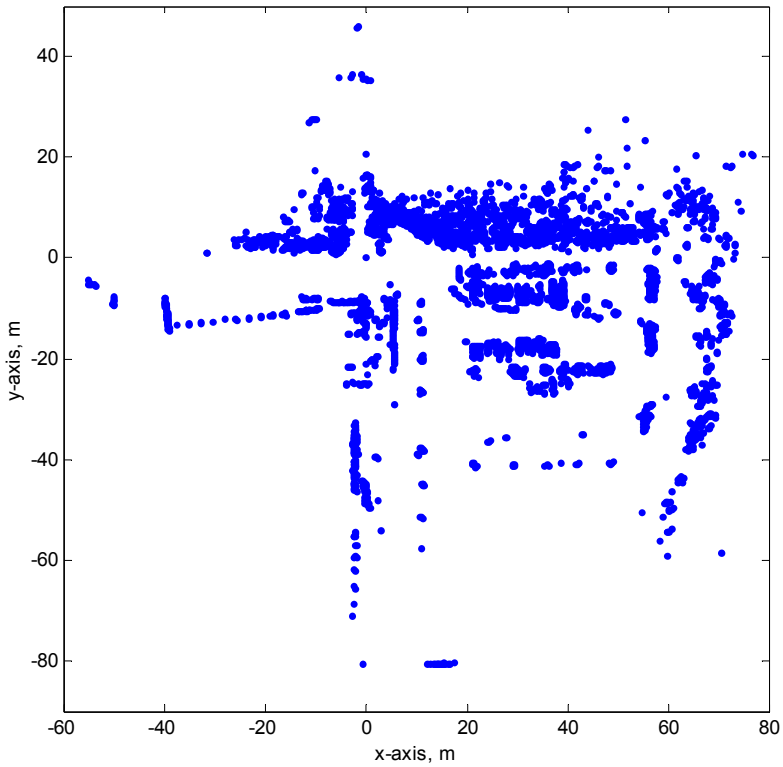

Figure 6.9 Map based on 640 successive sub maps in trial no. 16.

Persons that are standing are included in the map. Figure 6.9 presents the same area as in Fig. 6.7.

7. SUMMARY AND CONCLUSIONS

This work has presented an adaptive navigation system for outdoor mobile robots operating in unknown environments. Matching of successive laser range maps is used when the environment does not include known landmarks. Conventional wheel based odometry is not needed because the matching method is a global optimization method by nature. The method has an important advantage over to the wheel odometry. It is namely insensitive to slipping of wheels or other similar inaccuracies in kinematic calculations. A 2D horizontally scanning laser range finder has been used as the principal sensor. The navigation method has been verified in an environment that consists of trees, bushes, lampposts, walls, and cars. The successive laser range map matching, known as laser odometry, produces errors that grow without limit. The laser bearing step-size defines the incremental heading estimation error. The position and heading error is typically zero mean and behaves like a random walk. Error in the heading estimate is the main source of the position error.

In cyclic navigation tasks, the accumulated error in position and heading can be corrected by matching a perceived laser map with one built earlier in the vicinity of the current pose. Map matching is done in 3DOF search space including position and heading. Matching in 3DOF is not generally possible in real time because of the magnitude of the robot position and heading uncertainties. The method based on divide-and-conquer search will be tested in the future.

However, laser odometry is used only when there are no landmarks available. Occasionally the robot may recognize such landmarks as vertical cylinder objects or vertical planes. By using the Hough transform, the robot can estimate its heading with a 0,2° accuracy relative to a vertical plane. By using two orthogonal vertical planes, the robot position can be estimated with an accuracy of 1 cm. Vertical cylinders can also be used to estimate the robot position and heading. When the vertical cylinders are located in an orthogonal direction from the robot, a typical position accuracy of 0,1 m can be achieved. The accuracy of the heading estimate is better than 0,5° when using orthogonal vertical landmarks. When using landmarks, their position must be known in some local coordinates. A laser range finder has been shown to be an accurate sensor for making a consistent model of vertical cylinder and vertical plane landmarks.

Laser odometry or landmark navigation cannot be used in open fields. GPS velocity and gyro aided GPS heading can be used for navigation in such featureless environments. GPS heading error is colored noise that grows up to 40° because of low pass filtering used in the receiver. Gyro based prediction filter was used to minimize the GPS heading error. Kalman filter has been used to fuse angular gyro and GPS heading.

The navigation system was able to choose automatically the best navigation method depending on the structure of the environment.

The developed method has been verified with a centaur type WorkPartner robot in a University campus area. The robot motion range has been used in laser scan matching to reduce the required calculations. In addition, the limited search space minimizes the risk of erroneous matches. The initialization of the robot position in previously known coordinates has been verified by using tree trunks as landmarks. Walls have been used as landmarks for position and heading error correction. The results have also been used in simultaneous localization and mapping.

The developed method runs in real time but is rather time consuming. When computer speed increases in the future, the robot maximal velocity can also be increased.

People moving in the vicinity of the robot have been successfully detected by using the horizontally scanning laser range finder. The path of moving people has also been tracked. Neglecting moving objects from the laser range finder view decreases the possibility of making erroneous matches. Human target tracking is also required when the robot follows an operator.

Recognition of individual landmarks is still mainly based on an approximate knowledge of robot position. Often relative position between landmarks can be used for the identification. Reliable recognition of individual natural landmarks such as tree trunks remains a challenging task. This is particularly true when the distance between landmarks is less than the position error of the robot.

Bluetooth chips are now used in mobile phones and some car tires. In the future, mobile robots will be able to recognize such objects as people and cars by using wireless Bluetooth communication.

A great challenge in the future will be outdoor navigation in true 3D environments. Managing true 3D environmental landmarks in real time requires computers that are more powerful. However, I believe that this is a reachable goal in the next ten years because fast 3D laser scanners exist already.

REFERENCES

Arras, K. O. and Vestli [1998]. Hybrid, high-precision localization for the mail distributing mobile robot system. Proceedings of the 1998 IEEE International Conference on Robotics and automation, Leuwen, Belgium. Pp. 3134-3129.

Arras, K. O. and Tomatis, N. [1999]. Improving robustness and precision in mobile robot localization by using laser range finding and monocular vision. Third European Workshop on Advanced Mobile Robots, IEEE, 1999. Pp. 177-185.

Bailey, T. and Nebot, E. M. [2001]. Localisation in large-scale environments. Robotics and Autonomous Systems 37 (2001) 261-281.

Balaram, J. [2000]. Kinematic observers for articulated rovers. Proceedings of the 2000 IEEE International Conference on Robotics & Automation, San Francisco, April 2000. pp. 2597-2604.

Brumitt B., Stentz, A., Hebert, M., and CMU UGV group [2002]. Autonomous driving with concurrent goals and multiple vehicles: Experiments and mobility components. Autonomous Robots 12, 135-156, 2002.

Cooper, S. and Durrant-Whyte, H. [1994]. A Kalman filter model for GPS navigation of land vehicles. Proceedings of the IEEE International Conference on Intelligent Robots and Systems, Vol. 1, IEEE, 1994. Pp. 157-163.p

Corke, P. I. and Ridley, P. [2001]. Steering kinematics for a center-articulated mobile robot. IEEE Transactions on Robotics and Automation, Vol. 17, No. 2, April 2001. pp. 215-218.

Dellaert, F., Fox, D., Burgard, W., and Thrun, S. [1999]. Monte Carlo localization for mobile robots. Proceedings of the 1999 IEEE International Conference on Robotics & Automation, Detroit, May 1999. pp. 1322-1328.

Evans, J. M. [1994]. HelpMate: An autonomous mobile robot courier for hospitals. Proceedings of the 1994 IEEE International Conference on Intelligent Robots and Systems. Pp. 1695-1700.

Forsman, P. [2001]. Three-dimensional localization and mapping of static environments by means of mobile perception. Helsinki University of Technology, Automation Technology Laboratory, Series A: Research reports no. 23, November 2001. Dr thesis. 132 p.

Frohn, H. and v. Seelen, W. [1989]. VISOCAR: An autonomous industrial transport vehicle guided by visual navigation. Proceedings of the 1989 IEEE International Conference on Robotics and Automation. Pp. 1155-1159.

Grossmann, A. and Poli, R. [2001]. Robust mobile robot localization from sparse and noisy proximity readings using Hough transform and probability grids. Robotics and Autonomous Systems 37 (2001) 1-18.

Guivant, J., Nebot, E., and Baiker, S. [2000a]. High accuracy navigation using laser range sensors in outdoor applications. Proceedings of the 2000 IEEE International Conference on Robotics & Automation, San Francisco, April 2000. pp. 3817-3822.

Guivant, J., Nebot, E., and Durrant-Whyte, H. [2000b]. Simultaneous localization and map building using natural features in outdoor environments. Proceedings of 6th International Conference in Intelligent Autonmous Systems, Venice, 2000. pp. 581-588.

Gutmann, J.-S. and Konolige, K. [1999]. Incremental mapping of large cyclic environments. Proceedings of the IEEE International Symposium on Computational Intelligence in Robotics and Automation, 1999. pp. 318-325.

Halme, A., Leppänen, I., Ylönen, S., and Kettunen, I. [2001a]. WorkPartner – centaur like service robot for outdoors applications. Proceedings of the 3rd International Conference on Field and Service Robotics, June 11-13, 2001, Finland. Pp. 217-223.

Halme, A., Leppänen, I., Montonen, M., and Ylönen, S. [2001b]. Robot motion by simultaneously wheel and leg propulsion. Proceedings of the Fourth International Conference on Climbing and Walking Robots, September 24-26, 2001. pp. 1013-1019.

Hancock, J. A. [1999]. Laser Intensity-based Obstacle Detection and Tracking. PhD thesis, Carnegie Mellon University, 1999. 152 p.

Harris, K. D. and Recce, M. [1998]. Experimental modeling of time-of-flight sonar. Robotics and Autonomous Systems 24 (1998) 33-42.

Jensfelt, P. [1999]. Localization using laser scanning and minimalistic environmental models. Thesis, Royal Institute of Technology, 1999. 114 p.

Kim, J. H., Sukkarieh, S., Nebot, E. M., and Guivant, J. [2001]. On the effects of using heading information during in-flight alignment of a low-cost IMU/GPS integrated system. Proceedings of the 3rd International Conference on Field and Service Robotics, June 11-13, 2001, Finland. pp. 55-60.

Kong, X., Nebot, E., and Durrant-Whyte, H. [1998]. The use of quaternions in a low cost strapdown INS unit. In Field and Service Robotics, Springer, 1998. pp. 275-280.

Konolige, K. and Chou, K. [1999]. Markov localization using correlation. International Joint Conference on Artificial Intelligence, Stockholm, July 1999. 6 p.

Larsson, U., Forsberg, J., and Wernersson, Å. [1996]. Mobile robot localization: Integrating measurements from a time-of-flight laser. IEEE Transactions on Industrial Electronics, Vol. 43, No. 3, June 1996. pp. 422-431.

Lawitzky, G. [2001]. A navigation system for service robots: from research to products. Proceedings of the 3rd International Conference on Field and Service Robotics, June 11-13, 2001, Finland. Pp. 15-19.

Lillqvist, M. and Åkerlund, K. [1993]. A study of a gyroscope based on piezo crystals resonance. Project report, Helsinki University of Technology, Automation Technology laboratory, 1993. 9p. (In finnish)

Lu, F. and Milios, E. E. [1994]. Robot pose estimation in unknown environments by matching 2D range scans. Proceedings of the IEEE Conference on Computer Vision and Pattern Recognition, 1994. pp. 935-938.

Lu, F. [1995]. Shape registration using optimization for mobile robot navigation. PhD thesis, University of Toronto, 1995. 150 p.

Madhavan, R., Dissanayake, M. W. M. G., and Durrant-Whyte, H. F. [1998a]. Autonomous underground navigation of an LHD using a combined ICP-EKF approach. Proceedings of the 1998 IEEE International Conference on Robotics and Automation, Leuven, Belgium, May 1998. pp. 3703-3708.

Madhavan, R., Dissanayake G., and Durrant-Whyte, H. [1998b]. Map-building and map-based localization in an underground-mine by statistical pattern matching. Proceedings of the 14th International Conference on Pattern Recognition, Vol. 2, 1998. pp. 1744-1746.

Madhavan, R., Durrant-Whyte, H., and Dissanayake, G. [2002]. Natural landmark-based autonomous navigation using curvature scale space. Proceedings of the 2002 IEEE International Conference on Robotics & Automation, Washington, DC, May 2002. pp. 3936-3941.

Maybeck, P. S. [1979]. Stochastic models, estimation and control, Vol. 1. Academic press, 1979. 523 p.

Moravec, H. P. and Elfes, A. E. [1985]. High resolution maps from wide-angle sonar. Proceedings of the IEEE International Conference on Robotics and Automation, Washington D. C., USA. Pp. 116-121.

Moreno L., Pimentel, J., Puente, E. A., and Salichs, M. A. [1992]. Mobile robot multitarget tracking in dynamic environments. Proceedings of the 1992 IEEE International Conference on Intelligent Robots and Systems, Raleigh, NC, July 7-10, 1992. pp. 1464-1469.

Murrieta-Cid, R., Parra, C., and Devy, M. [2002]. Visual navigation in natural environments. Autonomous Robots 13 (2002) 143-168.

Mäkelä, Hannu [2001]. Overview of LHD navigation without artificial beacons. Robotics and Autonomous Systems 36 (2001) 21-35.

Nebot, E. M. and Durrant-Whyte, H. [1999]. Initial calibration and alignment of low cost inertial navigation units for land vehicle applications. Journal of Robotics Systems, Vol. 16, No. 2, February 1999. pp. 81-92.

Nebot, E. M., Bailey, T., and Guivant, J. [2000]. Navigation algorithms for autonomous machines in off-road applications. 19 p. (submitted to Journal of Autonomous Robots in November 2000). Publication available at http://www.usyd.edu.au/publications/.

Nilsson, B. [1997]. On Robot Control using Range Sensors. Linköping Studies in Science and Technology. Dissertations no. 511, 1997. 224 p.

Olson, C. F. [2000]. Probabilistic self-localization for mobile robots. IEEE Transactions on Robotics and Automation, Vol. 16, no. 1, February 2000. pp. 55-66.

Pears, N. E. [2000]. Feature extraction and tracking for scanning range sensors. Robotics and Autonomous Systems 33 (2000) 43-58.

Roberts, J. M., Duff, E. S., Corke, P. I., Sikka, P., Winstanley, G. J., and Cunningham, J. [2000]. Autonomous control of underground mining vehicles using reactive navigation. Proceedings of the 2000 IEEE International Conference on Robotics & Automation, San Francisco, April 2000. pp. 3790-3795.

Schultz, A. and Adams, W. [1998]. Continuous localization using evidence grids. Proceedings of the 1998 IEEE International Conference on Robotics & Automation, Leuwen, Belgium, May 1998. pp. 2833-2839.

Schulz, D., Burgard, W., Fox, D., and Cremers, A. B. [2001]. Tracking multiple moving targets with a mobile robot using particle filters and statistical data association. Proceedings of the 2001 IEEE International Conference on Robotics & Automation, Soul, Korea, May 21-26, 2001. pp. 1665-1670.

Selkäinaho, J. and Paanajärvi, J. [2000]. On tuning of Kalman filter. Proceedings of the 2nd International Symposium on Robotics and Automation, November 10-12, 2000, Monterrey, Mexico. pp 157-161.

Selkäinaho, J., Halme, A., and Paanajärvi, J. [2001]. Navigation system of an outdoor service robot with hybrid locomotion system. Proceedings of the 3rd International Conference on Field and Service Robotics, June 11-13, 2001, Finland. Pp. 79-83.

Shumway, R. and Stoffer, D. [1982]. An approach to time series smoothing and forecasting using the EM algorithm. Journal of Time Series Analysis, Vol. 3, No. 4, 1982. pp. 253-263.

Stroupe, A., Sikorski, K., and Balch, T. [2002]. Constraint-based landmark localization. Preprints of the 2002 International RoboCup Symposium, June 24-25, Fukuoka, Japan, 2002. pp 1-16.

Thrun, S., Bucken, A., Burgard, W., Fox, D., Fröhlingshaus, T., Hennig, D., Hofman, T., Krell, M., and Schmidt, Timo [1998a]. Map learning and high-speed navigation in RHINO. In AI based Mobile Robots, MIT Press, 1998.

Thrun, S., Fox, D., and Burgard, W. [1998b]. Probabilistic mapping of an environment by a mobile robot. Proceedings of the 1998 IEEE International Conference on Robotics & Automation, Leuwen, Belgium, May 1998. pp. 1546-1551.

HELSINKI UNIVERSITY OF TECHNOLOGY AUTOMATION TECHNOLOGY LABORATORY RESEARCH REPORTS

No. 11 Yang, H.,
Using landmarks for the vehicle location measurement, February 1994.

No. 12 Halme, A., Zhang, X.,
Experimental study of bioelectrochemical fuel cell using bacteria from Baltic sea, February 1995.

No. 13 Zhang, X.,
Aspects of modelling and control of bioproceses: Application of conventional approach, and functional state concept, October 1995.

No. 14 Yang, H.,
Vision methods for outdoor mobile robot navigation, November 1995.

No. 15 Wang, Y.,
Spherical rolling robot, February 1996.

No. 16 Hartikainen, K.,
Motion planning of a walking platforms designed to locomote on natural terrain, November 1996.

No. 17 Zhang, X., Halme, A.,
Effect of size and structure of a bacteria fuel cell on the electricity production and energy conversion rate, March 1997.

No. 18 Visala, A.,
Modeling of nonlinear processes using Wiener-NN representation and multiple models, November 1997.

No. 19 Xu, B.,
An interactive method for robot control and its application to deburring, November 1998.

No. 20 Zhang, X., Halme A.,
A biofilm reactor for a bacteria fuel cell system, August 1999.

No. 21 Vainio, M.,
Intelligence through interactions – Underwater robot society for distributed operations in closed aquatic environment, October 1999.

No. 22 Appelqvist, P.,
Mechatronics design of a robot society – A case study of minimalist underwater robots for distributed perception and task execution, November 2000.

No.23 Forsman, P.,
Three-dimensional localization and mapping of static environments by means of mobile perception, November 2001.

ISBN 951-22-6230-4
ISSN 0783-5477